DIPLOMARBEIT

BIAS-T FOR PULSED APPLICATIONS

AUSGEFÜHRT ZUM ZWECKE DER ERLANGUNG DES AKADEMISCHEN GRADES EINES DIPLOM-INGENIEURS UNTER DER LEITUNG VON

DI DR MARKUS MAYER

UND

UNIV. PROF. DI DR GOTTFRIED MAGERL
INSTITUT FÜR ELEKTRISCHE MESS- UND SCHALTUNGSTECHNIK
Inst. Nr. E354

EINGEREICHT AN DER TECHNISCHEN UNIVERSITÄT WIEN
FAKULTÄT ELEKTROTECHNIK UND INFORMATIONSTECHNIK VON

MARKUS RABERGER
MATR. NR. 9525139
ALAUNTALSTRASSE 50
3500 KREMS

WIEN, IM APRIL 2004

Kurzfassung

Zweck dieser Diplomarbeit war es, ein Bias-T für gepulste Anwendungen zu entwickeln und zu bauen. Dieses Bias-T ist notwendig bei der Messung der Eigenschaften von Hochfrequenz-Transistoren, um während der Zeit der Messung den Einfluss der Selbsterwärmung zu eliminieren. Um dies zu ermöglichen, ist es notwendig HF-Spannung, gepulste Gleichspannung und Gleichspannung zu kombinieren. Der Frequenzbereich, in dem das Bias-T arbeiten soll, ergab sich aus den Anwendungen in der Mobilkommunikation für die man zur Zeit HF-Transistoren mit großer Leistung benötigt. Werden diese Transistoren im Großsignalbetrieb verwendet, werden Harmonische der Grundschwingung mit höherer Ordnung erzeugt. Diese harmonischen Signalanteile müssen vom Bias-T definiert abgeschlossen werden.
Kapitel 1 beinhaltet eine genaue Beschreibung für die Notwendigkeit des Bias-Ts und die Spezifikationen, die von ihm erfüllt werden müssen.
Die theoretischen Grundlagen, welche für die Erarbeitung dieser Diplomarbeit notwendig waren, sind in Kapitel 2 angeführt.
In Kapitel 3 sind die einzelnen Entwicklungsstufen und deren Probleme dargestellt. Begonnen wurde mit der Realisierung mit diskreten Bauteilen, danach kommt der Versuch, einen eigenen Koppler zu bauen und zuletzt das endgültige Design mit kommerziell verfügbaren 3 dB 90° Hybriden. Das Bias-T wurde schließlich in mehrere Bias-Ts aufgeteilt, um eine höhere Flexibilität in der Anwendung zu erhalten. Gebaut wurde schließlich ein Bias-T mit Anpassung für Harmonische, das alle Spezifikationen erfüllt, zwei ohne einer Anpassung für unterschiedliche, eingeschränktere Frequenzbereiche und dann noch zwei, um gepulste Gleichspannung mit Gleichspannung zu kombinieren.
Kapitel 4 enthält die Ergebnisse der Messungen der verschiedenen Bias-Ts und eine Auflistung der notwendigen Modifikationen, um die gewünschten Spezifikationen zu erreichen.
Abschließend gibt es eine Zusammenfassung und Tipps für die Entwicklung weiterer Bias-Ts.
Im Anhang befinden sich Programme, Dokumentationen und Datenblätter, welche für die Hardwareentwicklung benötigt wurden.

Abstract

The aim of this diploma thesis was to design and build a bias-T for pulsed applications which is needed to measure RF transistors without the influence of self-heating during the time of measurement. In order to accomplish this, DC, pulsed DC and RF have to be combined with this bias-T. The frequency range of the bias-T is defined by the frequency bands of mobile communication systems, where high power RF transistors are needed. At large signal excitation, the transistor produces harmonics. These harmonics should be terminated by the bias-T.
In chapter 1, the motivation to build such a bias-T is described more detailed and the specifications which are necessary for the implementation are given in detail.
The theory, which is essential to solve the arised problems is summarized in chapter 2.
In chapter 3, the different steps of development as well as their according problems and solutions are explained in detail. Two design approaches were evaulated for the realization of the bias-T to combine RF and an already combined pulse and DC. The first approach which was based on lumped elements, turned out to be not feasible. A second design approach was based on 3 dB 90° hybrids. Starting with a new design of a broadband coupler, the final design was realized with commercially available hybrids. The bias-T was finally splitted to a set of different bias-Ts to offer high flexibility. To combine RF and an already combined pulse, a bias-T with up to 3^{rd} order harmonic matching was built; fulfilling all required specifications. Additionally, two bias-Ts, which do not comprise harmonic matching for a frequency range, for different limited frequency ranges were built.
In order to combine the DC pulse with a bandwidth of 200 MHz and DC offset, two additional bias-Ts in classical design with lumped components were built.
Chapter 4 comprised the results of the measurements that were performed on the bias-Ts and which modifications were necessary to reach the required specifications.
A summary, which sums up the specifications of the chosen implementations and an outlook summing up hints for further bias-T designs conclude this thesis.
In the appendix descriptions of additionally developed software tools and required documents for the hardware development can be found.

Acknowledgement

I would like to thank my parents, who made it possible for me to study, and my wife, who always supported me with love and energy through my studies and this Diploma Thesis.
I also would like to thank all members of the microwave engineering group of the Institute for Electrical Measurement and Circuit Design at the Vienna University of Technology. Special thanks go to Univ. Prof. Gottfried Magerl, my advisor DI Dr Markus Mayer for his support with practical experience and his participation in inspiring discussions that led to new ideas for the realization of my work.

Contents

List of Acronyms **IX**

List of Symbols **X**

1 Introduction **1**
1.1 Motivation . . . 1

1.2 System Overview . . . 2
1.3 Specifications of the Pulser . . . 3
1.4 Specifications of the Pulsed Bias-T . . . 3

2 Theory **4**
2.1 Basic Definitions of Inductors and Capacitors . . . 4
2.1.1 Inductors . . . 4
2.1.2 Capacitors . . . 8
2.2 Microwave Network Theory . . . 11
2.2.1 Introduction . . . 11
2.2.2 Actual and Equivalent Voltages and Currents . . . 11
2.2.3 Scattering Matrix . . . 16
2.3 Broadside-Coupled Lines . . . 18
2.3.1 Broadside-Coupled Striplines . . . 18
2.3.2 Broadside-Coupled Suspended Microstrip Lines . . . 18
2.3.3 Broadside-Coupled Offset Striplines . . . 20
2.4 Directional Coupler . . . 22

3 Hardware Design **24**
3.1 Design with Lumped Elements . . . 24
3.1.1 Simulations with Ideal Components . . . 24
3.1.2 Choosing a Substrate . . . 25
3.1.3 Simulation with Real Components . . . 26
3.1.4 Results of the Simulations . . . 26
3.2 Realization with Quadrature Hybrids . . . 27
3.2.1 General Aspects . . . 27
3.2.2 Design of the 3 dB Hybrid . . . 29
3.2.3 Internet Investigation of the Commercially Available 3-dB Hybrids . . . 35
3.2.4 Design of the Bias-T with Anaren Xinger® . . . 36

4 Measurements **45**
4.1 Bias-T with Harmonic Matching . . . 45
4.1.1 S-Parameters . . . 45
4.1.2 Thermal Tests with RF Power and DC Current . . . 51
4.1.3 Measured DC Pulses . . . 54
4.2 1^{st} Bias-T without Harmonic Matching . . . 55
4.2.1 S-Parameters . . . 55
4.2.2 Thermal Test with RF Power and DC Current . . . 57

4.2.3 Measured DC Pulses . . . 61
4.3 2^{nd} Bias-T without Harmonic Matching . . . 62
4.3.1 S-Parameters . . . 63
4.3.2 Thermal Test with RF Power and DC Current . . . 64
4.3.3 Measured DC Pulses . . . 65
4.4 Bias-T to combine DC-Pulse and DC . . . 66
4.4.1 Bias-T for Pulses up to 10 μs Pulsewidth . . . 66
4.4.2 Bias-T for Pulses up to 100 μs Pulsewidth . . . 71

5 Summary and Outlook **75**
5.1 Summary . . . 75
5.2 Bias-Ts Technical Data Sheets . . . 76
5.2.1 Bias-T with Harmonic Matching . . . 76
5.2.2 1^{st} Bias-T without Harmonic Matching . . . 77
5.2.3 2^{nd} Bias-T without Harmonic Matching . . . 78
5.2.4 1^{st} Bias-T for DC-Pulse and DC . . . 79
5.2.5 2^{nd} Bias-T for DC-Pulse and DC . . . 80
5.3 Outlook . . . 81

References **82**

6 Appendix **83**
6.1 Appendix A - MatLab® Function . . . 83
6.2 Appendix B - Directional Coupler - Design Parameters . . . 86
6.3 Appendix C - Directional Coupler - Table of Physical Parameters . . . 90
6.4 Appendix D - Datasheets of Anaren Xinger® Q-Hybrids . . . 92
6.5 Appendix E - Subtrates . . . 96

List of Figures

1.1 System Schematic 2
1.2 Operation Point 2
1.3 Pulser AVRF-2-B 3
1.4 Specifications 3

2.1 Loop Wire Configuration Showing Flux Area S, Current I, and Magnetic Flux B. 4
2.2 Magnetic Flux Lines in a Coil 5
2.3 (a) Self-Inductance in Parallel with Capacitance. (b) Series Inductance Resistance Representation. 6
2.4 Basic Parallel Plate Capacitor Configuration. 8
2.5 (a,b) Series Representation of Capacitor. 9
2.6 Equivalent Circuit of Parallel Plate Capacitor 10
2.7 Variation of Input Impedance of Ideal Series Inductor, Series Capacitor and Parallel Capacitor and Parallel Plate Capacitor. 10
2.8 Normalized and Unnormalized Voltage and Current Waves on Transmission Lines of a Two-Port Network. 11
2.9 A Two-Port Network Connected to a Source and Load 14
2.10 An N-Port Network 15
2.11 (a) Even-Mode, and (b) Odd-Mode Field Distribution of General Broadside Coupled Microstrip Lines. 19
2.12 Broadside Coupled Off-Set Stripline 20
2.13 Structure of the Directional Coupler 22
2.14 Weighting Function for the Directional Coupler 22

3.1 Ideal Bias-T 24
3.2 Simulation Results: Real Microstrip Lines with Ideal Lumped Elements 25
3.3 Simulation Results: Ideal Lumped Elements Optimized 25
3.4 Simulation Results: Real Components 26
3.5 Quadrature Hybrid 27
3.6 Branch-Line and Directional Coupler 27
3.7 Combination of 2 Hybrids 28
3.8 Bias-T with Hybrids 28
3.9 Edge & Broadside Coupled Striplines 29
3.10 Broadside Coupled Off-Set Stripline 31
3.11 MWO Model for Broadside Offset Coupled Lines 33
3.12 Simulation Results for both Design Methods 33
3.13 Structure of the Coupled Elements in MWO 34
3.14 Optimized Coupler 34
3.15 Theoretical S Parameters with Anaren 11306-3 36
3.16 Theoretical S Paramters with Anaren 1M803 37
3.17 Testprints for Mod. 11306-3 and 1M803 38
3.18 S-Parameters of the Test Prints 38
3.19 Heatsink of the Test Prints 39
3.20 Simulated S Parameters of Bias-T with Harmonic Matching 42

3.21 Layout of the Bias-Ts . . . 43
3.22 The Prints of the Bias-Ts . . . 43
3.23 Schematic of Bias-T to Combine Pulse and DC . . . 44

4.1 Final Bias-T with Harmonic Matching . . . 45
4.2 1^{st} Measured S-Parameters . . . 46
4.3 Modified Bias-T with Open Case . . . 47
4.4 Power Loss at Port 4 . . . 48
4.5 Closed Case . . . 48
4.6 Closed Case with Magnetic Absorber (a), Dielectric Absorber (b) . . . 49
4.7 Cap with Dielectric Absorber . . . 49
4.8 Final Bias-T for Harmonics . . . 50
4.9 Bias-T Temperature vs. RF Power . . . 51
4.10 Bias-T Temperature vs. Current . . . 52
4.11 Safe Operation Area of the Bias-T . . . 53
4.12 Configuration for Pulse Measurements . . . 54
4.13 Short Pulse Measured . . . 54
4.14 Long Pulse Measured . . . 54
4.15 Bias-T without Harmonic Matching . . . 55
4.16 Without Cap . . . 56
4.17 Closed Case . . . 56
4.18 Final Bias-T without Harmonics . . . 57
4.19 Bias-T Temperature vs. RF Power . . . 58
4.20 Bias-T Temperatur vs. DC Current . . . 59
4.21 Safe Operation Area of the Bias-T . . . 60
4.22 Short Pulse Measured . . . 61
4.23 Long Pulse Measured . . . 61
4.24 2^{nd} Bias-T without Harmonic Matching . . . 62
4.25 Finished Bias-T for Higher Frequencies . . . 63
4.26 Bias-T Temperature vs. DC Current . . . 64
4.27 Short Pulse Measured . . . 65
4.28 Longe Pulse Measured . . . 65
4.29 Circuit Schematic for Bias-T Pulse + DC . . . 66
4.30 Bias-T for Pulses up to 10 μs . . . 66
4.31 Small Bias-T for DC + Pulse . . . 67
4.32 Short Pulse . . . 68
4.33 Pulse Inside the Range of the Bias-T . . . 68
4.34 Maximum Pulsewidth . . . 69
4.35 Distorted Pulse . . . 69
4.36 Negative Pulse Through the Bias-T . . . 70
4.37 Pulse + DC . . . 70
4.38 Bias-T for Pulses up to 100 μs . . . 71
4.39 Large Bias-T for DC + Pulse . . . 71
4.40 Short Pulse . . . 72
4.41 Pulsewidth 20 μs . . . 72
4.42 Pulsewidth 50 μs . . . 73
4.43 Largest Available Pulse . . . 73
4.44 Negative Pulse with Pulsewidth 75 μs . . . 74
4.45 Pulse + DC . . . 74

5.1 Ports of the 1^{st} Bias-T . . . 76
5.2 Ports of the 2^{nd} Bias-T . . . 77
5.3 Ports of the 3^{rd} Bias-T . . . 78
5.4 Ports of the 4^{th} Bias-T . . . 79
5.5 Ports of the 5^{th} Bias-T . . . 80

List of Tables

3.1 Normalized Even-Mode Impedances for 3 dB Coupling 30
3.2 Weighting Factors 30
3.3 Physical Parameters 32
3.4 Electrical Specifications of Model 11306-3 36
3.5 Electrical Specifications of Model 1M803 37
3.6 Ohmic Resitance 39
3.7 Rogers R4003C 40

4.1 Resonance Frequencies 49
4.2 Table of S-Parameter 50
4.3 RF Power Measurement 51
4.4 DC Current Measurement 52
4.5 Limits of RF Power and DC Current 53
4.6 Resonance Frequencies 56
4.7 Insertion Loss of the Bias-T without Harmonic Termination 57
4.8 Measurement Results with RF Power 58
4.9 DC Current Measurement Results 59
4.10 Limits of RF Power and DC Current 60
4.11 Insertion Losses from 2.3 to 6.3 GHz 63
4.12 DC Current Measurement Results 64

List of Acronyms

Att	...	Attenuator
BW	...	Bandwidth
CW	...	Continuous Wave
DF	...	Dissipation Factor
DUT	...	Device Under Test
FOM	...	Figure of Merit
HP	...	High Pass Filter
I_D	...	Drain Current
I_G	...	Gate Current
LF	...	Low Frequency
LP	...	Low Pass Filter
MatLab®	...	MatLab Ver. 6.0
Microwave Office®	...	Microwave Office Ver. 5.51
PRF	...	Parallel Resonance Frequency
RF	...	Radio Frequency
TEM	...	Transversal Electromagnetic Mode
TRL	...	Thru, Reflect, Line Calibration Methode
SRF	...	Series Resonance Frequency
V_{DS}	...	Drain Source Voltage
V_{GS}	...	Gate Source Voltage
VSWR	...	Voltage Standing Wave Ratio
θ_{JC}	...	Thermal Resistance Junction Case

List of Symbols

B	...	bandwidth ratio
B_m	...	magnetic flux density
b	...	dielectric thickness of strip transmission lines
C	...	capacitance
c_0	...	velocity of light in free space
d	...	overall length of the coupler
f	...	frequency
f_0	...	center frequency
I^+	...	incident current wave
I^-	...	reflected current wave
I_n^+	...	normalized incident current wave
I_n^-	...	normalized reflected current wave
L	...	inductance
M	...	mutual inductance
P^+	...	incident power
P^-	...	reflected power
R	...	voltage coupling factor
S	...	spacing between coupled lines
s'	...	normalized spacing between coupled lines
S_{xy}	...	scattering parameter
t	...	conductor thickness
T	...	transmission coefficient
tan δ	...	dissipation factor
V^+	...	incident voltage wave
V^-	...	reflected voltage wave
V_n^+	...	normalized incident voltage wave
V_n^-	...	normalized reflected voltage wave
v_p	...	phase velocity
W_m	...	magnetic energy
W	...	line width of directional coupler
W_c	...	line overlap width of directional coupler
W_0	...	difference of w and w_c

w'	...	normalized line width of directional coupler
w_c'	...	normalized line overlap width of directional coupler
w_0'	...	normalized difference of w and w_c
Z	...	impedance
Z_{in}	...	input impedance
Z_L	...	load impedance
Z_0	...	characteristic impedance
Z_{0e}	...	even-mode characteristic impedance
Z_{0o}	...	odd-mode characteristic impedance
β	...	phase constant
γ	...	complex propagation constant
ε_0	...	permittivity of free space
ε_r	...	relative dielectric constant
σ	...	conductivity
λ	...	wave length
μ_0	...	permeability of free space
μ_r	...	relative permeability
Ψ	...	magnetic flux
Ψ_{ij}	...	phase of the transversal components el. and mag. field
τ	...	time constant
Γ	...	reflection coefficient
ω	...	angular frequency
ω_p	...	parallel resonance angular frequency
ω_s	...	series resonance angular frequency

Chapter 1

Introduction

1.1 Motivation

To operate a transistor as a microwave amplifier it is, on the one hand, necessary to combine DC voltage and RF voltage at the transistor´s input and, on the other hand, to separate DC and RF voltage at the transistor´s output. With the DC voltage the quiescent point at which the transistor should work is set and the RF voltage is amplified. It is not possible to combine RF and DC straightly, because the DC supply acts as a short circuit for the RF voltage. Therefore, a bias-T with three ports is needed. It combines RF and DC voltage at one port and decouples the two input ports of RF and DC. For the measurement of transistors it is a disadvantage if the transistor operates for a longer time at the quiescent point, because the self-heating of the transistor affects the measurement. As a result of this, only a short DC pulse is used to switch for the short time of measurement to the desired quiescent point, so that the effect of self-heating is eliminated.
Out of this reason, a "bias-T for pulsed applications" was designed at this diploma thesis.

1.2 System Overview

In Fig. 1.1 the principle structure of measuring a transistor with pulsed DC is shown. Therefore, firstly the pulse from the pulser is combined with DC in a bias-T for an offset. The next step is the combination of the DC+pulse with the RF in the second bias-T. If this combination is used at the gate and the drain of the transistor, the operation point can be moved for a short period of time to each direction, as shown in Fig. 1.2. At such a system it is possible to measure a transistor´s DC-IV curves at a certain bias point while not affecting the measurement due to self-heating.

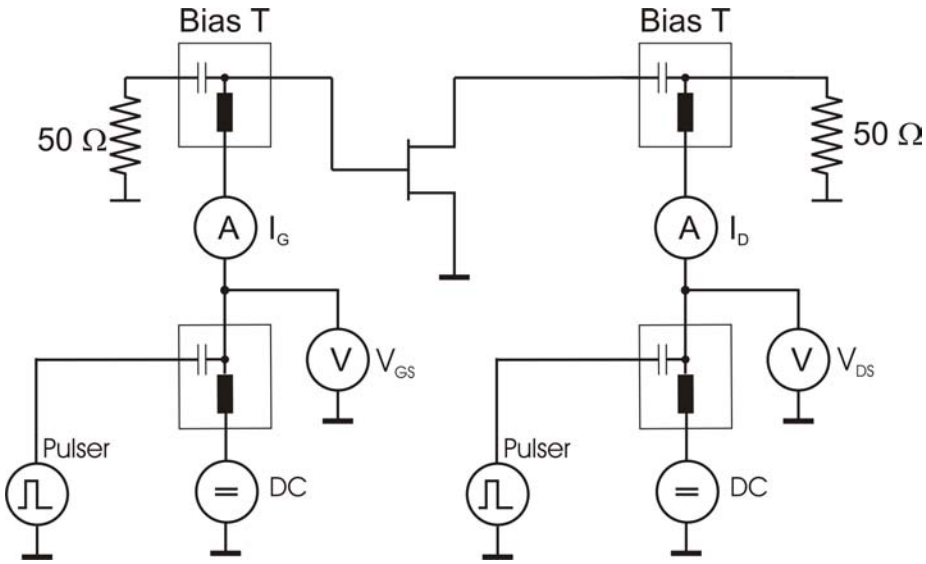

Figure 1.1: System Schematic

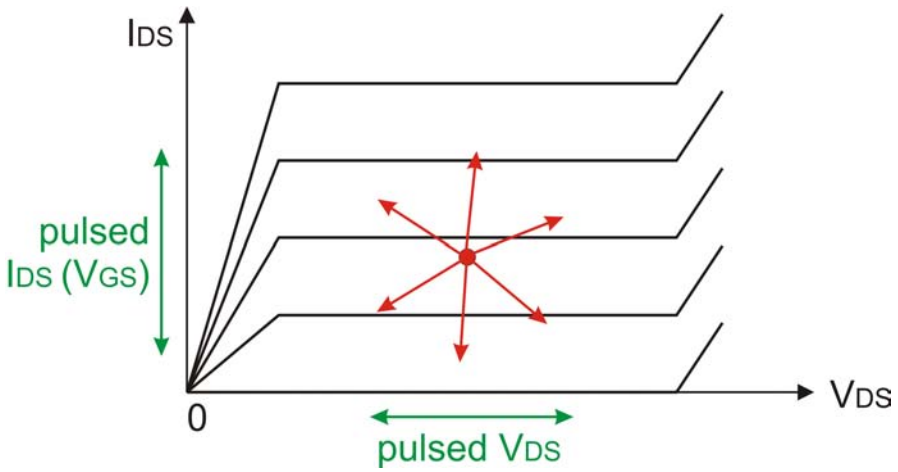

Figure 1.2: Operation Point

1.3 Specifications of the Pulser

Used Pulser: AVTECH AVRF-2-B

The specifications are:	
Amplitude at a 50 Ω load:	0 to 200 Volts
Rise time:	$\leq$ 2 ns
Fall time:	$\leq$ 2 ns
Pulse width:	0.1 to 100 μs
Pulse repetition frequency:	0 to 1 kHz
Duty cycle (max):	0.5%
Average power out:	4 Watts

Figure 1.3: Pulser AVRF-2-B

1.4 Specifications of the Pulsed Bias-T

The following basic requirements define the specifications of the bias-T:

First of all, it will be designed for a 50 Ω network. The bias-T should be used to measure transistors in the frequency band of mobile communication and wireless LAN, which is a frequency range of 1.8 GHz to 2.5 GHz and should also handle the harmonics up to the third order because at large signal excitation the transistor produces harmonics. These harmonics should be terminated by the bias-T. So, the required frequency range is 1.8 GHz to 8 GHz. The pulsed maximum current value of the pulser is 4 A at 50 Ω load. But the bias-T should be designed up to a maximum current of 8 A. Since DC current from the DC supply may go up to 8 A, this is a value taken from the practice of measuring transistors in the given bandwidth. The bias-T must not distort the shape of the DC pulse, which results in a bandwidth of 200 MHz. The resistance of the DC path should be as low as possible.
The return losses S_{11}(RF port) and S_{22} (RF+DC port), respectively, should be higher than 15 dB and the insertion loss should be as low as possible, aimed at $\leq$ 0.5 dB. The isolation between S_{23} (path DC to RF+DC port) and S_{21} (path RF to RF+DC port) should be higher than 20 dB.

Frequency Range:	1,8 to 8 GHz	Pulsed current	8 A
Return Loss S_{ii}:	$\geq$ 15 dB	DC-current:	8 A
Insertion Loss:	0.5 dB	Impedance:	50 Ω
Isolation S_{23} - S_{21}	20 dB		

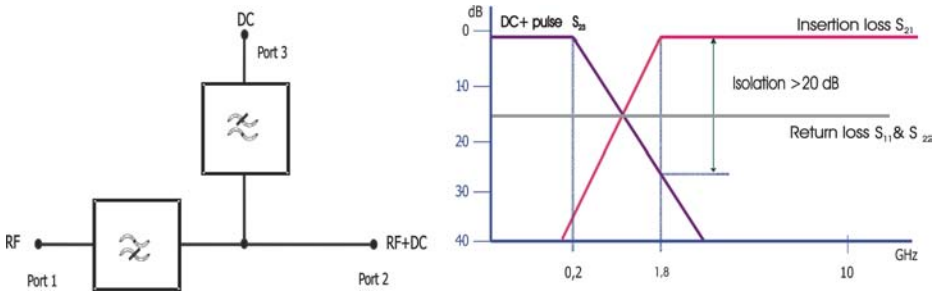

Figure 1.4: Specifications

Chapter 2

Theory

2.1 Basic Definitions of Inductors and Capacitors

The presented theory of inductors and capacitors is based on [1].

2.1.1 Inductors

Inductance

In electrical circuits, the effect of magnetic energy storage is represented by an inductance L, which is defined in terms of magnetic flux Ψ by

$$\begin{aligned} L &= \frac{1}{I}\oint_S B_m \cdot ds = \frac{\Psi}{I} \\ &= \mu_0\mu_r \frac{1}{I}\oint_l H \cdot dl \end{aligned} \tag{2.1}$$

where:
I = the current flowing through the conductor in amperes,
B_m = magnetic flux density expressed in tesla (T) or weber/m^2 = $\mu_0\mu_r H$,
where the magnetic field, H is expressed in A/m,
S = the surface area enclosed by the loop of wire of length l.

For perfect conductors $\mu_r = 1$. Free-space permeability is $\mu_0 = 4\pi \times 10^{-7} H/m$.
The current I produces magnetic flux in the area S bound by the loop as shown in Fig. 2.1.
In this case, L is also known as *self-inductance*. Fig. 2.2 shows the magnetic flux lines in a coil.

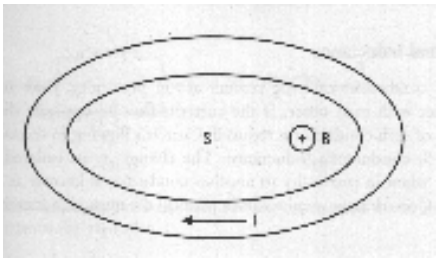

Figure 2.1: Loop Wire Configuration Showing Flux Area S, Current I, and Magnetic Flux B.

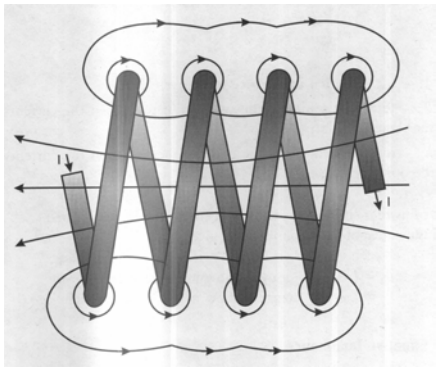

Figure 2.2: Magnetic Flux Lines in a Coil

Magnetic Energy

In an inductor, the magnetic energy is stored as long as the current keeps flowing through it and is given by

$$W_m = \frac{LI^2}{2} \tag{2.2}$$

where:
W_m = magnetic energy express in Joules ($W \cdot s = J$), W and s designate watt and second, respectively;
L = inductance in henrys (H);
I = current in amperes (A).

Mutual Inductance

When two conductors carrying current are in proximity, their magnetic flux lines interact with each other. If the currents flow in opposite directions, the inductance of each conductor is reduced. Currents flowing in the same direction increase each conductor´s inductance. The change in an isolated conductor´s inductance when in proximity to another conductor is known as their *mutual inductance*. Consider two conductors in parallel; the mutual inductance is defined by

$$M = L_m = \frac{L_a - L_0}{2} \tag{2.3}$$

where
$M = Lm$ = mutual inductance in henry (H);
L_a = total inductance of the two conductors when the current flows in the same direction;
L_0 = total inductance of the two conductors when the current flows in the opposite direction;

If L is the self-inductance of each conductor in the isolated case, then the total inductance of each conductor is given by

$$\begin{aligned} L_t &= L + M \quad \text{(current flow in the same direction)} \\ &= L - M \quad \text{(current flow in the opposite direction)} \end{aligned} \tag{2.4}$$

Effective Inductance

For chip inductors, the nominal inductance value is measured at low frequencies; however, the operating frequency range is much higher. Because the inductor has associated parasitic capacitance (due to

interturn and ground plane effects) in parallel with its inductance as shown in Fig. 2.3(a), the impedance of the inductor (neglecting series resistance) can be written as

$$Z_i = \frac{j\omega L \cdot \frac{1}{j\omega C_p}}{j\omega L + \frac{1}{j\omega C_p}} = \frac{j\omega L}{1 - \omega^2 L C_p} \tag{2.5a}$$

or

$$Z_i = j\omega L_e \tag{2.5b}$$

where

$$L_e = \frac{L}{1 - (\omega/\omega_p)^2} \quad . \tag{2.5c}$$

Here ω_p $(= 1/\sqrt{LC_p})$ is the parallel resonant frequency. The equivalent inductance L_e is known as *effective inductance*, and below the first resonance its value is generally greater than the nominal specified value.

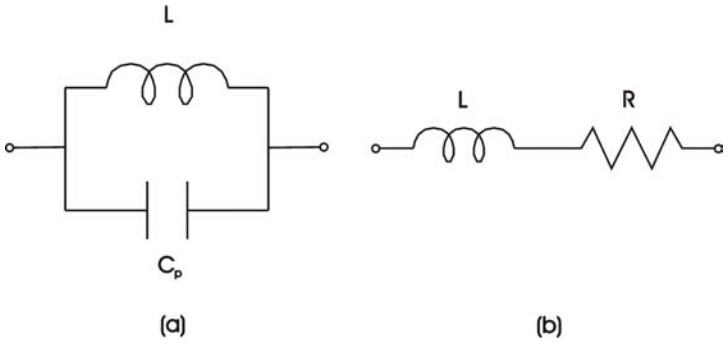

Figure 2.3: (a) Self-Inductance in Parallel with Capacitance. (b) Series Inductance Resistance Representation.

Impedance

The Impedance of an inductor is defined as

$$Z_L = \frac{V}{I} = j\omega L \tag{2.6}$$

where $\omega = 2\pi f$ and f is the operating frequency in hertz (Hz). The preceding equation shows that the sinusoidal current in a perfect inductor lags the voltage by 90°.

Time Constant

When a DC voltage is applied across a series inductor-resistor combination as shown in Fig. 2.3(b), the time required to charge the inductor to the applied voltage is known as the time constant τ and is given as

$$\tau = \frac{L}{R} \tag{2.7}$$

where τ, L and R are expressed in seconds, henries and ohms, respectively.

Quality Factor

Several different definitions of Q-factors for inductors have been used in the literature, but the most general definition of Q is based on ratio of energy stored, W_S, to power dissipated, P_D, in the inductor per cycle; that is

$$Q = \frac{\omega W_S}{P_D} \quad . \tag{2.8}$$

At low frequencies an inductor´s primary reactance is inductive and

$$Q = \frac{\omega \frac{1}{2} L i_0^2}{\frac{1}{2} R i_0^2} = \frac{\omega L}{R} \tag{2.9}$$

where i_0 is the rms value of the current. When the inductor is used as a resonant component close to its *self-resonance frequency* (RSF) f_{res}, a more appropriate definition of the Q-factor is in terms of its 3-dB bandwidth (BW) is given by

$$Q = \frac{f_{res}}{BW} \tag{2.10}$$

A third definition of Q-factor, which has been used for distributed resonators, is evaluated from the rate of charge of input reactance with frequency:

$$Q = \frac{f_{res}}{2R} \left[\frac{dX_{in}}{df} \right] \tag{2.11}$$

where X_{in} is the input reactance of the inductor and dX_{in}/df is determined at f_{res}.
In microwave circuits where the inductors are used far below the self-resonance frequency, the degree at which the inductor deviates from an ideal component is described by the effective quality factor Q_{eff}.

$$Q_{eff} = \frac{\mathrm{Im}\left[Z_{in}\right]}{\mathrm{Re}\left[Z_{in}\right]} = \frac{X}{R} = \frac{\omega L_e}{R} \tag{2.12}$$

where $Re[Z_{in}]$ and $Im[Z_{in}]$ are the real and imaginary parts of the input impedance of the inductor, respectively. This definition leads to the unusual condition that Q_{eff} becomes zero at resonance. Since in RF and microwave circuits, for series applications of inductors, the operating frequencies are well below the self-resonance frequency, the preceding definition is traditionally accepted.

Self-Resonant Frequency

The self-resonant frequency (f_{res}) of an inductor is determined when $Im[Z_{in}] = 0$; that is, the inductive reactance and the parasitic capacitive reactance become equal and opposite in sign. At this point, $Re[Z_{in}]$ is maximum due to parallel resonance and the angle of Z_{in} changes sign. The inductors´s first resonant frequency is of the parallel resonance type. Beyond the resonant frequency, the inductor becomes capacitive.

2.1.2 Capacitors

Introduction

When a voltage is applied across the two plates of a capacitor, the amount of energy stored depends on the work done in charging the capacitor. *Capacitance* is defined as the capacity to store energy in an electric field between two electrodes or efficiency of the structure in storing a charge when voltage difference exists between the plates. Its value depends on the area of the electrodes, separation between the electrodes, and the dielectric material between them. Dielectrics with high values of permittivity and higher breakdown voltage are the most desirable. The capacitor structure might have two or more conductors. The capacitance, C, in farads, of a capacitor structure consisting of two conductors is expressed as:

$$C = \frac{Q}{V} \tag{2.13}$$

where Q is the total charge in coulombs on each electrode or conductor and V is the voltage between the two conductors in volts. At the positive polarity the charge is positive, whereas at the negative polarity it is negative. Field lines start from the positive plate and terminate at negative plate.
The basic structure of a capacitor, as shown in Fig. 2.4, consists of two parallel plates also called electrodes, each of area A and separated by an insulator or dielectric material of thickness d and permittivity $\varepsilon_0\varepsilon_r$, where ε_0 and ε_r are free-space permittivity and relative dielectric constant.

$$Q = \oint_S \varepsilon_0 \varepsilon_r E_x \cdot ds = \varepsilon_0 \varepsilon_r E_x A \tag{2.14}$$

where E_x (V/d) is the electric field produced by the applied voltage V. From (2.13) and (2.14),

$$C = \varepsilon_0 \varepsilon_r \frac{A}{d} = \varepsilon_0 \varepsilon_r \frac{W \times l}{d} \tag{2.15}$$

where W and l are the width and length of one of the plates. Equation (2.15) does not include the effect of fringing field.

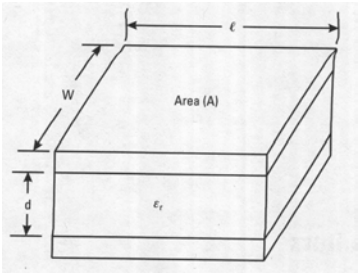

Figure 2.4: Basic Parallel Plate Capacitor Configuration.

Effective Capacitance

For chip capacitors, the nominal capacitance value is measured at 1 MHz and in typical RF applications the operating frequency is much higher. Because the capacitor has an associated parasitic series inductance as shown in Fig. 2.5(a), the impedance of the capacitance (neglecting series resistance) can be written

$$Z_c = j\left[\omega L_s - \frac{1}{\omega C}\right] = -\frac{j}{\omega C}\left[1 - \omega^2 L_s C\right] \tag{2.16}$$

or

$$Z_c = -\frac{j}{\omega C_e} \tag{2.17a}$$

where

$$Ce = C\left[1 - \omega^2 L_s C\right]^{-1} = C\left[1 - (\omega/\omega_s)^2\right]^{-1} \quad . \tag{2.17b}$$

Here ω_s is the series resonant frequency ($= 1/\sqrt{L_S C}$). The equivalent capacitance C_e is known as the effective capacitance and below the resonance frequency, its value is generally greater than the nominal specified value.

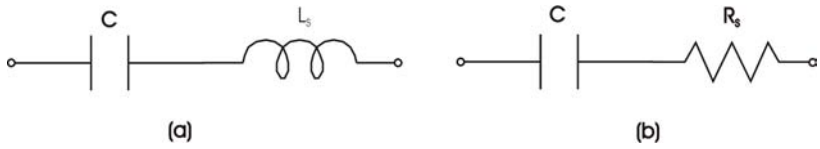

Figure 2.5: (a,b) Series Representation of Capacitor.

Quality Factor

Quality factor is an important FOM for capacitors and measures the capacitor´s capability to store energy. When a capacitor is represented by a series combination of capacitance C and resistance R_s as shown in Fig. 2.5(b), the quality factor, Q is defined by the following relation:

$$Q = \frac{1}{\omega C R_S} = \frac{1}{2\pi f C R_S} \tag{2.18}$$

where $\omega = 2\pi f$, and is the operating frequency. For discrete capacitors, the value of Q is typically measured at low frequencies.

Series and Parallel Resonances

Unlike inductors from the equivalent circuit shown in Fig. 2.6, we see that capacitors have both series and parallel resonance frequencies where the series and first parallel resonance frequencies are dominant. Below the series resonance frequency, the capacitor works as a capacitor as designed. However, above the resonance frequency, the capacitor´s total reactance is inductive and it becomes again capacitive after the first parallel resonance frequency.
A lumped-element equivalent circuit of a capacitor is shown in Fig. 2.6, where L_S is the electrode inductance and C_p is the parasitic parallel capacitance. The impedance of the capacitance between the two electrodes can be written as follows:

$$Z_C = \frac{1}{j\omega C_p + (R_S + j\omega L_S + \frac{1}{j\omega C})^{-1}} \quad . \tag{2.19}$$

Thus, the value of Z_C is infinite (because of C and C_p) at DC and decreases with frequency. Finally, it becomes zero at infinite frequency (because of inductance L_S). However, as shown in Fig. 2.7, the behavior of Z_C is nonideal. Fig. 2.7 also shows variations of an ideal inductor L, for an ideal capacitor C, and for a parasitic capacitor C_p. When $C \gg C_P$, at frequency ω_s, the reactances of series elements C and L_S become equal, that is, $\omega_S L_S = \frac{1}{\omega_S C}$, resulting in total reactance equal zero. The frequency ω_S at which this happens is called the *series resonant frequency* (SRF), and the capacitor´s impedance is equal to resistor R_S. Thus, at SRF, a capacitor mounted in a series configuration is represented by a small resistor and its insertion loss is low. As the frequency increases, the reactance of the capacitance becomes very small and the reactances of the parallel elements L_S and C_p become equal, that is, $\omega pLS = \frac{1}{\omega pCp}$. The frequency ω_p at which this occurs is known as the *parallel resonant frequency* (PRF), and the capacitor becomes a very large resistor whose value is given by

$$R_p = \frac{1}{R_S(\omega_p C_p)^2} \quad . \tag{2.20}$$

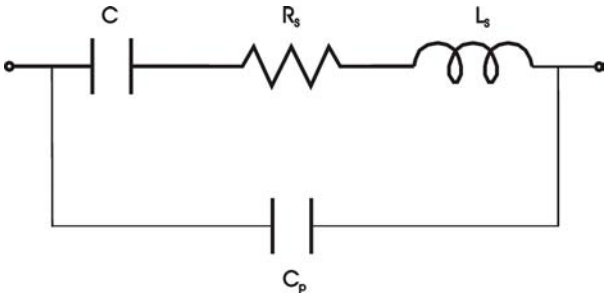

Figure 2.6: Equivalent Circuit of Parallel Plate Capacitor

Thus, at PRF, R_p is infinite when $R_S = 0$.

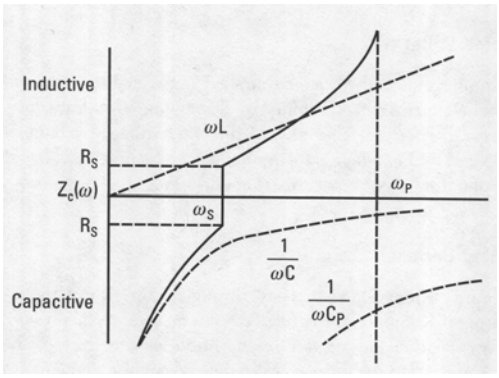

Figure 2.7: Variation of Input Impedance of Ideal Series Inductor, Series Capacitor and Parallel Capacitor and Parallel Plate Capacitor.

Dissipation Factor or Loss Tangent

The dissipation factor (DF) of a capacitor is defined as a ratio of the capacitor´s series resistance to its capacitive reactance, that is,

$$DF = \omega C R_S = \frac{1}{Q} = \tan\delta \tag{2.21}$$

where Q was defined earlier in (2.18). The dissipation factor tells us the approximate percentage of power lost in the capacitor and converted into heat. For example, $DF = tan\delta = 0.01$ means that the capacitor will absorb 1% of total power. To dissipate negligible power, one needs a capacitor with very high Q on the order of 1,000 to 10,000.

Time Constant

In a circuit when an ideal capacitor C is connected in series with an resistor R, and a DC voltage is applied, it takes affinity time τ to charge the capacitor to the applied voltage. This is known as the *time constant* and is given by

$$\tau = RC \tag{2.22}$$

where τ, R and C are expressed in seconds, ohms and farads, respectively.

2.2 Microwave Network Theory

2.2.1 Introduction

In order to characterize microwave systems and subsystems it is important to determine their input-output characteristics. Such a microwave system can be classified as a N-port network, e.g. a two-port, three-port, four-port, and so on. The behavior of a linear microwave network can be described in many different ways [2], like its impedance, admittance or scattering parameters (S-parameters). Because a network is usually constructed to have specified reflection and transmission properties, one can directly express the desired response in terms of a scattering matrix. These quantities can also be easily measured using a vector network analyzer. In this chapter, the S-parameters will be described in more detail.

2.2.2 Actual and Equivalent Voltages and Currents

Unique voltages and currents can be defined (and measured) at various locations in a circuit at low frequencies. Unfortunately, this is not true at microwave frequencies and beyond, where it is not possible to define unique quantities for transmission lines carrying power in Transversal Electro-Magnetic (TEM) mode. Examples of transmission lines supporting the TEM mode of propagation are striplines or microstrip lines. Therefore, one resorts to the concept of equivalent voltages and currents, and this can be applied to both TEM- and non-TEM-mode transmission lines. Relationships involving equivalent voltages or currents lead to unique physical quantities such as reflection and transmission coefficients, normalized input impedance, and the like. Equivalent voltages and currents can be defined on a normalized or unnormalized basis. Because the representative matrix of a network may define a relationship between normalized and unnormalized quantities, it is essential to be mentioned.

Normalized Voltages and Currents

Fig. 2.8 shows a two-port network. The power flows into and out of the network by means of transmission lines connected to the network. Each transmission line may carry a wave propagating toward the network defined as the incident wave or away from the network defined as the reflected wave. Assuming that the power flows in positive z-direction, the z-variation of the incident electromagnetic wave can be described by a simple factor $e^{-j\beta_1 z}$, where β_1 is a unique quantity and denotes the phase constant of the wave in the transmission line of port 1.

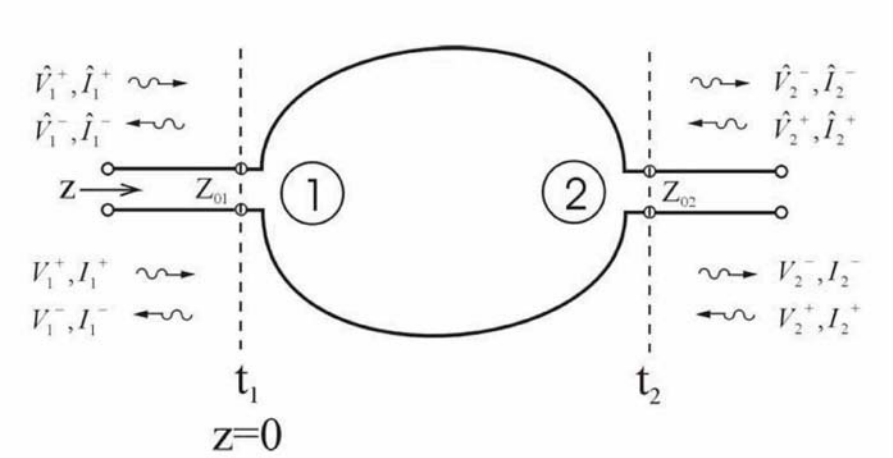

Figure 2.8: Normalized and Unnormalized Voltage and Current Waves on Transmission Lines of a Two-Port Network.

If we assume that the incident voltage and current waves have the same phase as that of the transverse electric and magnetic field components of the incident electromagnetic wave, we can determine the normalized voltage and current waves. If the z-variation of voltage and current waves is also given by the same factor as that for the field components $e^{-j\beta_1 z}$, the normalized incident voltage and current waves in the transmission line of port 1 can be expressed as

$$\hat{V}_1^+(z) = \hat{V}_{10}^+ e^{-j\beta_1 z} = \left|\hat{V}_{10}^+\right| e^{j\Psi_{i1}} e^{-j\beta_1 z} \tag{2.23}$$

and

$$\hat{I}_1^+(z) = \hat{I}_{10}^+ e^{-j\beta_1 z} = \left|\hat{I}_{10}^+\right| e^{j\Psi_{i1}} e^{-j\beta_1 z} \tag{2.24}$$

where Ψ_{i1} denotes the phase of the incident wave at z=0, and $\hat{V}_{10}^+$ and $\hat{I}_{10}^+$ are the complex voltage and current, respectively, at the same terminal plane (z=0). To reemphasize, the value of Ψ_{i1} is the same as that of the transverse components of the electric and magnetic fields of the incident wave. The symbol "^" has been added to denote that the respective quantities are normalized. When the characteristic impedance of the transmission line is real, the voltage and current waves can be expressed in terms of incident and reflected power. At microwave frequencies, the characteristic impedance of practical transmission lines are generally real. To compute the value of $\left|\hat{V}_{10}^+\right|$ and $\left|\hat{I}_{10}^+\right|$, we force the condition that the average power flow is given by

$$\left|\hat{V}_{10}^+\right| \left|\hat{I}_{10}^+\right| = P_1^+ \tag{2.25}$$

where P_1^+denotes the incident power, and $\left|\hat{V}_{10}^+\right|$ and $\left|\hat{I}_{10}^+\right|$ denote the rms quantities.

To determine $\left|\hat{V}_{10}^+\right|$ and $\left|\hat{I}_{10}^+\right|$, we need to have another relation between them. To define normalized quantities, we choose

$$\frac{\left|\hat{V}_{10}^+\right|}{\left|\hat{I}_{10}^+\right|} = 1 \tag{2.26}$$

and hence from (2.25) and (2.26):

$$\left|\hat{V}_{10}^+\right| = \left|\hat{I}_{10}^+\right| = \sqrt{P_1^+} \quad . \tag{2.27}$$

Substituting the values of $\left|\hat{V}_{10}^+\right|$ and $\left|\hat{I}_{10}^+\right|$ from the above equation in (2.23) and (2.24), we obtain

$$\hat{V}_1^+(z) = \hat{I}_1^+(z) = \sqrt{P_1^+} e^{j\Psi_{i1}} e^{-j\beta_1 z} \quad . \tag{2.28}$$

When the incident power reaches the network, a part of it (say, P_1^-) is reflected back. By analogy with incident voltage and current waves, the reflected waves can be expressed as

$$\hat{V}_1^-(z) = \hat{I}_1^-(z) = \sqrt{P_1^-} e^{j\Psi_{i1}} e^{j\beta_1 z} \tag{2.29}$$

where the superscript "-" is used to denote the reflected waves. Ψ_{i1} is the phase of the transversal components of the electric and magnetic fields of the reflected wave at z=0 and is a unique quantity. Because the reflected wave propagates in the negative z-direction, its z-dependence is described by the factor $e^{j\beta_1 z}$.

The total normalized voltage (at any value of z) in the transmission line of port 1 is those given by,

$$\hat{V}_1(z) = \hat{V}_1^+(z) + \hat{V}_1^-(z) = \sqrt{P_1^+} e^{j\Psi_{i1}} e^{-j\beta_1 z} + \sqrt{P_1^-} e^{j\Psi_{i1}} e^{j\beta_1 z} \quad . \tag{2.30}$$

On the other hand, the total current at any value of z is given by

$$\hat{I}_1(z) = \hat{I}_1^+(z) - \hat{I}_1^-(z) = \hat{V}_1^+(z) - \hat{V}_1^-(z) = \sqrt{P_1^+} e^{j\Psi_{i1}} e^{-j\beta_1 z} + \sqrt{P_1^-} e^{j\Psi_{i1}} e^{j\beta_1 z} \quad . \tag{2.31}$$

Because the current flows in the axial direction, the net current is given by the difference of the currents flowing in the positive and negative z-direction. The net power flows into the network across any

z=constant plane in the transmission line of port 1 and is given by $P = Re(\hat{V}_1\hat{I}_1^*)$. Using (2.30) and (2.31) we obtain

$$P = Re(\hat{V}_1\hat{I}_1^*) = P_1^+ - P_1^- \quad . \tag{2.32}$$

Unnormalized Voltages and Currents

If the ratio between the voltage and current of the incident wave (and the reflected wave) is chosen to be different from unity (2.26), the resulting quantities are called unnormalized. For TEM transmission lines, this ratio is generally chosen to be equal to the actual characteristic impedance of the line. In that case, the unnormalized voltages and currents reduce to actual quantities in the line. For non-TEM transmission lines, the characteristic impedance depends on the definition used. Referring to Fig. 2.8, the unnormalized incident voltage and current waves in the transmission line of port 1 can be expressed as

$$V_1^+(z) = \sqrt{Z_{01}P_1^+}e^{j\Psi_{i1}}e^{-j\beta_1 z} \tag{2.33}$$

$$I_1^+(z) = \sqrt{\frac{P_1^+}{Z_{01}}}e^{j\Psi_{i1}}e^{-j\beta_1 z} \tag{2.34}$$

where Z_{01} denotes the characteristic impedance of the transmission line of port 1. In the above equations the symbols "^" has been dropped to denote unnormalized quantities.
The unnormalized reflected voltage and current waves in the transmission line of port 1 can be expressed as

$$V_1^-(z) = \sqrt{Z_{01}P_1^-}e^{j\Psi_{i1}}e^{j\beta_1 z} \tag{2.35}$$

$$I_1^-(z) = \sqrt{\frac{P_1^-}{Z_{01}}}e^{j\Psi_{i1}}e^{j\beta_1 z} \quad . \tag{2.36}$$

Reflection Coefficient, VSWR and Input Impedance

Referring to Fig. 2.9, the voltage reflection coefficient $\Gamma_1(z)$ in the transmission line of port 1 is defined as

$$\Gamma_1(z) = \frac{\hat{V}_1^-(z)}{\hat{V}_1^+(z)} = \frac{V_1^-(z)}{V_1^+(z)} \quad . \tag{2.37}$$

Substituting values of $\hat{V}_1^-(z)$ and $\hat{V}_1^+(z)$ from (2.28) and (2.29) in (2.37), we have

$$\Gamma_1(z) = \frac{\left|V_{10}^-\right|e^{j\Psi_{1r}}e^{+j\beta_1 z}}{\left|V_{10}^+\right|e^{j\Psi_{1i}}e^{-j\beta_1 z}} = \sqrt{\frac{P_1^-}{P_1^+}}e^{j(\Psi_{1r}-\Psi_{1i})}e^{2j\beta_{1z}} \quad . \tag{2.38}$$

We easily conclude from (2.38) that the reflection coefficient is a unique quantity, and the square of its modulus gives the fraction of the incident power that is reflected back. The return loss (in decibels), which is a positive quantity, is given by

$$L_R(dB) = -10\log|\Gamma_1(z)|^2 = -20\log|\Gamma_1(z)| \quad . \tag{2.39}$$

The voltage standing wave ratio ($VSWR$) in the transmission line of port 1 is given by

$$VSWR = \frac{1+|\Gamma_1(z)|}{1-|\Gamma_1(z)|} \tag{2.40}$$

More often, it is the practice to use the ratio of total voltage and current, which can be termed as input impedance. The ratio of total normalized voltage and current is defined as the normalized impedance and is given by

$$\hat{Z}_{in}(z) = \frac{\hat{V}_1(z)}{\hat{I}_1(z)} = \frac{\hat{V}_1^+(z)+\hat{V}_1^-(z)}{\hat{V}_1^+(z)-\hat{V}_1^-(z)} = \frac{1+\Gamma_1(z)}{1-\Gamma_1(z)} \quad . \tag{2.41}$$

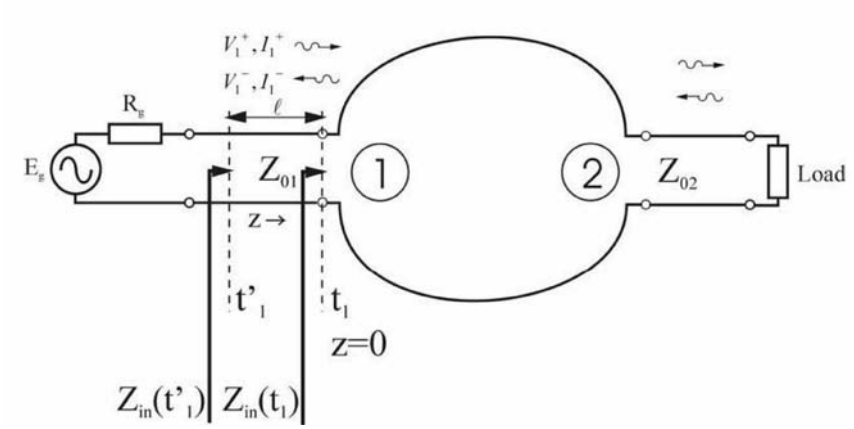

Figure 2.9: A Two-Port Network Connected to a Source and Load

Because $\Gamma_1(z)$ is a unique quantity, the normalized input impedance is also a unique quantity. Similarly, the unnormalized input impedance Z_{in} is given by

$$Z_{in}(z) = Z_{01}\frac{1+\Gamma_1(z)}{1-\Gamma_1(z)} \tag{2.42}$$

where Z_{01} denotes the characteristic impedance of the transmission line connected to port 1. Using (2.41), the reflection coefficient in terms of normalized input impedance is expressed as

$$\Gamma_1(z) = \frac{\hat{Z}_{in}(z)-1}{\hat{Z}_{in}(z)+1} \tag{2.43}$$

and in terms of the unnormalized input impedance:

$$\Gamma_1(z) = \frac{\frac{Z_{in}(z)}{Z_{01}}-1}{\frac{Z_{in}(z)}{Z_{01}}+1} = \frac{Z_{in}(z)-Z_{01}}{Z_{in}(z)+Z_{01}} \quad . \tag{2.44}$$

Transformation of Impedance
With $Z_{in}(t_1)$ as the input impedance at the terminal plane t_1 looking into the network, the input impedance at the terminal plane t_1' (which is closer to the generator compared with terminal plane t_1) is

$$Z_{in}(t_1') = Z_{01}\frac{Z_{in}(t_1)+jZ_{01}\tan(\beta_1 l)}{Z_{01}+jZ_{in}(t_1)\tan(\beta_1 l)} \tag{2.45}$$

where l is the distance between terminal planes t_1 and t_1'. If $Z_{in}(t_1')$ denotes the load impedance Z_L, the input impedance Z_{in} at distance l away (towards the generator) can be expressed as

$$Z_{in} = Z_{01}\frac{Z_L+jZ_{01}\tan(\beta_1 l)}{Z_{01}+jZ_L\tan(\beta_1 l)} \tag{2.46}$$

where $\beta_1 = 2\pi/\lambda_g$ denotes the propagation constant of the line, which is assumed to be lossless.

Quantities Required to Describe the State of a Transmission Line

Consider an N-port network as shown in Fig. 2.10. The ports are numbered from $m = 1$ to $m = N$. The power is carried into and away from the network by means of transmission lines connected to each port. The characteristic impedance of the transmission line of the m_{th} port is denoted by Z_{0m}, because the voltages and currents vary along the length of the transmission line, fictitious terminal planes are located in each transmission line. Voltage or current at port m denotes the respective quantity at the

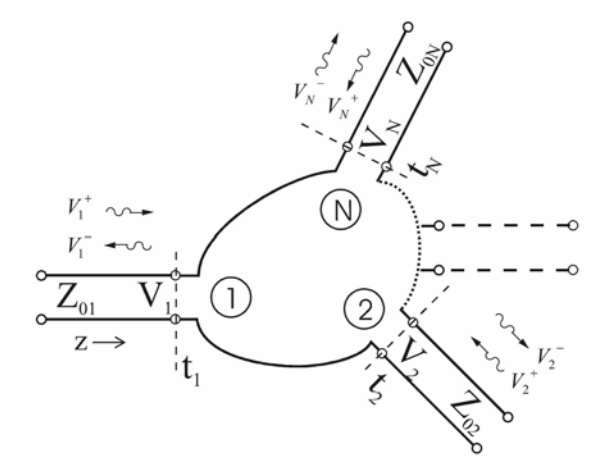

Figure 2.10: An N-Port Network

specified terminal plane in the transmission line of port m. We use the notation of the sections above for normalized and unnormalized quantities and incident and reflected quantities.

Note that $\hat{V}_n^+$ and $\hat{I}_n^+$ (similarly, $\hat{V}_n^-$ and $\hat{I}_n^-$) are not independent quantities. The normalized quantities satisfy following relationships:

$$\frac{\hat{V}_n^+}{\hat{I}_n^+} = \frac{\hat{V}_n^-}{\hat{I}_n^-} = 1 \quad . \tag{2.47}$$

If the two quantities $\hat{V}_n^+$ (or $\hat{I}_n^+$) and $\hat{V}_n^-$ (or $\hat{I}_n^-$) are known, the total voltage and current can be determined using

$$\hat{V}_n = \hat{V}_n^+ + \hat{V}_n^- = \hat{I}_n^+ + \hat{I}_n^- \tag{2.48}$$

and

$$\hat{I}_n = \hat{I}_n^+ - \hat{I}_n^- = \hat{V}_n^+ - \hat{V}_n^- \quad . \tag{2.49}$$

Therefore, if any two of the four quantities $\hat{V}_n$, $\hat{I}_n$, $\hat{V}_n^+$ (or $\hat{I}_n^+$), and $\hat{V}_n^-$ (or $\hat{I}_n^-$) are known, all others can be determined. the same conclusion holds for unnormalized quantities if the characteristic impedance of all transmission lines are known. For unnormalized quantities:

$$\frac{V_n^+}{I_n^+} = \frac{V_n^-}{I_n^-} = Z_{0n} \tag{2.50}$$

$$V_n = V_n^+ + V_n^- = Z_{0n}(I_n^+ + I_n^-) \tag{2.51}$$

and

$$I_n = I_n^+ - I_n^- = \frac{V_n^+ - V_n^-}{Z_{0n}} \tag{2.52}$$

Relationship Between Normalized and Unnormalized Quantities
The normalized and unnormalized quantities are related by

$$\hat{V}_n^\pm = \frac{V_n^\pm}{\sqrt{Z_{0n}}} \tag{2.53}$$

$$\hat{V}_n = \frac{V_n}{\sqrt{Z_{0n}}} \tag{2.54}$$

$$\hat{I}_n^\pm = I_n^\pm \sqrt{Z_{0n}} \tag{2.55}$$

$$\hat{I}_n = I_n \sqrt{Z_{0n}} \quad . \tag{2.56}$$

2.2.3 Scattering Matrix

A very popular method of representing microwave networks is by the scattering matrix. The scattering matrix is generally represented in a normalized form. In this representation, the normalized reflected voltage at each port of the network as shown in Fig. 2.10 is related to the normalized incident voltages at the ports of the network as follows:

$$\begin{array}{ccccccc} \hat{V}_1^- = & \hat{S}_{11}\hat{V}_1^+ + & \hat{S}_{12}\hat{V}_2^+ + & \cdots + & \hat{S}_{1N}\hat{V}_N^+ \\ \hat{V}_2^- = & \hat{S}_{21}\hat{V}_1^+ + & \hat{S}_{22}\hat{V}_2^+ + & \cdots + & \hat{S}_{2N}\hat{V}_N^+ \\ \vdots & \vdots & \vdots & \vdots & \vdots \\ \hat{V}_N^- = & \hat{S}_{N1}\hat{V}_1^+ + & \hat{S}_{N2}\hat{V}_2^+ + & \cdots + & \hat{S}_{NN}\hat{V}_N^+ \end{array} \tag{2.57}$$

In matrix notation, the above set of equations can be expressed as

$$\left[\hat{\mathbf{V}}^-\right] = \left[\hat{\mathbf{S}}\right] \cdot \left[\hat{\mathbf{V}}^+\right] \tag{2.58}$$

where

$$\left[\hat{\mathbf{V}}^-\right] = \begin{bmatrix} \hat{V}_1^- \\ \vdots \\ \hat{V}_N^- \end{bmatrix} \tag{2.59}$$

$$\left[\hat{\mathbf{V}}^+\right] = \begin{bmatrix} \hat{V}_1^+ \\ \vdots \\ \hat{V}_N^+ \end{bmatrix} \tag{2.60}$$

and

$$\left[\hat{\mathbf{S}}\right] = \begin{bmatrix} \hat{S}_{11} & \hat{S}_{12} & \cdots & \hat{S}_{1N} \\ \hat{S}_{21} & \hat{S}_{22} & \cdots & \hat{S}_{2N} \\ \vdots & \vdots & \vdots & \vdots \\ \hat{S}_{N1} & \hat{S}_{N2} & \cdots & \hat{S}_{NN} \end{bmatrix} . \tag{2.61}$$

The scattering parameter $\hat{S}_{mn}$ is therefore given by

$$\hat{S}_{mn} = \frac{\hat{V}_m^-}{\hat{V}_n^+} \Big|_{\hat{V}_p^+ = 0 \ where \ p=1,...,N; p \neq n} . \tag{2.62}$$

In terms of the incident power P_n^+ in the n^{th} transmission line, the amplitude of the normalized incident voltage wave at the n^{th} port is given by

$$\left|\hat{V}_n^+\right| = \sqrt{P_n^+} . \tag{2.63}$$

Similarly, the amplitude of the normalized reflected voltage wave at the m^{th} port is given by

$$\left|\hat{V}_m^-\right| = \sqrt{P_m^-} \tag{2.64}$$

where P_m^- denotes the reflected power at port m.
When the values of $\left|\hat{V}_n^+\right|$ and $\left|\hat{V}_m^-\right|$ from the last two equations are substituted in (2.62), we obtain

$$\left|\hat{S}_{mn}\right| = \frac{\left|\hat{V}_m^-\right|}{\left|\hat{V}_n^+\right|} = \sqrt{\frac{P_m^-}{P_n^+}} . \tag{2.65}$$

From the above equation, we see that $\left|\hat{S}_{mn}\right|^2$ denotes the ratio of power coupled from port n to port m when $\hat{V}_p^+ = 0$, where $p = 1, ..., N; p \neq n$. The last condition is readily ensured by exciting only the n^{th}

port and terminating all the ports in matched loads. Similarly:

$$\left|\hat{S}_{nn}\right|^2 = |\Gamma_n|^2 = \frac{\left|\hat{V}_n^-\right|^2}{\left|\hat{V}_n^+\right|^2} = \frac{P_n^-}{P_n^+} \tag{2.66}$$

where Γ_n denotes the reflection coefficient at port n. Further, $\left|\hat{S}_{nn}\right|^2$ denotes the fraction of the incident power that is reflected back at port n.
The ports of a typical microwave network are usually match-terminated. Therefore, if some power is incident in one of the ports, the reflected power and the power coupled to the other ports of the network can be easy determined if the normalized scattering matrix is known.

2.3 Broadside-Coupled Lines

2.3.1 Broadside-Coupled Striplines

General broadside-coupled microstrip lines are shown in Fig. 2.11. For $\varepsilon_{r1} = \varepsilon_{r2} = \varepsilon_r$, the structure reduces to broadside- coupled striplines. For coupled striplines, the even- and odd-mode effective dielectric constant are the same and given by

$$\varepsilon_{ree} = \varepsilon_{reo} = \varepsilon_r \tag{2.67}$$

The characteristic impedance of the odd-mode can be found using the following expression:

$$Z_{0o}\sqrt{\varepsilon_r} = Z^a_{0\infty} - \Delta Z^a_{0\infty} \tag{2.68}$$

where

$$Z^a_{0\infty} = 60 \ln\left(\frac{3S}{W} + \sqrt{\left(\frac{S}{W}\right)^2 + 1}\right) \tag{2.69}$$

and

$$\begin{aligned} \Delta Z^a_{0\infty} &= \begin{cases} P & \text{for} \frac{W}{S} \leq 1/2 \\ PQ & \text{for} \frac{W}{S} \geq 1/2 \end{cases} \\ P &= 270\left[1 - \tanh\left(0.28 + 1.2\sqrt{\frac{b-S}{S}}\right)\right] \\ Q &= 1 - \tan^{-1}\left[\frac{0.48\sqrt{\frac{2W}{S} - 1}}{\left(1 + \frac{b-S}{S}\right)2}\right] \quad . \end{aligned} \tag{2.70}$$

Further, the even-mode characteristic impedance can be found using

$$Z_{0e} = \frac{60\pi}{\sqrt{\varepsilon_r}} \frac{K(k')}{K(k)} \tag{2.71}$$

where

$$k = \tanh\left(\frac{293.9S/b}{Z_{0e}\sqrt{\varepsilon_r}}\right) \quad . \tag{2.72}$$

It has been reported in [7] that (2.68) and (2.71) offer an accuracy within 1% of spectral domain results.

2.3.2 Broadside-Coupled Suspended Microstrip Lines

The structure shown in Fig. 2.11 reduces to broadside-coupled suspended microstrip lines for $\varepsilon_{r1} = \varepsilon_r \geq 1$, $\varepsilon_{r2} = 1$. The even- and odd-mode characteristic impedances of broadside-coupled suspended microstrip lines are given by

$$Z_{0e} = \frac{Z^a_{0e}}{\sqrt{\varepsilon_{ree}}} \tag{2.73}$$

$$Z_{0o} = \frac{Z^a_{0o}}{\sqrt{\varepsilon_{reo}}} \tag{2.74}$$

where Z^a_{0e} and Z^a_{0o} are the even- and odd-mode characteristic impedances of the corresponding air-filled homogeneous broadside-coupled striplines. Their values can be found using (2.68) and (2.71). Further the even- and odd-mode effective dielectric constants are given by

$$\varepsilon_{reo} = \frac{1}{2}(\varepsilon_r + 1) + q\frac{(\varepsilon_r - 1)}{2} \tag{2.75}$$

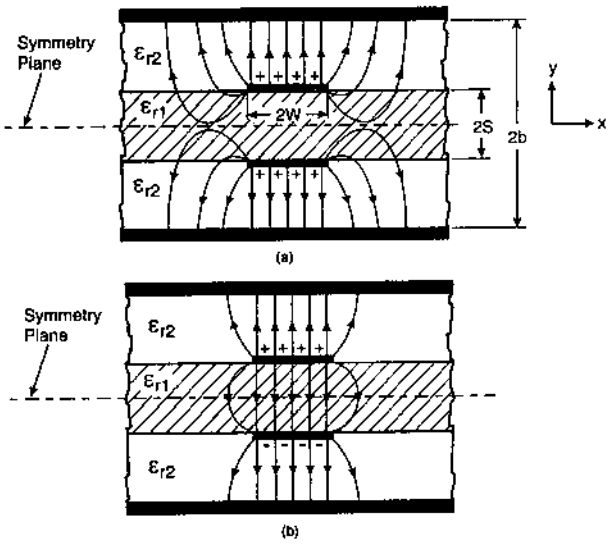

Figure 2.11: (a) Even-Mode, and (b) Odd-Mode Field Distribution of General Broadside Coupled Microstrip Lines.

where

$$\begin{aligned} q &= q_\infty q_c \\ q_\infty &= \left(1+\frac{5S}{W}\right)^{-a(U)b(\varepsilon_r)} \\ a(U) &= 1+\frac{1}{49}\ln\left[\frac{U^4+(U/52)^2}{U^4+0.432}\right]+\frac{1}{18.7}\ln\left[1+\left(\frac{U}{18.1}\right)^3\right] \\ U &= 2W/S \\ b(\varepsilon_r) &= 0.564\left(\frac{\varepsilon_r-0.9}{\varepsilon_r+3}\right)^{0.053} \end{aligned}$$

and

$$\begin{aligned} q_c &= \tanh\left[1.043+0.121\left(\frac{b-S}{S}\right)-1.164\left(\frac{S}{b-S}\right)\right] \\ \varepsilon_{ree} &= \left[1+\frac{S}{b}\left(a_1-b_1\ln\left(\frac{W}{b}\right)\right)\left(\sqrt{\varepsilon_r}-1\right)\right]^2 \end{aligned} \tag{2.76}$$

where

$$\begin{aligned} a_1 &= \left[0.8145-0.05824\ln\left(S/b\right)\right]^8 \\ a_2 &= \left[0.7581-0.07143\ln\left(S/b\right)\right]^8 \quad . \end{aligned}$$

The above equations offer an accuracy of about 1% for $\varepsilon r \leq 16$, $S/b \leq 0.4$, and $W/b \leq 1.2$. These conditions are usually met in practice.

2.3.3 Broadside-Coupled Offset Striplines

Broadside-coupled offset striplines are shown in Fig. 2.12. This structure is more general than the broadside-coupled stripline configuration. Shelton [3] has given closed-form expressions for the analysis and synthesis of broadside-coupled offset lines. Here, we present the synthesis equations only as they are more frequently used. Two sets of equations are given, one for tightly coupled lines and the other for loosely coupled lines. The conditions for tight and loose coupling are defined by

Tight coupling case:

$$\begin{aligned} \frac{w'}{1-s'} &\geq 0.35 \\ \frac{w'_c}{s'} &\geq 0.7 \end{aligned} \tag{2.77}$$

Loose coupling case:

$$\begin{aligned} \frac{w'}{1-s'} &\geq 0.35 \\ \frac{2w'_0}{1+s'} &\geq 0.85 \end{aligned} \tag{2.78}$$

In the above equations, $s' = S/b$, $w' = W/b$, $w'_c = Wc/b$, and $w'_0 = W_0/b$ denote the normalized

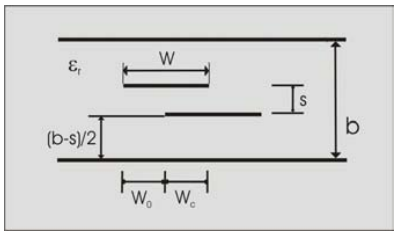

Figure 2.12: Broadside Coupled Off-Set Stripline

values. The coupling between TEM lines can be expressed in terms of even- and odd-mode characteristic impedances. For a TEM coupler that is matched at all its ports:

$$\frac{Z_{0e}}{Z_0} = \frac{Z_0}{Z_{0o}} \tag{2.79}$$

Define ρ as

$$\sqrt{\rho} = \frac{Z_{0e}}{Z_0} = \frac{Z_0}{Z_{0o}} \tag{2.80}$$

we obtain the synthesis equations given below:

Tight coupling case:

$$\begin{aligned}
A &= \exp\left[\frac{60\pi^2}{\sqrt{\varepsilon_r}Z_0}\left(\frac{1-\rho s'}{\sqrt{\rho}}\right)\right] \\
B &= \frac{A-2+\sqrt{A^2-4A}}{2} \\
p &= \frac{(B-1)\left(\frac{1+s'}{2}\right)+\sqrt{(B-1)^2\left(\frac{1+s'}{2}\right)+4s'B}}{2} \\
r &= \frac{s'B}{p} \\
C_{f0} &= \frac{1}{\pi}\left[-\frac{2}{1-s'}\ln s' + \frac{1}{s'}\ln\left(\frac{pr}{(p+s')(1+p)(r-s')(1-r)}\right)\right] \\
C_0 &= \frac{120\pi\sqrt{\rho}}{\sqrt{\varepsilon_r}Z_0} \\
w' &= \frac{s'(1-s')}{2}\left(C_0 - C_{0f}\right) \\
w'_0 &= \frac{1}{2\pi}\left[(1+s')\ln\frac{p}{r} + (1-s')\ln\left(\frac{(1+p)(r-s')}{(s'+p)(1-r)}\right)\right]
\end{aligned} \tag{2.81}$$

Loose coupling case:

$$\begin{aligned}
C_0 &= \frac{120\pi\sqrt{\rho}}{\sqrt{\varepsilon_r}Z_0} \\
\Delta C &= \frac{120\pi}{\sqrt{\varepsilon_r}Z_0}\frac{(\rho-1)}{\sqrt{\rho}} \\
K &= \frac{1}{\exp\left(\frac{\pi\Delta C}{2}\right)-1} \\
a &= \sqrt{\left(\frac{(s'-K)}{(s'+1)}\right)^2+K} - \frac{(s'-K)}{(s'+1)} \\
q &= \frac{K}{a} \\
C_{f0} &= \frac{2}{\pi}\left[\frac{1}{1+s'}\ln\frac{1+a}{a(1-q)} - \frac{1}{1-s'}\ln q\right] \\
w'_c &= \frac{1}{\pi}\left[s'\ln\frac{q}{a} + (1-s')\ln\left(\frac{1-q}{1+a}\right)\right] \\
C_{f(a=\infty)} &= -\frac{2}{\pi}\left[\frac{1}{1+s'}\ln\left(\frac{1-s'}{s}\right) + \frac{1}{1-s'}\ln\left(\frac{1+s'}{s}\right)\right] \\
w' &= \frac{1-s'^2}{4}\left[C_0 - C_{f0} - C_{f(a=\infty)}\right]
\end{aligned} \tag{2.82}$$

2.4 Directional Coupler

After a study of [4] a nonuniform broadband TEM directional coupler was chosen to be best suitable as directional coupler for the design presented in section 3.2. This type of coupler is applicable in a wide frequency range which is its most important property. More details on choosing the directional coupler and the different development steps are stated in subsection 3.2.2. The principal structure of a symmetrical multisection nonuniform directional coupler is shown in Fig. 2.13. It is built of several sections that have different line widths and spacings according to the different odd- and even-mode impedances of each section.
Every section causes a different coupling such that the overall coupling and the directivity should be equal over the whole frequency range. The structure of the coupler is symmetrical with respect to the vertical and horizontal axes that are plotted dashed in Fig. 2.13. For the measurement of the length of the coupler there are two different scales. On the one hand there is the u-axis that measures the length in degrees and is used for the determination of the odd- and even-mode impedances and on the other hand there is the x-axis that measures the length in mm and is used to calculate the physical dimensions of the coupler. As shown by θ all the elements have the same length.

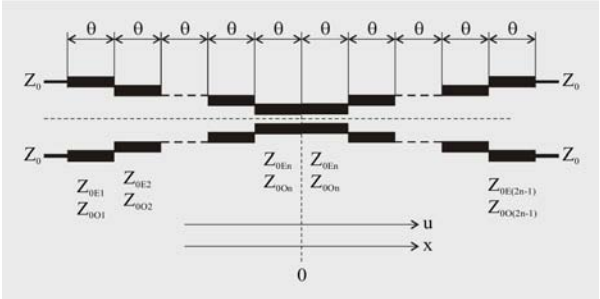

Figure 2.13: Structure of the Directional Coupler

For the determination of the odd- and even-mode impedance of the different sections of the coupler a weighting function is used. This weighting factor is precalculated and listed in tables in [4]. We will come back to use this tables later. The values of the weighting function are symmetrical with respect to the vertical axis of the directional coupler. They are different for different sections. The principal weighting function over the u-axis is shown in Fig. 2.14.

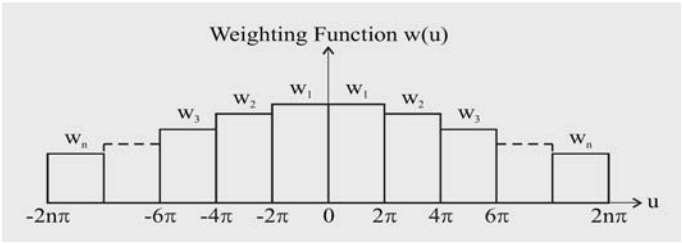

Figure 2.14: Weighting Function for the Directional Coupler

The first step in the development procedure is to define the lower frequency f_L and upper frequency f_U of the application frequency range. Further, the desired coupling C and the ripple factor δ that describes the ripple of the coupling versus frequency have to be defined in dB. With equations (2.83) to (2.85) the voltage-coupling factor R, the center frequency f_0 and the bandwidth ratio B can be determined.

$$R = 10^{-\frac{C}{20}} \tag{2.83}$$

$$f_0 = \frac{f_L + f_U}{2} \tag{2.84}$$

$$B = \frac{f_U}{f_L} \tag{2.85}$$

With this characteristics the values of the normalized impedances Z_{0e} and Z_{0o} can be looked up in appendix B. These impedances are used to determine the weighting factors. In the table the number of used sections N can be found too. Using equation (2.86) the minimum number of sections n can be determined.

$$n = \frac{N+1}{2} \tag{2.86}$$

From the values of the normalized impedance $Z_{0e}(i) = Z_{0ei}$ given in the table the values of the weighting coefficient w_1 to w_n can be determined using equation (2.87). For the value of Z_{0e} the nominal impedance Z_0 of the coupler has to be used.

$$w_i = \frac{\pi}{4R} \ln \frac{Z_{0e}\,(n-i+1)}{Z_{0e}(n-i)} \text{ for } i = 1 \text{ to } n \tag{2.87}$$

Since all values for the calculation of the even-mode impedances of the directional coupler on certain positions are defined now, one can determine them with equation (2.88) where equation (2.89) is already substituted into the last expression.

$$\frac{1}{2} \ln \frac{Z_{0e(u)}}{Z_0} = \frac{R}{\pi} \cdot \int_{-\frac{d}{2}}^{u} w(u) \cdot p(u) \cdot du = -\frac{R}{\pi} \cdot \int_{-\frac{d}{2}}^{u} w(u) \cdot \frac{\sin^2\left(\frac{u}{2}\right)}{\frac{u}{2}} \cdot du \tag{2.88}$$

$$p(u) = \frac{\sin^2\left(\frac{u}{2}\right)}{\frac{u}{2}} \tag{2.89}$$

As the coupler is symmetrical with respect to the vertical and horizontal axis at position 0 only the values for $u < 0$ have to be calculated. The variable $w(u)$ is the weighting value for a certain position u that can be determined according to Fig. 2.14.
The limits of u are given by $-2\pi n \leq u \leq 2\pi n$. For the evaluation of equation (2.88) the value of $\frac{d}{2}$ is set to $2\pi n$. This also shows the relation between the x- and u-axis, which is given in equation (2.90).

$$x = \frac{ud}{4\pi n} \tag{2.90}$$

The overall length d can be calculated from the center frequency by equation (2.91), where ε_r is the relative dielectric constant of the used substrate.

$$d = \frac{n\pi}{\beta_0} = \frac{nc_0}{2f_0\sqrt{\varepsilon_r}} \tag{2.91}$$

With the calculations above, the even-mode impedance at a certain position on every section of the coupler can be derived. Using equation (2.79) the odd-mode impedance can be calculated. Further, with equations (2.81) and (2.82) the physical dimensions of the directional coupler can be determined.

Chapter 3

Hardware Design

Generally, a bias-T is built by a high pass filter in the RF path and by a low pass filter in the DC path. Therefore, it is started in section 3.1 with the classic design based on lumped elements. But with high and low pass filters of higher order, problems occured because of the resonance frequencies of the coils. Therefore, in section 3.2, an alternative design based on 3 dB 90° hybrids without coils was forced.

3.1 Design with Lumped Elements

3.1.1 Simulations with Ideal Components

The design of the bias-T fulfilling the specifications was started by a conventional design with lumped elements, which are a low pass filter in the DC-path and a high pass filter in the RF-path. All simulations were done with Microwave Office®, starting with ideal transmission lines and ideal lumped elements. In general, a large bandwidth of the bias-T can turn into a problem. But with a low and a high pass filter of fourth order, the S-parameters of the bias-T fulfill the requirements, as shown in Fig. 3.1.

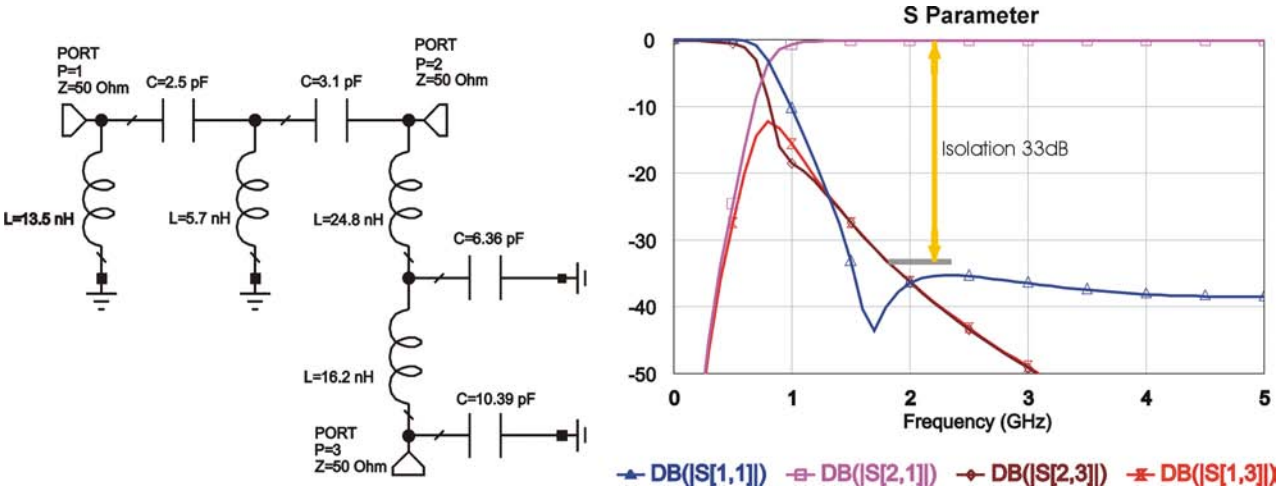

Figure 3.1: Ideal Bias-T

3.1.2 Choosing a Substrate

The substrate "Taconic RF-35-0300-C1/C1" was chosen for the design of the bias-T. "RF-35" is an organic-ceramic laminate in the ORCER family of Taconic products. It is based on woven glass reinforcement. The dielectric constant parameter is 3.5 and the dissipation factor is 0.0018 at 1.9 GHz.
"RF-35" marks the dielectric constant parameter, for the thickness of 0.76 mm (0.030") which is "0300" in the product code and "C1/C1" indicates the copper thickness of 35 μm of both sides of the laminate. For detailed information see Appendix F. The width of the microstrip line for 50 Ω-characteristic impedance is 1.73 mm at 6 GHz and there is no damage of the microstrip line up to a DC current of 10 Ampere. The resistance of the line is 1.077 $\mu\Omega/mm$.
A TRL calibration kit and test prints, in order to measure and characterize lumped elements, were designed for this laminate. While the prints were manufactured, ideal components were exchanged with real components in Microwave Office®.
First, 50 Ω microstrip transmission line models were set between the ideal lumped elements and also microstrip models for steps, junctions and gaps have been added. The influence of these real line segments can be seen in Fig 3.2. There are several resonances in the desired frequency range and also with the optimization tool of Microwave Office®, it was not possible to eliminate completely these points of resonance, as it is shown in Fig. 3.3.

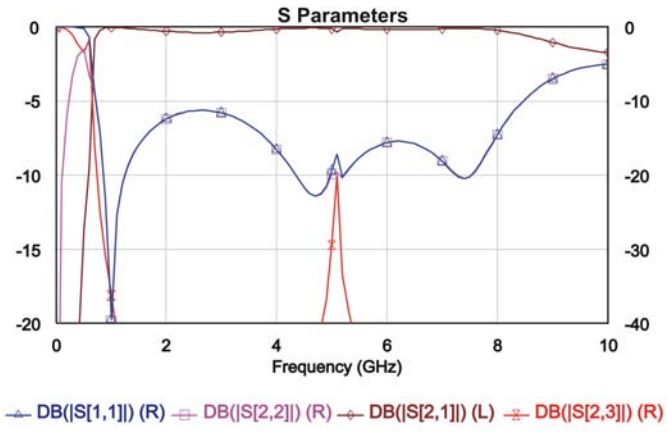

Figure 3.2: Simulation Results: Real Microstrip Lines with Ideal Lumped Elements

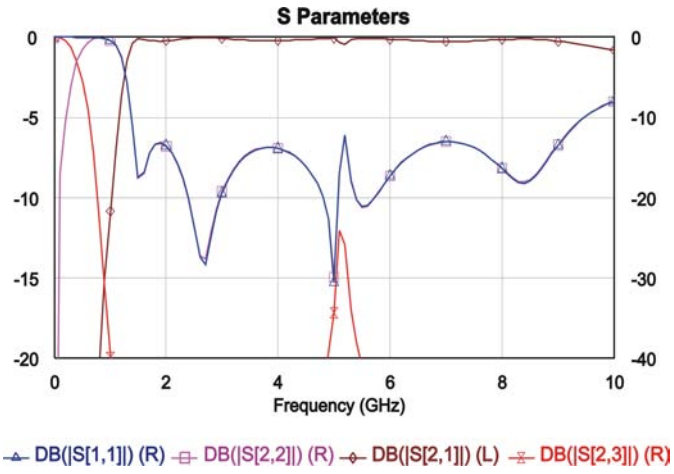

Figure 3.3: Simulation Results: Ideal Lumped Elements Optimized

3.1.3 Simulation with Real Components

In Fig. 3.4, we can see the simulation results of the S-parameters of the bias-T designed in microstrip technology with the Taconic substrate and real components. These are capacitors of the ATC 500 series from American Technical Ceramics and inductors of the 603CS series from Coilcraft. The S-parameters of the inductors are defined in the frequency range from 50 MHz to 6 GHz only and so, only within this bandwidth, the S-parameters of Fig. 3.4 are shown. We can clearly see resonances at 2.85 GHz and 4.95 GHz. Additionally, the insertion loss in the important frequency range, is more than 0.6 dB. But this value is required not to exceed the limit of 0.5 dB at its worst case scenario.
The next problem is that the inductors from coilcraft are built for a current up to 2.4 A only and will be destroyed by a current up to 8 A. There are no inductors from other companies available for these currents, too.

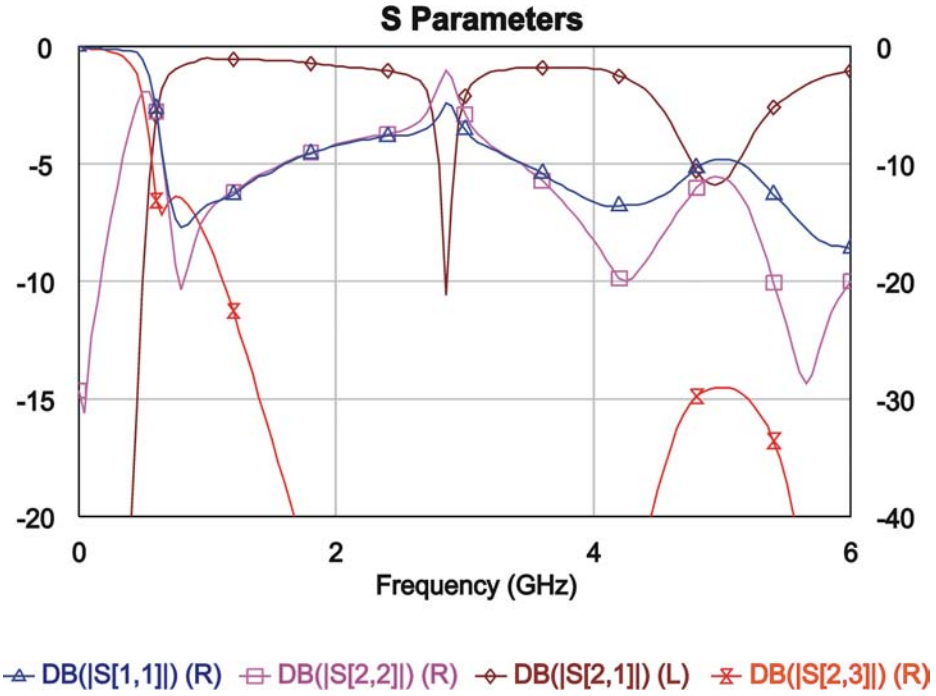

Figure 3.4: Simulation Results: Real Components

3.1.4 Results of the Simulations

As we have already seen, fundamental problems with the design of the bias-T with the required specifications have occurred. The inductivities with their resonance frequencies are causing major problems. It is possible to move the resonance frequencies, but it is not possible to eliminate them completely from the required frequency range. Furthermore, a high inductivity value with a high current capability is needed but it is not possible to buy this as a lumped component. So, it would be necessary to design a new inductor to solve this problem.
These problems are the reason why we thought of the possibility of finding another way to solve the problem with the bias-T, best without lumped elements. Fortunately, an alternative solution was found, as it is presented in the next subchapters.

3.2 Realization with Quadrature Hybrids

3.2.1 General Aspects

A 3 dB hybrid coupler, as shown in Fig. 3.5, which is also called a quadrature coupler, is a four-port device that is used either to split an input signal with a resultant 90° phase shift between output signals equally or to combine two signals with 90° phase shift while maintaining high isolation between them. Additionally, two ports are always connected straightly in a directional design coupler. Here, in a cross over design, port 1 is connected with port 4 and port 2 with port 3.

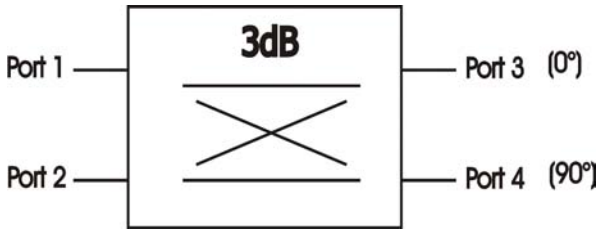

Figure 3.5: Quadrature Hybrid

Most of the 3 dB quadrature hybrids are designed as branche-line couplers, as shown in Fig. 3.6 (a), there, all four ports are physically connected by transmission lines. It would be no problem for the RF to use branch-line couplers for a bias-T, but for DC there would be no separation between the ports and consequently no separation between the RF-source, the DC-source and the DUT. Therefore, it is necessary to use the design of directional couplers, as shown in Fig. 3.6 (b), because there are only two ports connected by transmission lines in one branch for DC and consequently there is no physical connection between RF- and DC-source, as it will be demonstrated next.

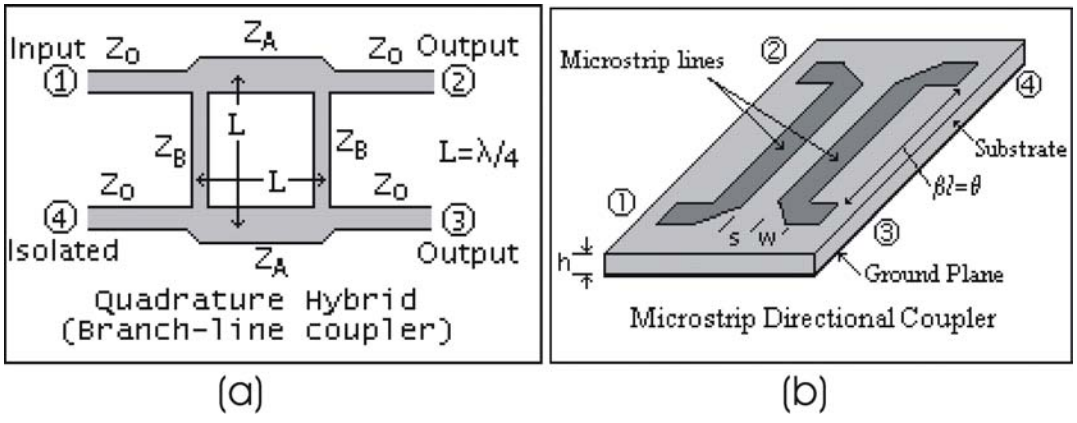

Figure 3.6: Branch-Line and Directional Coupler

The idea was to connect two of these hybrids, as it is shown in Fig. 3.7, so that the splitted RF power is combined again at the RF+DC port. But what is the advantage of this? The big advantage of this, as shown in Fig. 3.8, is the pathlayout of the connected ports. There is the RF path, which is terminated on the right side with an impedance of 50 Ω, because the whole RF power will be coupled to the other path, the DC path. As a result of this, there are three ports left, the RF port, the DC port and the port with RF plus DC. Theoretically, there are no losses but practically there is the insertion loss of the two hybrids. Between the coupled paths and in the DC path the ohmic resistance of the conductor will cause a voltage drop and self-heating at high current. But this will be less than by inductors. Furthermore, the pulse, frequency range 100 Hz to 200 MHz, and the RF operation bandwidth of the hybrids are in a different frequency range, so that there should be no distortion of the pulse.
It was decided to force this design for the construction of a bias-T for pulsed applications.

Figure 3.7: Combination of 2 Hybrids

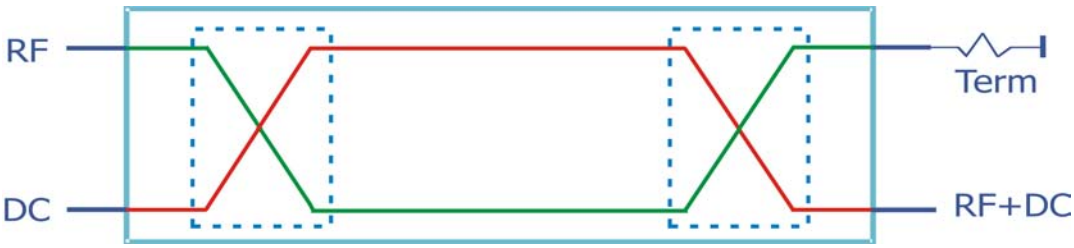

Figure 3.8: Bias-T with Hybrids

3.2.2 Design of the 3 dB Hybrid

For the design of the bias-T the aim was to design a 3 dB Hybrid for the given bandwidth of 6.2 GHz. The question, which basic principle is to use, arose: edge coupled striplines or broadside coupled striplines, shown in Fig. 3.9. Because of the tight coupling of 3 dB, the broadside coupled stripline design was chosen. This was verified in simulation with Microwave Office®.

Figure 3.9: Edge & Broadside Coupled Striplines

Material

For the core substrate, it was decided to use the CuFlon from Polyflon with the following specifications:

Thickness		0.1 mm
ε_r		2.1
tan δ		0.00045
Copper		17,5 μm

So, the coupled lines can be positioned exactly because they are placed on the upper and lower side of the substrate. The only impreciseness comes from the manifacturing of the prints and those are less.
For the boundary surface, Polyguide from Polyflon was chosen.

Thickness		3.175 mm
ε_r		2.32
tan δ		0.0002
Copper		35.6 μm

These substrates, see also Appendix F, were used in previous projects for similar applications and it was found out that the low dielectric constant makes the implementation less sensitive to production inaccuracies.

Implementation

The implementation of the hybrid is based on the theory of coupled lines and development procedures for directional couplers, that was explained in section 2.11.

Characterization

First of all, the main characteristics of the directional coupler had to be established. Since the application frequency range of the bias-T should be from 1.8 GHz to 8 GHz and should allow an appropriate offset the frequency range of the directional coupler was defined to be from $f_L = 1$ GHz to $f_U = 10$ GHz. Using equations (2.84) and (2.85), the center frequency and the bandwidth ratio were calculated to be $f_0 = 5.5$ GHz and $B = 10$. The coupling C of the hybrid should be 3 dB and from this, the value of $R = 0.708$ was evaluated. The ripple factor δ should be as low as possible. Using these design parameters, I looked up the value of the normalized even-mode impedances in table 6.1 of [4] which is added in Appendix B. The part of the table that is important for my 3 dB hybrid is shown in the next subsection, where the whole development process is described.

Simulation

The normalized even-mode impedances for a coupling of 3 dB for different ripple factors and bandwidth ratios are shown in Tab. 3.1. Additionally, it can be found in the table that $N = 9$ sections have to be used for the directional coupler. The whole table is shown in Appendix B.

$\boldsymbol{\delta}$	Z_{0e1}	Z_{0e2}	Z_{0e3}	Z_{0e4}	Z_{0e5}	B
0.05	1.02680	1.09163	1.24706	1.66958	4.93133	7.365
0.10	1.04112	1.12024	1.29488	1.74863	5.18240	9.030
0.15	1.05391	1.14328	1.33137	1.80742	5.36886	10.356
0.20	1.06598	1.16366	1.36260	1.85696	5.52654	11.528
0.25	1.07763	1.18248	1.39075	1.90116	5.66814	12.615

Table 3.1: Normalized Even-Mode Impedances for 3 dB Coupling

Using equation (2.86) the minimum number of elements can be calculated to be $n = 5$. Using this parameter, the constraints for u were determined as in equation (3.1) which results in a length of $20 \cdot \pi$.

$$-10 \cdot \pi \leq u \leq 10 \cdot \pi \tag{3.1}$$

The weighting factors were calculated from the used even-mode impedances (2.87). Since the bandwidth ratio is 10, the values for $\delta = 0.15$ and $B = 10.356$ were used. These values were chosen, because this gives the lowest ripple within the required bandwidth. With this choice, the required properties should be met. The resulting weighting factors and the according u-range are given in Tab. 3.2.

u-Range	$w_i\,(u)$
$-2\pi \leq u \leq 0$	1.2092
$-4\pi \leq u \leq -2\pi$	1.0186
$-6\pi \leq u \leq -4\pi$	0.9458
$-8\pi \leq u \leq -6\pi$	0.6323
$-10\pi \leq u \leq -8\pi$	0.5248

Table 3.2: Weighting Factors

The evaluation of the integral (2.88) is shown in equation (3.2). According to the weighting factors, the constraints of the ranges were chosen. In equation (3.2) the value for u is calculated to be -π. After a simple transformation, the value for $Z_{oe|u=-\pi}$ was determined using equation (2.79).

For my implementation, I chose 80 elements over the whole length of the directional coupler. So, the odd- and even-mode impedances had to be calculated on 41 different positions, since the direction coupler is symmetrical to its vertical axis.

$$\begin{aligned}\frac{1}{2} \cdot \ln \frac{Z_{0e|u=-\pi}}{Z_0} &= -\frac{R}{\pi} \cdot \left[w_5 \cdot \int_{-10\pi}^{-8\pi} \frac{\sin^2(\frac{u}{2})}{\frac{u}{2}} \cdot du + w_4 \cdot \int_{-8\pi}^{-6\pi} \frac{\sin^2(\frac{u}{2})}{\frac{u}{2}} \cdot du \right] + \\ &+ -\frac{R}{\pi} \cdot \left[w_3 \cdot \int_{-6\pi}^{-4\pi} \frac{\sin^2(\frac{u}{2})}{\frac{u}{2}} \cdot du + w_2 \cdot \int_{-4\pi}^{-2\pi} \frac{\sin^2(\frac{u}{2})}{\frac{u}{2}} \cdot du + w_1 \cdot \int_{-2\pi}^{-\pi} \frac{\sin^2(\frac{u}{2})}{\frac{u}{2}} \cdot du \right]\end{aligned} \tag{3.2}$$

The experience from another project [5] has shown that the number of 80 elements is a good trade off between exact results and economic implementation.

Broadside-Coupled Offset Striplines

Broadside-coupled offset striplines are shown in Fig. 3.10. Shelton [3] has given closed-form expressions for the analysis and synthesis of broadside-coupled offset lines. Here, we present the synthesis equations as they are more frequently used Two sets of equations are given, one for tightly coupled lines and the other one for loosely coupled lines. The conditions for tight and loose coupling are defined by

Tight coupling case:

$$\begin{aligned} \frac{w'}{1-s'} &\geq 0.35 \\ \frac{w'_c}{s'} &\geq 0.7 \end{aligned} \tag{3.3}$$

Loose coupling case:

$$\begin{aligned} \frac{w'}{1-s'} &\geq 0.35 \\ \frac{2w'_0}{1+s'} &\geq 0.85 \end{aligned} \tag{3.4}$$

In the above equations, $s' = S/b$, $w' = W/b$, $w'_c = W_c/b$, $w'_0 = W_0/b$ denote the normalized values

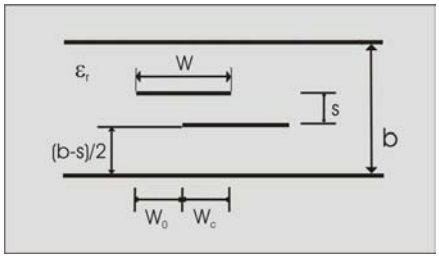

Figure 3.10: Broadside Coupled Off-Set Stripline

With the MatLab® program developed in [5] which has been modified for broadside coupled off-set stripline, see also Appendix A, the following parameters were calculated and are summed up in Tab. 3.3: Angular position U; absolute position x; Z_{even} *and* Z_{odd}; the line dimensions W, W_0 for the case of tight coupling and W, W_C for the case of loose coupling and the limits for the validity of loose and tight coupling.

U	x/mm	Z_{0e}/Ω	Z_{0o}/Ω	W_{tight}/mm	W_{0tight}/mm
-31.415	-45.575	50.00	50.00	6.822	7.107
-30.630	-44.435	50.03	49.97	6.817	7.102
-29.845	-43.296	50.22	49.77	6.786	7.068
-29.059	-42.156	50.66	49.34	6.716	7.994
⋮	⋮	⋮	⋮	⋮	⋮
⋮	⋮	⋮	⋮	⋮	⋮
-6.283	-9.115	90.88	27.50	3.211	3.164
-5.497	-7.975	91.57	27.30	3.179	3.127
-4.712	-6.836	96.59	25.88	2.957	2.872
-3.927	-5.696	110.81	22.56	2.445	2.266
-3.141	-4.557	139.67	17.89	1.749	1.389
-2.356	-3.418	187.87	13.30	1.114	0.450
-1.570	-2.278	235.02	9.88	0.715	complex
-0.785	-1.139	315.69	7.91	0.551	complex
0	0	342.60	7.29	0.5176	complex

W_{loose}	W_{Cloose}	$tight \geq 0.35$	$tight \geq 0.7$	$loose \geq 0.35$	$loose \geq 0.85$
void	void	1.07	**-2.84**	void	void
5.542	-12.340	1.07	**-2.84**	0.87	5.46
5.541	-8.223	1.06	**-2.82**	0.87	4.20
5.539	-6.008	1.05	**-2.77**	0.87	3.52
⋮	⋮	⋮	⋮	⋮	⋮
⋮	⋮	⋮	⋮	⋮	⋮
3.210	0.042	0.50	**0.46**	0.50	0.96
3.178	0.049	0.50	**0.51**	0.50	0.95
2.957	0.082	0.46	**0.85**	0.46	0.87
2.445	0.174	0.38	1.78	0.38	**0.69**
1.749	0.348	**0.27**	3.60	**0.27**	**0.42**
1.114	0.623	**0.17**	6.64	**0.17**	**0.14**
0.715	0.980	**0.11**	**complex**	**0.11**	**-0.08**
void	void	**0.08**	**complex**	**void**	**complex**
void	void	**0.08**	**complex**	**void**	**complex**

Table 3.3: Physical Parameters

It is not necessary to show all 40 elements of the coupler in Tab.3.3 to explain the basic problem. The whole table is shown in Appendix C. In Tab. 3.3, the parameters, where the theory of tight and loose coupled off-set striplines are not valid, are marked bold. This is the case where coupling should be strongest. The physical length of the directional coupler is $d = 91.2\ mm$, calculated with equation (3.5), so that the minimum length of the bias-T would be more than 183 mm.

$$d = \frac{n\pi}{\beta_0} = \frac{nc_0}{2f_0\sqrt{\varepsilon_r}} \tag{3.5}$$

There is a risk of damaging the whole bias-T, if the width W of coupled lines would be too narrow for the maximum flowing current. For a solution of these problems, this structure of 80 elements was simulated and optimized in Microwave Office®.

Simulations with Microwave Office®

In Microwave Office®, models of broad side coupled offset striplines, see Fig. 3.11, were used to build the directional coupler with 80 elements.
There are two possibilities to determine the physical dimensions of the elements. Firstly, by the theory

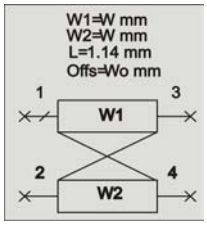

Figure 3.11: MWO Model for Broadside Offset Coupled Lines

of broadside coupled offset striplines. But the elements in the middle of the directional coupler had invalid values because of the limited validity of the theory. So, I tried to find the optimum dimensions of these elements with the optimization tool from Microwave Office® resulting in physically impossible dimensions. Secondly, it is also possible with Microwave Office® to optimize the physical parameters of broadside coupled offset striplines with the values of Z_{0even} and Z_{0odd} which are known from section 6.3 for each element. For this method the results were unphysical as well. Simulation results for both methods can be seen in Fig. 3.12. The structure of the coupled elements, used for simulation in Microwave Office®, is shown in Fig. 3.13.

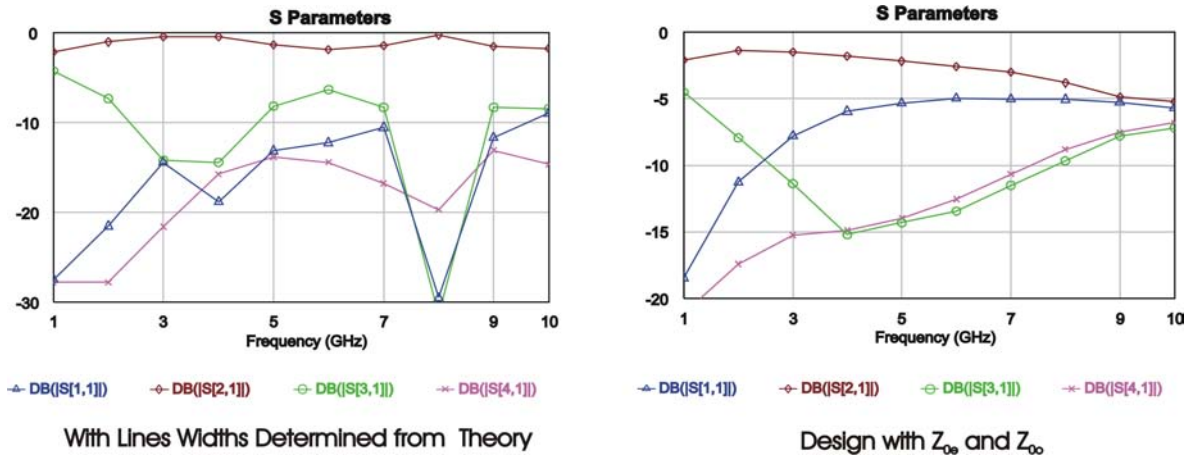

Figure 3.12: Simulation Results for both Design Methods

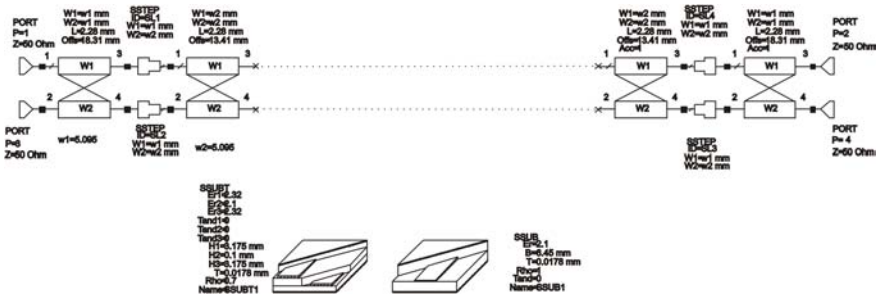

Figure 3.13: Structure of the Coupled Elements in MWO

So, the next step was to optimize these results with Microwave Office®. There were a lot of runs with modified optimization goals. One run took about one week until I could see if the results got better. In Fig. 3.14, one of the best results of these optimizations is shown.

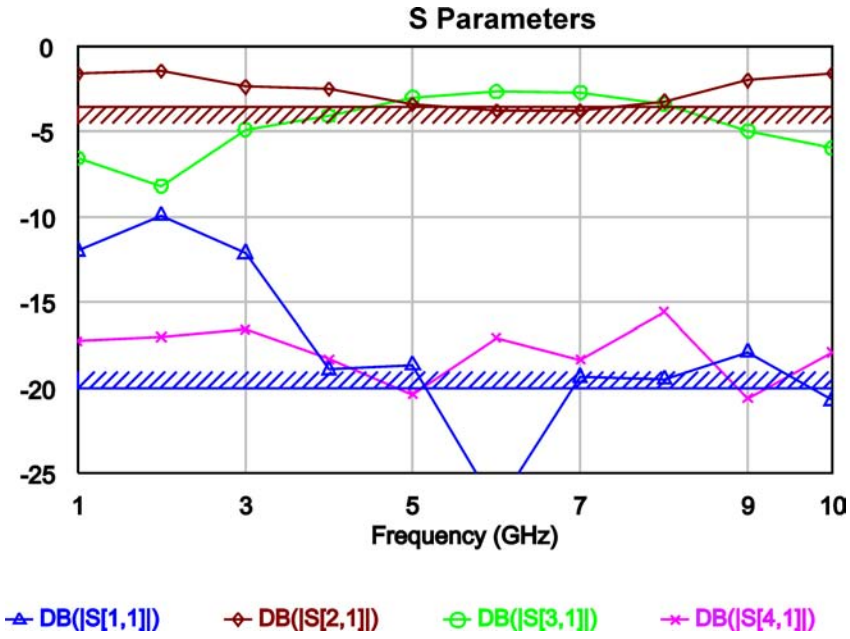

Figure 3.14: Optimized Coupler

Then, I also tried to optimize the direction coupler starting with one frequency point for 3 dB coupling. I enlarged the frequency range step by step up to the desired bandwidth. But there was no chance to get the 3 dB coupling over the whole bandwidth.
The next idea was to leave the concept of symmetrical broadside coupled lines, so that Microwave Office® could optimize with different values of W1 and W2 from Fig. 3.11. Because of this, the number of parameters to optimize was doubled and so the time for the optimization also increased. The results of these optimizations were better, if only the S-parameters of the coupler are noticed. But having a look at the physical dimensions of the lines and the offsets, it became clear that these results are not usable, because of the big differences of the width and the offset of the adjacent elements. So, partly, there is no possibility of physical connection between these elements.

3.2.3 Internet Investigation of the Commercially Available 3-dB Hybrids

Because of the nonsatisfying results of the development of an own 3 dB hybrid and the large unfavorable dimensions of one directional coupler, I started an investigation on 3 dB directional couplers in the internet. I found some models from the following companies: Krytar, Merrimac, Sage-Filtronic, ETI.

Krytar:	**frequency range**	**isolation**	**insertion loss**	**average power**	**price**
Mod. 3020080	2.0 to 8.0 GHz	$>$ 19 dB	$<$ 0.65 dB	20 W	538 €
Mod. 1230	1.0 to 12.4 GHz	>20 dB	<1.4 dB	20 W	980 €

Merrimac:					
Mod. QHD-3C-10G	2.0 to 18.0 GHz	15 dB	2 dB	30 W	280€

ETI:					
Mod. HY 112-90	1.0 to 5.0 GHz	>20 dB	1.2 dB	20 W	750 $
Mod. HY-059-90	0.5 to 9.0 GHz	>20 dB	1.2 dB	20 W	995 $

Sage-Filtronic:					
Mod. 2375-3	2.0 to 8.0 GHz	20 dB	0.4 dB	50 W	592 €

Theoretically, it would be possible to build the bias-T with all of them. Disadvantages are either the high costs or the minimum number of items to order. All of them should be tested to find the one with the best RF properties and the maximum DC current. It would be too expensive to loose one of them at these tests. Besides, they are all built in cases with large dimensions with coaxial connectors like SMA. Comprising, I can say that there are only a few of 3 dB directional couplers with the required bandwidth to find on the commercial market and those are expensive. So, I started to search for cost efficient directional couplers with reduced bandwidth and I found some at Anaren, which will be presented in the next subsection.

3.2.4 Design of the Bias-T with Anaren Xinger®

On the homepage of Anaren I found 3 dB Hybrids which have small physical dimensions and have a surface mount package design which is easy to use. The price is also acceptable, but it was clear that it is not possible to cover the whole required bandwidth with one coupler. Therefore, firstly, I had to choose those which have the best characteristics for my thesis. For each coupler, there is a file of the S-parameters available on the hompage of Anaren. So, with Microwave Office®, it was possible for me to make a choice and so, I decided for the Models 11306-3 and 1M803. For detailed information see Appendix E.

Anaren Xinger® Model 11306-3

The specifications of this model are:

Frequency Range:	2.0 - 4.0 GHz
Isolation	$>$ 20 dB
Insertion Loss	$<$0.35 dB
Power (Ave. CW)	60 W
Θ_{JC}	24.6 $°C/W$
Operating Temp.	-55 to +85 $°C$

Table 3.4: Electrical Specifications of Model 11306-3

With the S-parameters provided from Anaren a bias-T built with two of these hybrid couplers has theoretically the following characteristics.

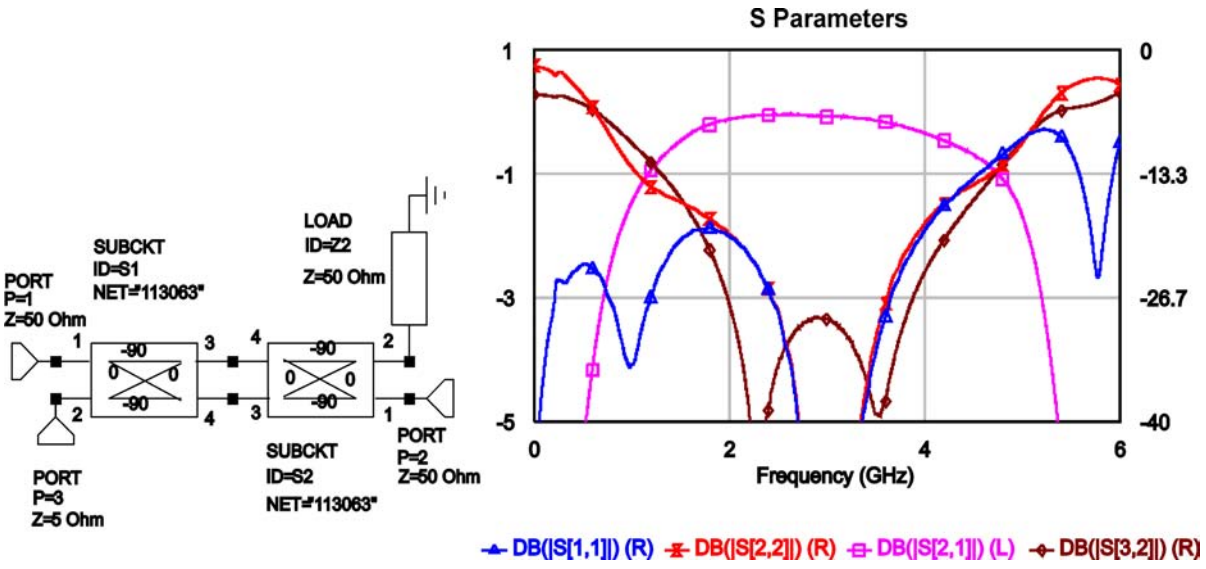

Figure 3.15: Theoretical S Parameters with Anaren 11306-3

In Fig. 3.15 it is possible to see, that a bias-T with an insertion loss of 0.5 dB and a return loss of better than 15 dB at port 1 and port 2 would have a frequency range from 1.48 GHz to 4.2 GHz. The idea was to build one bias-T with a frequency range from 1.8 GHz to 2.5 GHz with a return loss at port 2 up to 7.5 GHz better than 10 dB. Because at large signal excitation transistors produce harmonics and these harmonics should be terminated by the bias-T. A second one for the whole possible bandwidth with no additional matching of S_{22}.

Anaren Xinger® Model 1M803

The specifications of this model are:

Frequency Range:	5.0 - 6.0 GHz
Isolation	> 20 dB
Insertion Loss	<0.25 dB
Power (Ave. CW)	20 W
Θ_{JC}	78.1 $°C/W$
Operating Temp.	-55 to +85 $°C$

Table 3.5: Electrical Specifications of Model 1M803

With the S-parameters provided from Anaren a bias-T built with two of these hybrid couplers has theoretically the following characteristics.

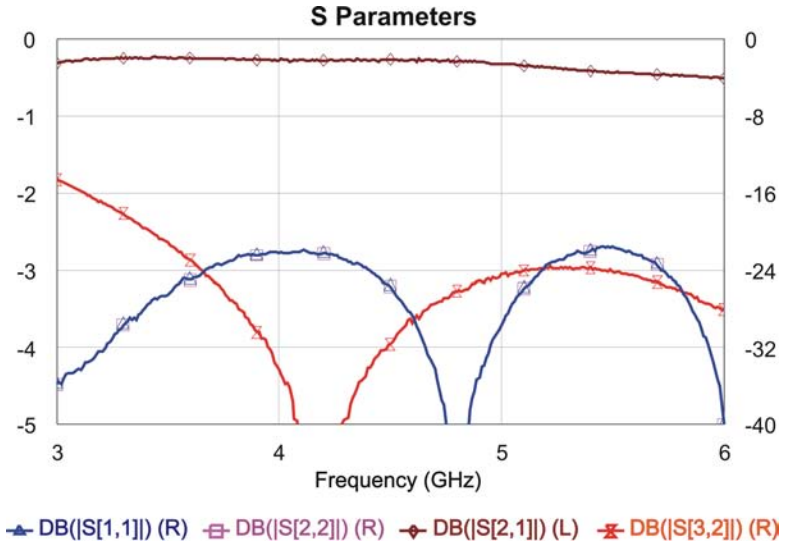

Figure 3.16: Theoretical S Paramters with Anaren 1M803

The S-parameters of the Model 1M803 are only specified from 3 GHz to 6 GHz and, therefore, the insertion loss S_{12}, in Fig. 3.16, becomes positive and invalid outside this frequency range. Within this bandwidth, the insertion loss and the matching of S_{11} and S_{22} are very good.

The next step was to define the DC current characteristics of these two Hybrids and their RF characteristics over the whole bandwidth of 10 GHz.

Tests of the Hybrid Couplers

Firstly, I tested how much current can flow through the couplers without destroying them. Therefore, I measured the case temperature of the coupler at slowly increasing DC current level up to a maximum case temperature of 85° C The maximum current depends directly from the used heatsink and the heat transmission from the coupler to the cooling element.
With the substrate Taconic RF-35-0300-C1/C1, see appendix F, small test prints for both couplers, see Fig 3.17. were designed to get more realistic S-parameters for bias-T over the whole bandwidth and to test which cooling method is the best.

Figure 3.17: Testprints for Mod. 11306-3 and 1M803

In Fig. 3.17 the packages of the couplers are marked with green color. For the proper function of the couplers it is necessary that there is a good connection to the ground of the package. Therefore, there has to be a high number of vias underneath the couplers. At these test prints, they were made by drill holes and hand soldered thin wires before the coupler got soldered onto the prints.

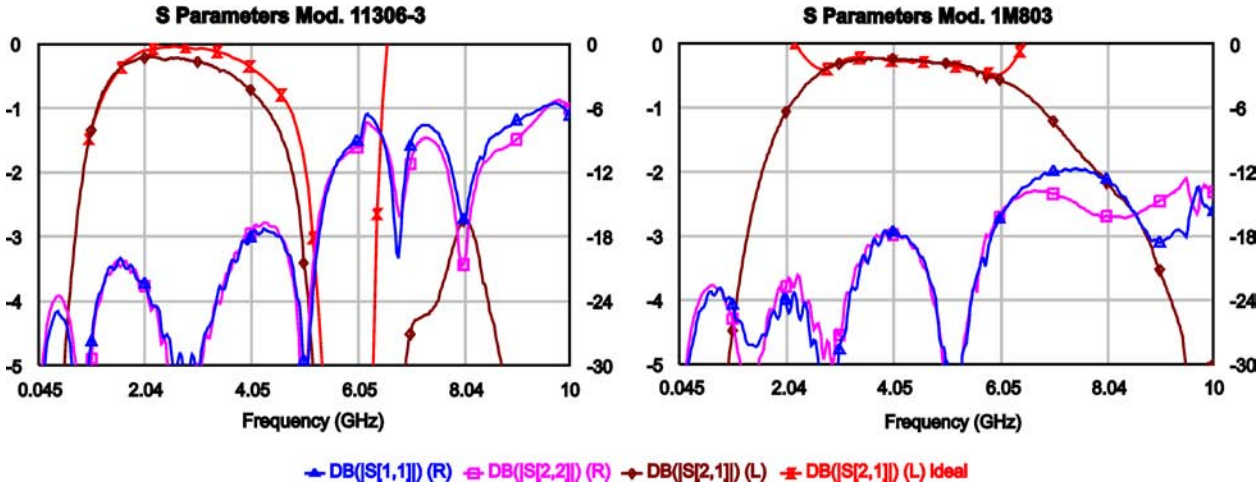

Figure 3.18: S-Parameters of the Test Prints

In Fig. 3.18, the S-parameters of the bias-Ts mounted on the Taconic substrate is shown. The red marked graph shows the insertion loss, given by the specification of the couplers in an ideal environment.
The bias-T for the lower frequency range has an insertion loss of 0.5 dB from 1.43 GHz to 3.7 GHz, the return loss of S_{11} and S_{22} is always better than 16 dB within this bandwidth.
The bias-T for the higher frequency range, has an insertion loss of 0.5 dB from 2.6 GHz to 5.7 GHz, the return loss of S_{11} and S_{22} is always better than 17 dB within this bandwidth.
The testprints were connected via SMA female connectors and during this measurement, the DC-port

and the Termination-port were terminated with 50 Ω. If the DC-port is terminated with a short circuit to simulate a power supply, the insertion losses do not change and the S_{11} and S_{22} parameters only get worse outside the bandwidth of good coupling.
I futher observed that it is only possible to place a cooling element under the coupler on the ground plane of the prints, because a cooling element directly placed on the couplers detesiosates the S-parameter performance of the couplers. For the test prints, a heatsink was adapted with the dimensions 58 mm x 20 mm x 50 mm, see Fig. 3.19.

Figure 3.19: Heatsink of the Test Prints

The temperature at a current of 8 Ampere was 73.7 $°C$ at the package of the couplers of Mod. 11306-3 and 72.7 $°C$ at the heatsink. At the bias-T with the two couplers of the Mod. 1M803, the temperature of the couplers was 51 $°C$ and the temperature of the heatsink was 41 $°C$. The difference of the temperature between the case of the coupler Mod. 1M803 and the heatsink is 10 $°C$. The reason therefore is, that the case of the coupler 1M803 has smaller dimensions than the package of the Mod. 11306-3 and so, the thermal resistance is higher because of the lower area for heat conduction.
At these measurements, I also identified the ohmic resistance of the coupler, which are as follows:

Model	**Resistance**
11306-3	27 $m\Omega$
1M803	13 $m\Omega$

Table 3.6: Ohmic Resitance

The difference of the electrical resistance of the coupler is the reason why Mod. 11306-1 had a higher temperature at the same current as Mod. 1M803.
Next, I tested if the couplers distort the DC-pulse from the pulser, but there was no distortion to observe.
Last, I checked if the couplers would physically bear a current of 8 Ampere. They did, the small lines inside the coupler were not destroyed like a fuse, but they needed a larger heatsink to eliminate the thermal dissipation loss.
Now, it was clear that these couplers fulfill all demands for the bias-T, so that the final design was able to get started.

Final design of the Bias-Ts

The first question was, how many different bias-Ts would be necessary to build? I decided as follows:

- One to combine the pulse with DC.
- One for the fundamental frequency range from 1.8 to 2.5 GHz with a return loss for the harmonics up to 3_{rd} order (3.6 to 7.5 GHz) at the RF+DC port of $\geq$ 10 dB.
- One for the lower frequency range, aprox. 2 to 4 GHz, with a bandwidth as large as possible.
- One for the upper frequency range, aprox. 4 to 6 GHz, with a bandwidth as large as possible.

The second question was, which case should be taken for the bias-Ts to have a compact design as well as enough space to place the heatsink. I chose cases from Telemeter Electronic GmbH company, the series SG for the bias-T for pulse and DC and the series PGS for the others. The bottom of the case was exchanged with the heatsink, which was aligned to the dimension of the cases. The ground plane of the prints had to have a direct and absolutely plane contact to the heatsink for a low thermal resistance.
So, thirdly, I had to choose another substrate for the bias-Ts where it was possible for Printex company to make vias automatically. There was no big choice and I took the Rogers R04003C. Please, also check appendix F.

ε_r	3.38
$tan\delta$	0.0021
thickness	508 μm
copper cladding	34 μm
W of 50 Ω line	1.18 mm

Table 3.7: Rogers R4003C

Implementation of the Bias-T with Harmonic Matching
With Microwave Office®, a circuit which not only allows to eliminate the harmonics but also to measure them was designed, see Fig. 3.2.4. But the attention does not lay on a reduced insertion loss from the RF+DC port and the harmonics port, but rather on a good matching of the RF+DC port within the frequency range of the harmonics.

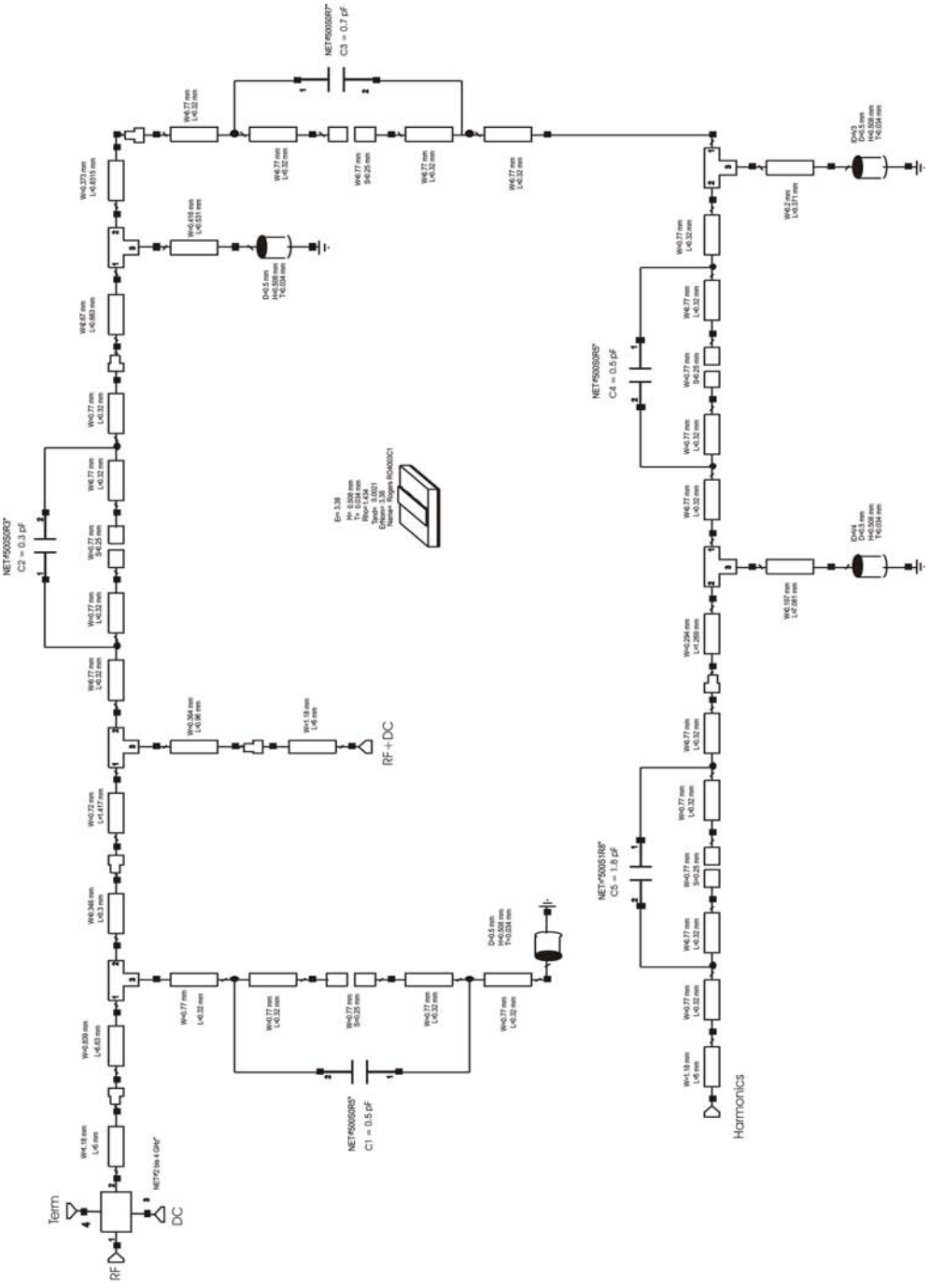

Schematic of Bias-T with Harmonic Matching

In the schematic depicted in Fig. 3.2.4 the capacitors are from ATC and the required inductivities are designed as lines. The simulated S-parameters are shown in Fig. 3.20, where S_{11} belongs to the RF port, S_{22} to the RF+DC port and S_{33} to the port of the harmonics.

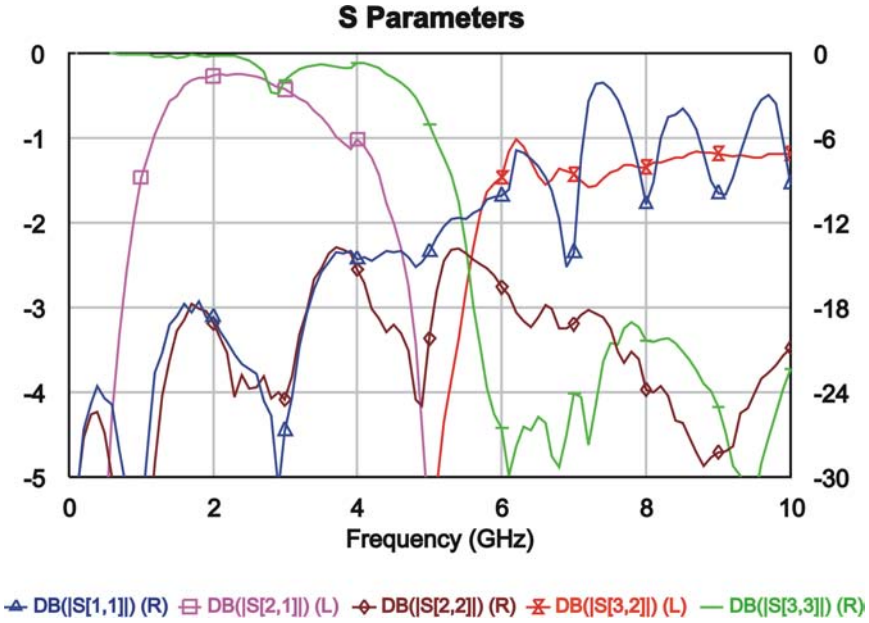

Figure 3.20: Simulated S Parameters of Bias-T with Harmonic Matching

In the simulation, the bandwidth of the insertion loss of 0.5 dB ranges from 1.5 GHz up to 3.1 GHz and within this bandwidth, the return loss of S_{11} and S_{22} is better than 18 dB. Outside this bandwidth, the return loss of S_{22} is also better than 13 dB.

So, a layout for this circuit and the bias-Ts with the couplers Mod.11306-3 and Mod.1M803, as shown in Fig. 3.21, were designed and then produced by Printex company.

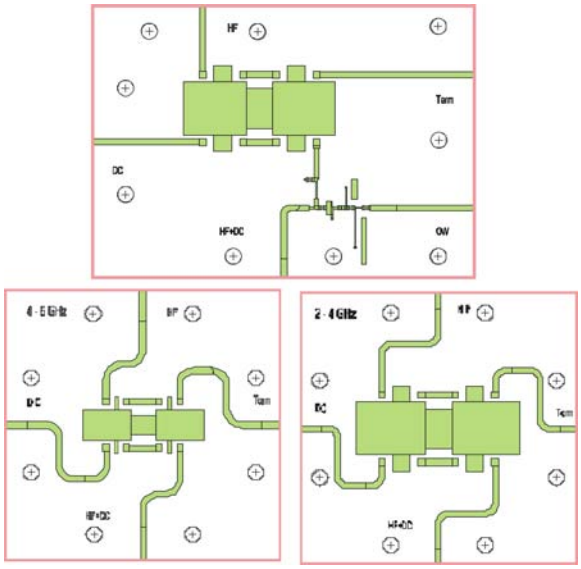

Figure 3.21: Layout of the Bias-Ts

For the bias-T with harmonic matching, the case PGS60-80-22-TR was chosen. Therefore, the dimensions of the print are 72 x 52 mm and for the other two bias-Ts the case PGS60-60-22-TR was chosen and so the prints are 52 x 52 mm, as shown in Fig. 3.22.

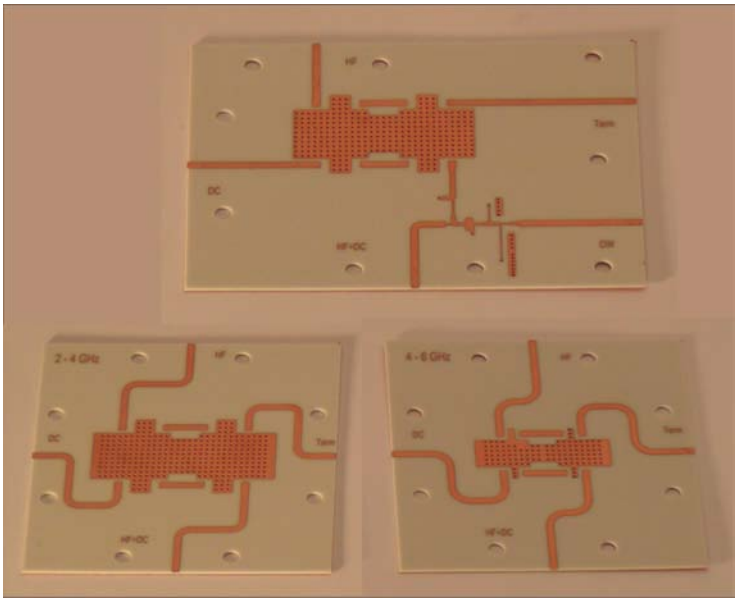

Figure 3.22: The Prints of the Bias-Ts

Implementation of the Bias-T to combine Pulse and DC
The bandwidth of the pulse is 200 MHz and so it is necessary to build a bias-T for low frequency. This is only possible with lumped elements, as shown in Fig 3.23. The most important thing at this bias-T is, that the pulse will not be distorted. With field-tests without a case, I found that with a capacitor of 300 μF and an inductor of 100 mH the droop of a pulse with a pulsewidth of 100 μs is about 2.5 %. The inductivity of 100 mH is built by two inductivities of 50 mH and both of them are made with a ring ferrite with the dimensions of $\oslash$ = 50 mm and h = 20 mm and A_l = 8700. The inductivity of the coil is $L = A_l * N^2$ where N is the number of windings, at this case $N = 76$.
One coil has an ohmic resistance of 115 $m\Omega$, so, the complete resistance is 230 $m\Omega$. That is quite a lot and the potential drop became a nasty problem at higher current. Most of the measurements with the pulser will be done with smaller pulse and so, I also built an inductivity with only one coil with a thicker wire of 1.5 mm^2 instead of 1 mm^2, with only $N = 48$ number of windings and an inductivity of 20 mH. The exact performance is shown in subsection 4.4.

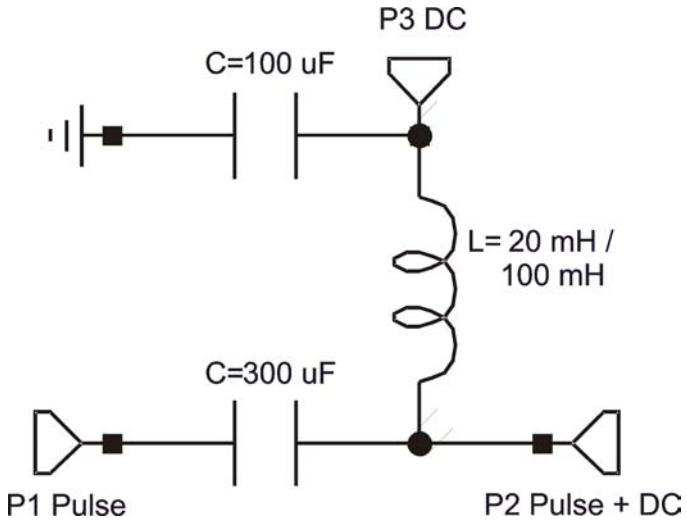

Figure 3.23: Schematic of Bias-T to Combine Pulse and DC

Chapter 4

Measurements

This chapter gives an overview of the final design of the bias-Ts, where modifications were necessary, the resulting and their final electrical parameters.

4.1 Bias-T with Harmonic Matching

4.1.1 S-Parameters

The final main bias-T, as shown in Fig. 4.1, should have a fundamental frequency range from 1.8 GHz to 2.5 GHz with an insertion loss of 0.5 dB and a return loss S_{22} at the RF+DC port for the harmonics up to the 3^{rd} order in the frequency range of 3.6 GHz up to 7.5 GHz of 10 dB.
This bias-T has five ports:

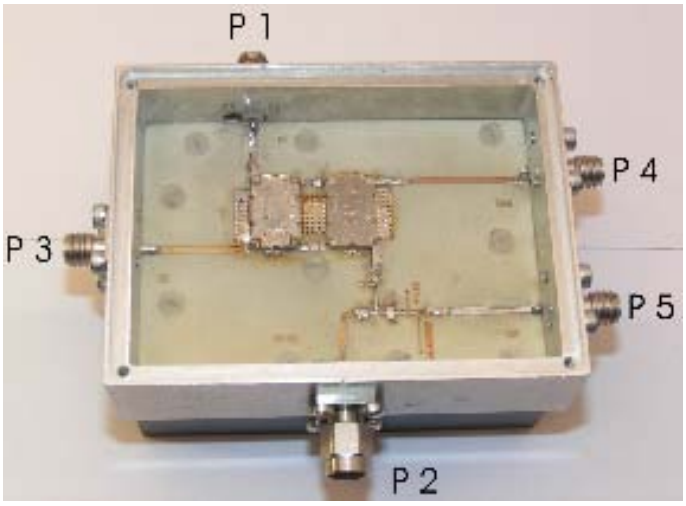

Figure 4.1: Final Bias-T with Harmonic Matching

Port 1	RF
Port 2	RF+DC
Port 3	DC
Port 4	Termination
Port 5	Harmonics

The first measurement results of the most important S-parameters are shown in Fig. 4.2. It can be seen, that the insertion loss S_{12} is $\leq$ 0.5 dB and also the return losses S_{11} and S_{22} are better than 15 dB in

the frequency range from 1.8 GHz to 2.5 GHz. But the return loss S_{22} within the frequency range from 5 GHz to 5.5 GHz has a less good performance and is lower than 10 dB. At this measurement, all ports, except port 3, were terminated with 50 Ω, port 3 was terminated with a short circuit to simulate the low resistance of a DC-voltage supply and the case was open.
In order to get a better performance of the return loss, modifications of the circuit were necessary.

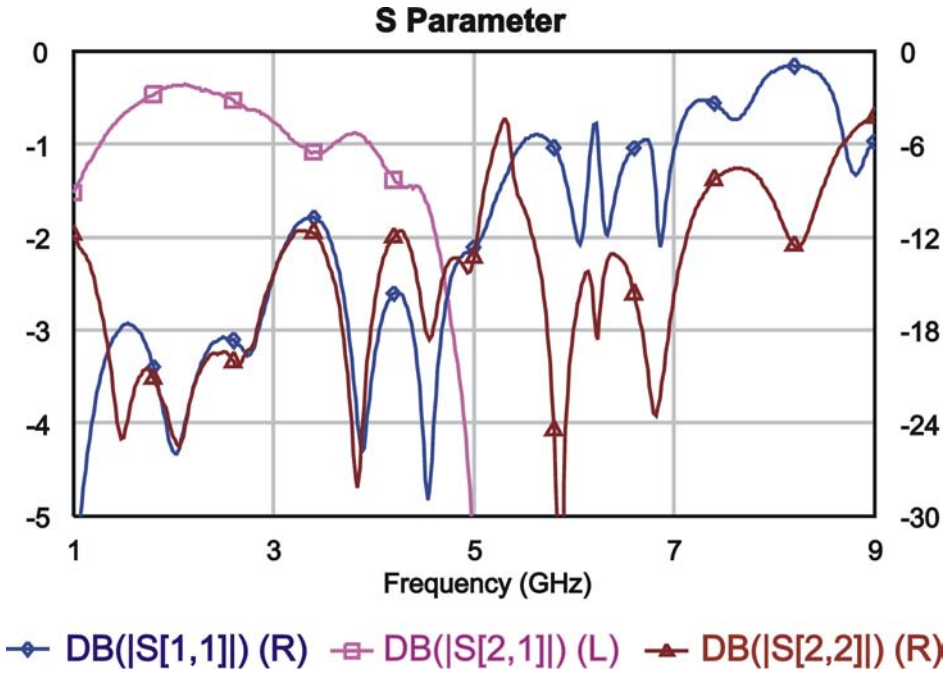

Figure 4.2: 1^{st} Measured S-Parameters

There were different possibilities to optimize S_{22}. Firstly, by the values of the capacitors and inductivitors. By the capacitors in order to exchange them with capacitors of different value of capacity and by the inductivitors by altering the length of the lines. Secondly, by trimming the width of the transmission lines to vary the impedance of the transmission lines. This can be done by cutting to make them thinner and soldering thin copper foil on the transmission lines to make them wider.
The same effect as simulated was observed for changes. Reducing the peak of S_{22} at 5.3 GHz below -10 dB, in most of the cases, it also reduces the frequency range of S_{12} and the insertion loss of S_{21} increases. I tried to find a compromise with the aim to increase the return loss S_{22} of 10 dB and hold the insertion loss of S_{21} as low as possible.

The best trade-off was found by leaving the inductivitors unchanged. Only the 0.5 pF capacitor $C1$ to ground in Fig. 3.2.4 was replaced by a capacitor of 0.7 pF. Most of the modifications of the S-parameters were done by trimming the transmission lines.
A full five port measurement of the S-parameters was done where all ports were terminated with 50 Ω and the top of the case was open. To have a clear overview of the S-parameters, the most important ones like S_{11}, S_{22}, S_{21} and S_{52} are shown in Fig. 4.3.

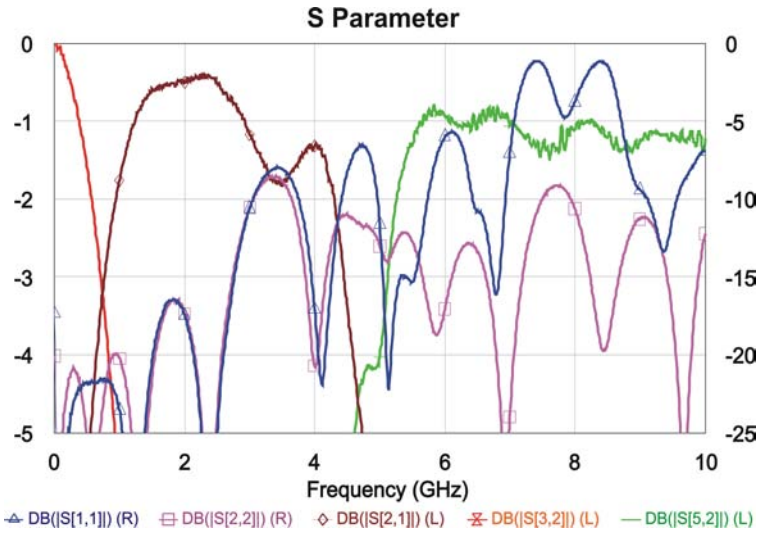

Figure 4.3: Modified Bias-T with Open Case

The insertion loss between 1.8 GHz and 2.5 GHz is now $\leq$ 0.516 dB, which is a little bit worse than in the original configuration. The return loss of port 1 and port 2 within this frequency range is still better than 15 dB. The return loss of port 2 in the frequency range of the harmonics up to 3^{rd} order, which ranges from 3.6 GHz to 7.5 GHz, is now better than 10 dB.
There is only a low ripple in the frequency range between 7.5 GHz and 7.9 GHz, where the insertion loss is worse than 10 dB and where the peak value is 9.13 dB. In the frequency range from 7.9 GHz up to 10 GHz the return loss is again better than 10 dB. Consequently, there is also a good return loss up to the harmonics of 5^{th} order for RF frequencies between 1.8 GHz and 2 GHz.
The insertion loss S_{32} between port 2 and port 3 for pulse and DC is better than 3.5 dB within the frequency range from 0 to 200 MHz.
The insertion loss S_{52} of the harmonics of 3^{rd} and 5^{th} order from port 2 (RF+DC) to port 5 (Harmonics) is better than 1.5 dB.
In Fig. 4.4 the insertion losses S_{41} and S_{42} are shown. This is the part of the RF power from port 1 and port 2 that has to be absorbed by the termination at port 4. Because of the fact that the power loss in the termination is directly proportional to the RF power levels at port 1 and port 2, the termination was not realized on the substrate as a SMD 50 Ω resistor to allow high power termination at the SMA connector and to characterize isolation by S-parameter measurement.

The minimum of the insertion loss of port 4 is at 6.5 GHz with 1.8 dB, but this is fairly out of the specified frequency range of port 1. Within this specified frequency range from 1.8 GHz to 2.5 GHz, the insertion loss S_{41} is $\geq$ 18.5 dB and the insertion loss S_{42} is $\geq$ 28 dB. The minimum insertion loss S_{42} is 13 dB at 4 GHz.

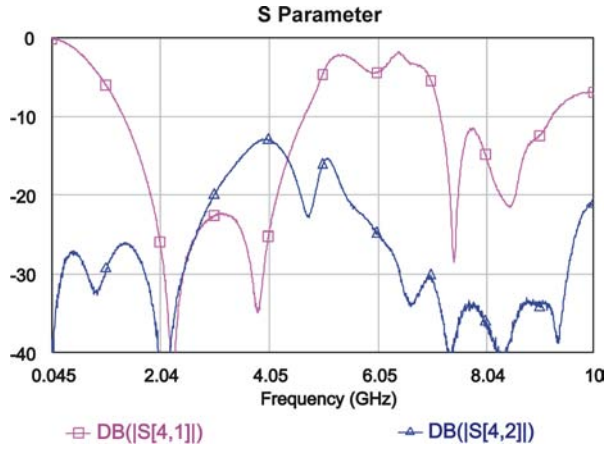

Figure 4.4: Power Loss at Port 4

Next, the bias-T was measured with closed case. The result of this is shown in Fig. 4.5 where it can be seen that there are resonance frequencies at:
3.5 GHz, 4.97 GHz, 6.05 GHz, 7 GHz, 8.61 GHz, 9.3 GHz and 9.5 GHz

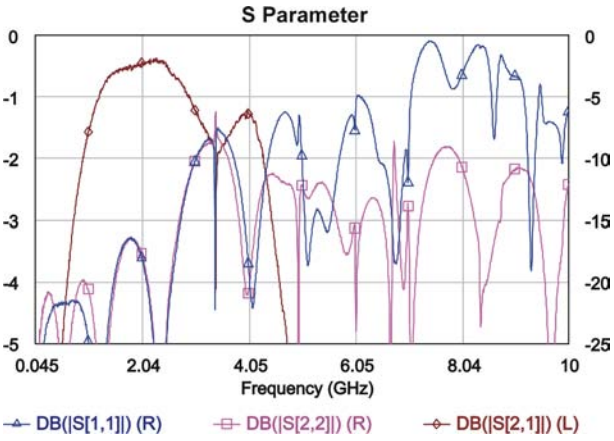

Figure 4.5: Closed Case

This resonance frequencies can be illustrated by the theory of the cavity [6]. The resonance frequencies are given by

$$f_{res,mnp} = \frac{c_0}{2} \cdot \sqrt{\left(\frac{m}{x_1}\right)^2 + \left(\frac{n}{y_1}\right)^2 + \left(\frac{p}{z_1}\right)^2} \tag{4.1}$$

where c_0 is the speed of the light, x_1 is the inner width, y_1 the inner height and z_1 the inner length of the case. For this case the following numbers are valid:

x_1	52 mm
y_1	12 mm
z_1	72 mm

For TE_{mnp} mode oscillations m or n can be 0 but p must not be 0.

TE_{101}	3.55 GHz
TE_{102}	5.06 GHz
TE_{201}	6.12 GHz
TE_{202}	7.10 GHz
TE_{301}	8.89 GHz
TE_{302}	9.59 GHz
TE_{303}	10.66 GHz

Table 4.1: Resonance Frequencies

To eliminate the resonance frequencies, an electromagnetic absorber was placed on the inner side of the cap, as shown in Fig. 4.7. Two different absorber materials were tested, both from the ARC Technologies company:

- Magnetic Absorber UD-11554 with a thickness of 4.4 mm and a frequency range from 2 to 6 GHz (Fig. 4.6 a)
- Dielectric Absorber LS-10055 with a thickness of 3.1 mm and a frequency range from 4 to 26 GHz (Fig. 4.6 b)

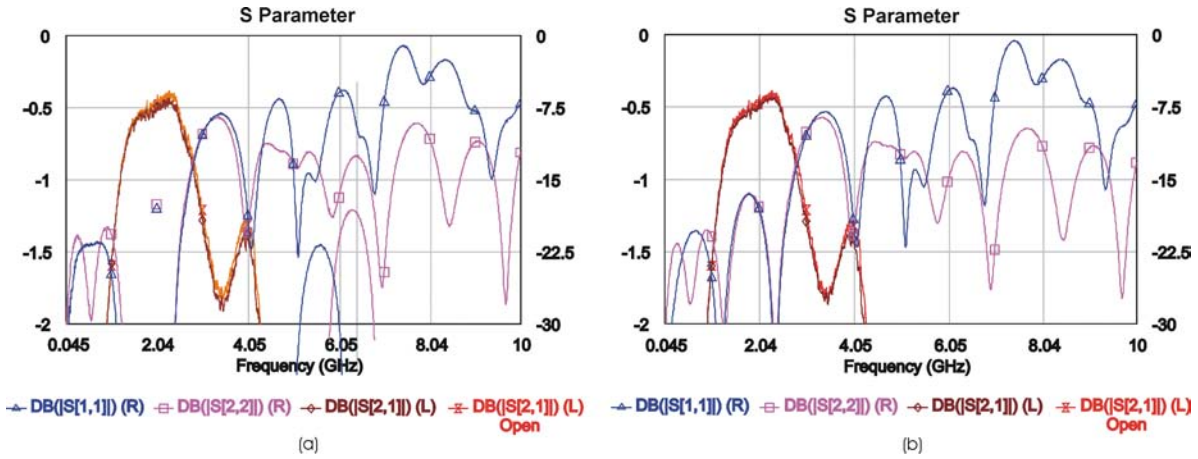

Figure 4.6: Closed Case with Magnetic Absorber (a), Dielectric Absorber (b)

Both absorber materials eliminate the resonance frequencies, but they also absorb RF energy and as a result of this, the insertion loss becomes worse. With the dielectric absorber LS-10055, this effect was not so strong as with the magnetic absorber. Finally, the dielectric absorber LS-10055 was chosen, as shown in Fig. 4.7.

Figure 4.7: Cap with Dielectric Absorber

Finally, the S-parameters of the bias-T with closed case and a short circuit at port 3 (DC) to simulate the effect of a power supply, were measured. The results are shown in Fig. 4.8.

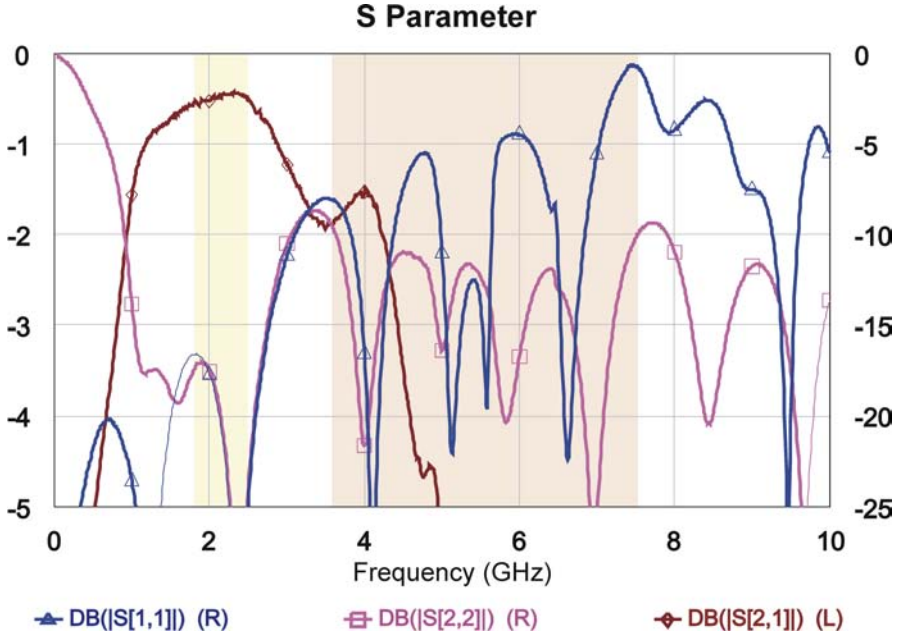

Figure 4.8: Final Bias-T for Harmonics

Concluding, the final specifications of this bias-T are summed up in table 4.2.

Insertion Loss S_{21}	$\leq$ 0.53 dB
Return Loss S_{11} & S_{22}	$\geq$ 17 dB
Return Loss S_{22} harm.	$\geq$ 10 dB
Additional Parameters:	
Isolation S_{21} to S_{23}	$\geq$ 20 dB
$S_{33} \leq$ 2GHz	$\leq$ -20 dB
$S_{44} \leq$ 200 MHz	$\leq$ -20 dB
$S_{55} \geq$ 5.1 GHz	$\leq$ -9 dB
S_{23} 0 - 200 MHz	$\leq$ 3.5 dB
$S_{52} \geq$ 5.4 GHz	$\geq$ 1.5 dB

Table 4.2: Table of S-Parameter

Beside a negligible degradation in insertion loss (0.53 dB instead of required 0.5 dB), this bias-T satisfies all required specifications for pulsed application and high current levels.

4.1.2 Thermal Tests with RF Power and DC Current

RF Power

Next, the bias-T was tested with an RF signal of 1.96 GHz up to a power of 70 W. At this frequency, the bias-T has an insertion loss of 0.53 dB. The power was measured at the input and at the output of the bias-T and the temperature was measured at the cases of the couplers and at the heatsink of the bias-T. The ambient temperature during the measurement was 22 °C.

P_{in} [dB]	P_{out} [dB]	P_{Δ} [dB]	P_{in} [w]	P_{out} [W]	P_{Δ} [W]	T_{coup} [°C]	T_{case} [°C]	ΔT [°C]
30.25	29.71	0.54	1.06	0.94	0.12	25.4	25.2	0.2
33.52	33.00	0.52	2.25	2.00	0.25	25.9	25.5	0.4
36.90	36.38	0.52	4.90	4.35	0.55	26.6	25.8	0.8
40.07	39.53	0.54	10.16	8.97	1.19	28.4	26.8	1.6
42.87	42.34	0.53	19.36	17.14	2.22	31.7	28.6	3.1
45.40	44.89	0.51	34.67	30.83	3.84	41.3	35.7	5.6
46.21	45.70	0.51	41.78	37.15	4.63	45.0	38.0	7.0
46.94	46.42	0.52	49.43	43.8	5.58	49.2	41.3	7.9
47.61	47.07	0.54	57.68	50.93	6.74	53.6	44.0	9.6
48.17	47.63	0.54	65.61	57.94	7.67	57.3	46.7	10.6
48.41	47.87	0.54	69.34	61.24	8.11	59.2	47.6	11.6
48.45	47.90	0.55	69.98	61.44	8.32	59.8	48	11.8

Table 4.3: RF Power Measurement

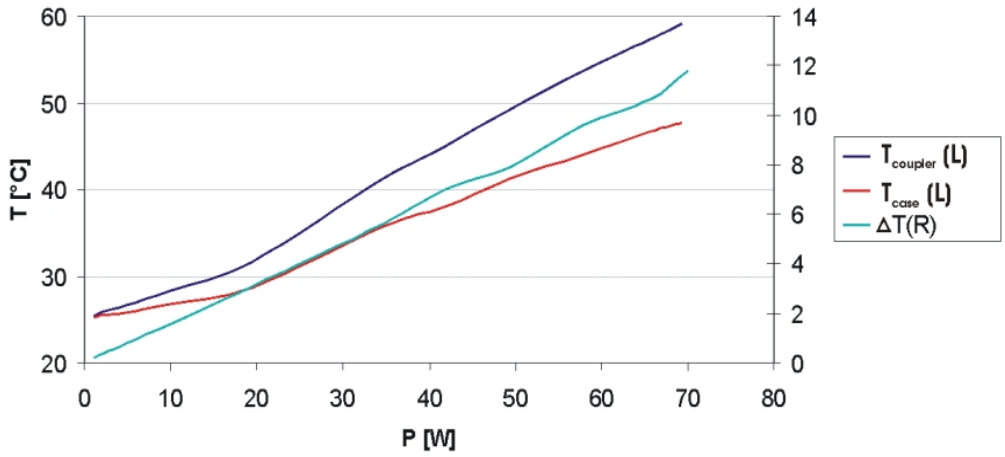

Figure 4.9: Bias-T Temperature vs. RF Power

With an input power of 70 W the power loss in the bias-T is 8.32 W. The temperature of the couplers is 59.8 °C and the temperature of the heatsink is 48 °C. The maximum temperature of the couplers should be kept below 85 °C. Consequently, reading the thermal limit, it would be possible to use the bias-T for more input RF power. But the maximum RF power for continuous wave is given from Anaren with 60 W. Though, the 70 W were no problem for the couplers. But there is no guarantee that more RF power would not destroy the hybrids.

DC Current

The heating of the bias-T with DC current was tested up to a current of 8 Ampere. The resistance of the DC path is 78 mΩ and the ambient temperature during the measurement was 22 °C.

I [A]	P [W]	T_{coup} [°C]	T_{case} [°C]	ΔT [°C]
1	0.08	24	23.8	0.2
2	0.31	26.1	24.9	1.2
3	0.70	30	27	3
4	1.25	35.2	29.5	5.7
5	2.00	42.2	33.3	8.9
6	2.80	52.8	39.3	13.5
7	3.82	64.7	44.5	20.2
8	5.0	78.5	50.3	28.2

Table 4.4: DC Current Measurement

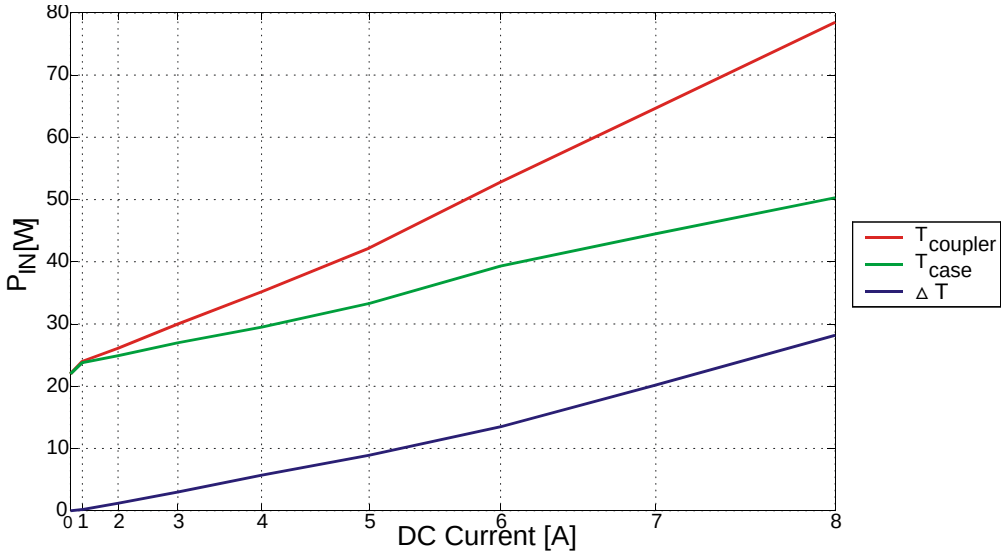

Figure 4.10: Bias-T Temperature vs. Current

With a DC current of 8 A the power loss is 5 W resulting in a temperature of the couplers of 78.5 °C and in a temperature of the heatsink of 50.3 °C. For a maximum temperature of the couplers of 85 °C the current has to be limited to 8 A.

Summary of Thermal Measurements

Since RF power will be lost mainly in the couplers due to their ohmic resistance, the thermal resistance for DC power is much worse than for RF power. RF power loss will not only occur in the couplers but also in the microstrip transmission lines and, therefore, resulting in a lower temperature increase than for DC power.
With a maximum temperature of the couplers, there is a safe operation area of the bias-T with the combination of RF power and DC current, as shown in Fig. 4.11. This figure is only valid for an RF frequency of 1.96 GHz and an ambient temperature of 22 °C. Although it can be assumed to be sufficiently correct for the whole operation bandwidth. The safe operation area for different ambient temperature may be derived by

$$T = T_{AMB} + P_{RF} \cdot R_{Th,RF} + I_{DC}^2 \cdot R_{DC} \cdot R_{Th,DC} \tag{4.2}$$

where the resulting temperature my not exceed $85°C$.

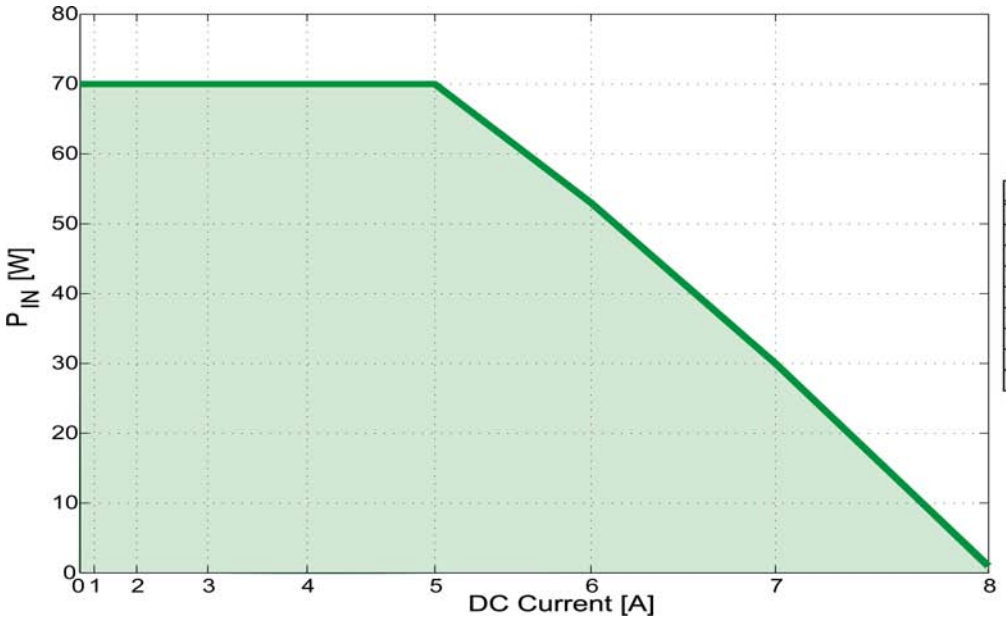

I [A]	Pin [W]
0	70
1	70
2	70
3	70
4	70
5	70
6	53
7	30
8	1

Figure 4.11: Safe Operation Area of the Bias-T

I_{max}	8 A	$T_{coupler}$ = 79 °C	T_{case} = 50 °C
P_{maxCW}	70 W	$T_{coupler}$ = 60 °C	T_{case} = 48 °C
$T_{maxCoupler}$	85 °C		
R_{DCpath}	78 mΩ		
$R_{Th,RF}$	1.4 °/W		
$R_{Th,DC}$	4.8 °/W		

Table 4.5: Limits of RF Power and DC Current

4.1.3 Measured DC Pulses

To check if a DC pulse is distorted by the bias-T, the shortest pulse from the pulser AVRF-2-B with 100 ns and the longest one, with 100 μs were measured at the input and output of the bias-T. The measurement setup is shown in Fig. 4.12. The bias-T (DUT) is placed between two attenuators of 10 dB. The first one is used because the pulser has an output impedance of only 6 Ω. Using the attenuator, the bias-T faces an impedance of 50 Ω. The second attenuator in front of the input of the oscilloscope is needed because the maximum voltage at the input of the scope may not exceed 5 V at an input impedance of 50 Ω.

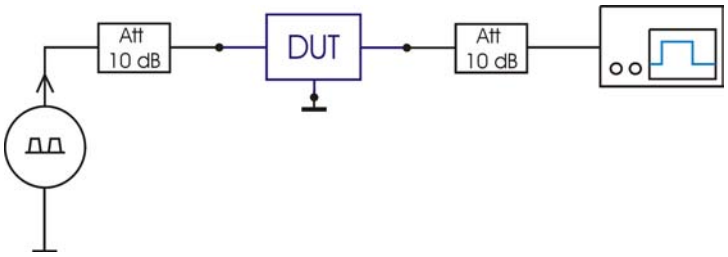

Figure 4.12: Configuration for Pulse Measurements

In Fig. 4.13 results with pulses with a pulsewidth of 100 ns are shown. One pulse was directly from the pulser output and the other one at the bias-T output. There is no distortion of the pulse by the bias-T. Only a short delay time of the pulse through the bias-T is seen.
In Fig. 4.14, the result with the longest pulse possible with the used pulser is shown. The length of this pulse is 100 μs and there is also no distortion of the pulse by the bias-T at this pulsewidth.

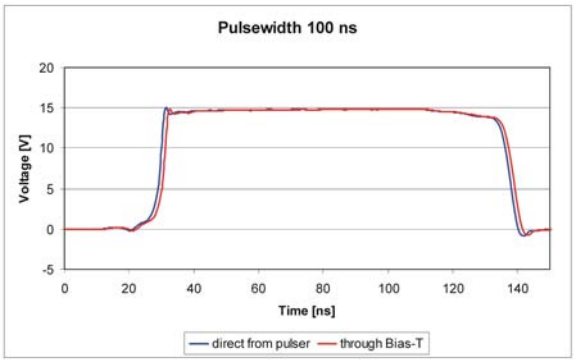

Figure 4.13: Short Pulse Measured

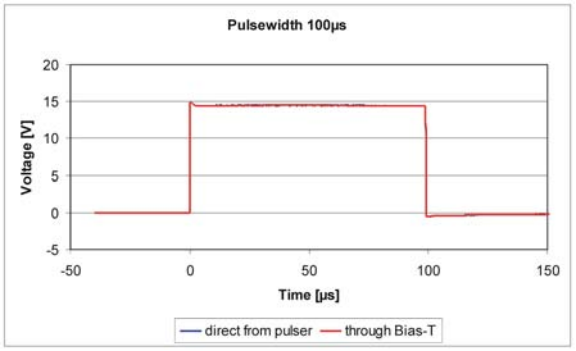

Figure 4.14: Long Pulse Measured

4.2 1^{st} Bias-T without Harmonic Matching

A bias-T with the same coupler type was built for applications where a matching of harmonics is not necessary.

4.2.1 S-Parameters

The final bias-T, as it is shown in Fig. 4.15, is a four port device. The frequency range depends on the acceptable insertion loss value.

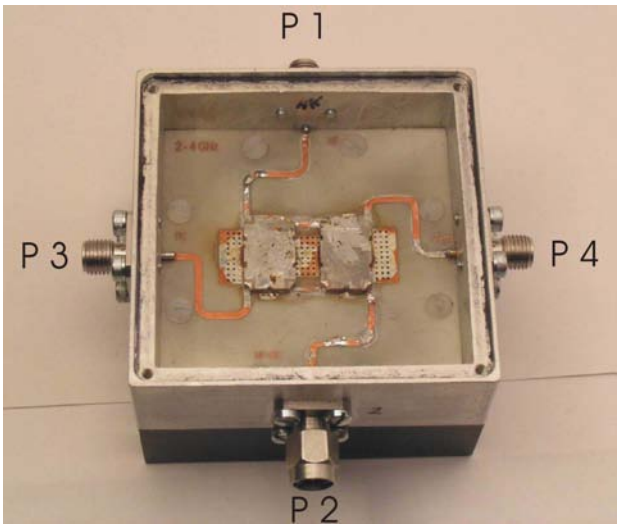

Figure 4.15: Bias-T without Harmonic Matching

Port 1	RF
Port 2	RF+DC
Port 3	DC
Port 4	Termination

In Fig. 4.15, the S-parameters of the bias-T with opened cap are shown. The return losses S_{11} and S_{22} are better than 17 dB and the insertion loss depends on the following frequency ranges:

Insertion Loss [dB]	Frequency Range [GHz]
0.5	1.68...2.35
0.6	1.50...3.30
0.7	1.43...3.80
0.8	1.35...4.10
0.9	1.28...4.26
1.0	1.25...4.33

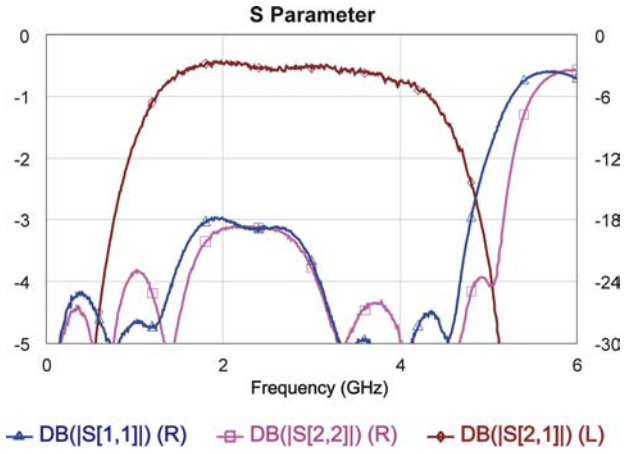

Figure 4.16: Without Cap

With equation 4.1, the resonance frequencies with closed cap are calculated. The parameters are: $x_1 = 52$ mm, $y_1 = 12$ mm and $z_1 = 52$ mm. The table of the resonance frequencies is:

TE_{101}	4.08 GHz
TE_{102}	6.44 GHz
TE_{201}	6.44 GHz
TE_{202}	8.15 GHz

Table 4.6: Resonance Frequencies

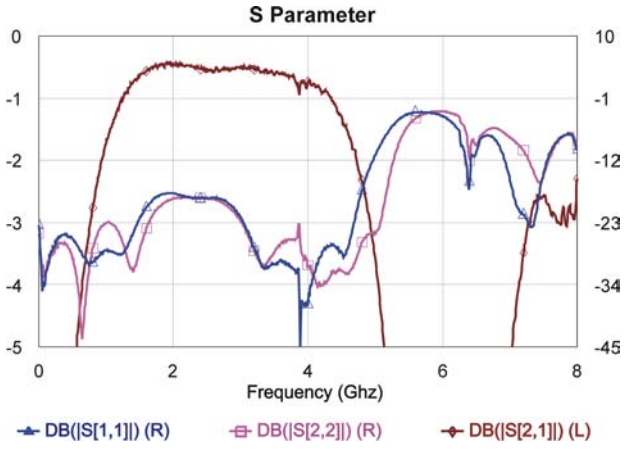

Figure 4.17: Closed Case

In Fig. 4.17 the measured points of resonance frequencies are shown. They are close to the calculated points. To eliminate these resonance frequencies, the dielectric absorber LS-10055 with a thickness of 3.1 mm and a frequency range from 4 to 26 GHz was used.

The last measurement of the S-parameters, shown in Fig. 4.18, was done with a closed case.

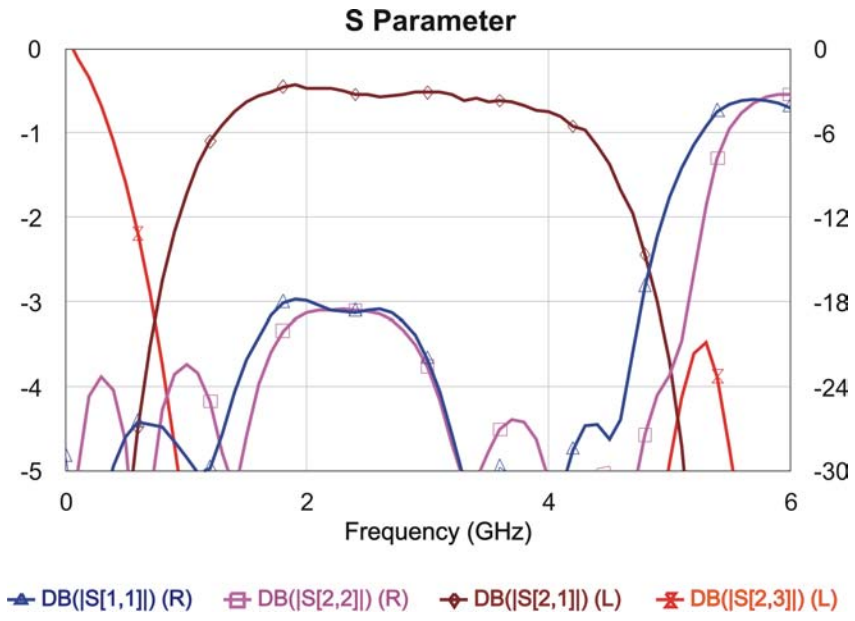

Figure 4.18: Final Bias-T without Harmonics

The return losses S_{11} and S_{22} are better than 17.7 dB and the insertion loss is listed in the table below:

Insertion Loss [dB]	Frequency Range [GHz]
0.5	1.68...2.35
0.6	1.50...3.30
0.7	1.43...3.80
0.8	1.35...4.10
0.9	1.28...4.26
1.0	1.25...4.33

Table 4.7: Insertion Loss of the Bias-T without Harmonic Termination

4.2.2 Thermal Test with RF Power and DC Current

RF Power

In the next step, the bias-T was tested with an RF signal of 1.96 GHz up to a power level of 70 W. At this frequency, the bias-T has an average insertion loss of 0.56 dB. The power was measured at the input and at the output of the bias-T and the temperature was measured at the cases of the couplers and on the heatsink of the bias-T. The ambient temperature during the measurement was 25 °C.

P_{in} [dB]	P_{out} [dB]	P_{Δ} [dB]	P_{in} [w]	P_{out} [W]	P_{Δ} [W]	T_{coup} [°C]	T_{case} [°C]	ΔT [°C]
30.20	29.68	0.52	1.05	0.93	0.12	25.4	25.2	0.2
33.44	32.99	0.45	2.21	1.99	0.22	25.6	25.3	0.3
36.80	36.26	0.54	4.79	4.23	0.56	26.5	25.9	0.6
39.94	39.34	0.55	9.86	8.69	1.17	28.1	26.9	1.2
42.74	42.19	0.55	18.79	16.56	2.24	31.4	29.0	2.4
45.35	44.79	0.56	34.28	30.13	4.15	37.6	32.9	4.7
46.11	45.52	0.59	40.83	35.65	5.19	39.6	34.0	5.6
46.84	46.25	0.60	48.31	42.17	6.14	42.5	35.9	6.6
47.51	46.91	0.61	56.36	49.09	7.27	46.8	39.9	7.5
48.08	47.47	0.61	64.27	55.85	8.42	50.8	41.8	9.0
48.32	47.71	0.61	67.92	59.02	8.90	53.1	43.1	10.0
48.44	47.83	0.61	69.82	60.67	9.15	53.2	43.2	10.0

Table 4.8: Measurement Results with RF Power

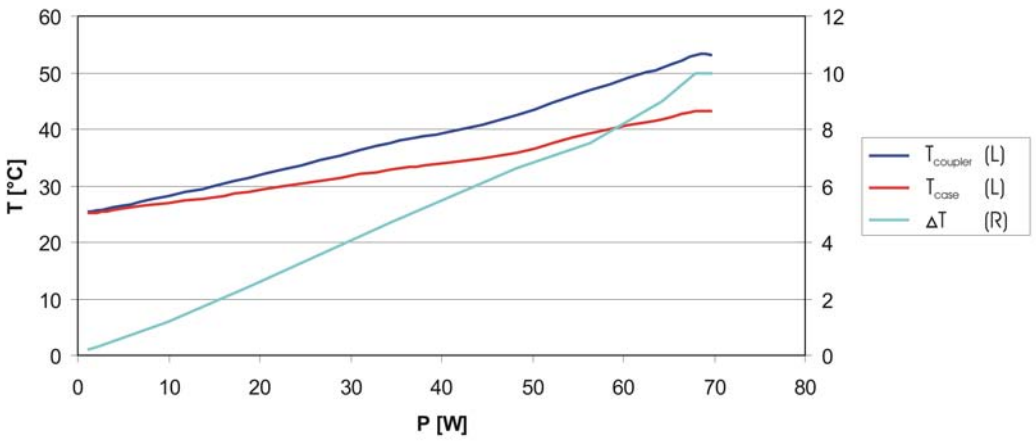

Figure 4.19: Bias-T Temperature vs. RF Power

With an input power of 70 W the power loss is 9.15 W, the temperature of the couplers is 53.2 °C and the temperature of the heatsink is 43.2 °C. The maximum temperature of the couplers shall not exceed 85 °C and the maximum RF power shall not exceed 60 W CW. But 70 W were no problem for the couplers, but there is no guarantee that more RF power would not destroy the hybrids.

DC Current

The heating of the bias-T with DC current was tested up to a current of 8 Ampere. The resistance of the DC path is 78 mΩ and the ambient temperature during measurement was 25 °C.

I [A]	P [W]	T_{coup} [°C]	T_{case} [°C]	ΔT [°C]
1	0.08	25.2	25.1	0.1
2	0.30	26.6	25.8	0.8
3	0.67	30.0	28.1	1.9
4	1.20	34.1	30.7	3.4
5	1.88	41.6	36.5	5.1
6	2.70	48.8	40.6	8.2
7	3.68	58.3	46.5	11.8
8	4.8	71.0	54.5	16.5

Table 4.9: DC Current Measurement Results

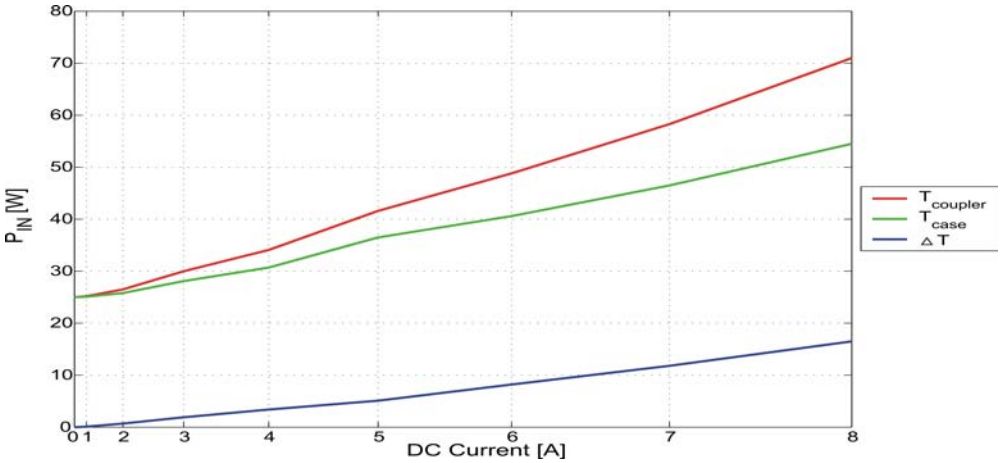

Figure 4.20: Bias-T Temperatur vs. DC Current

With a DC current of 8 A the power loss is 4.8 W, the temperature of the couplers is 71 °C and the temperature of the heatsink is 54.5 °C. For a maximum temperature of 85 °C of the couplers, the current of 8 A is not the absolute limit, since maximum temperature is not reached by 14 °C.

Summary of Thermal Measurements

Since RF power will be lost mainly in the couplers due to their ohmic resistance, the thermal resistance for DC power is much worse than for RF power. RF power loss will not only occur in the couplers but also in the microstrip transmission lines and, therefore, resulting in a lower temperature increase than for DC power.
With a maximum temperature of the couplers, there is a safe operation area of the bias-T with the combination of RF power and DC current, as shown in Fig. 4.21. This figure is only valid for an RF frequency of 1.96 GHz and an ambient temperature of 25 °C. Although it can be assumed to be sufficiently correct for the whole operation bandwidth. The safe operation area for different ambient temperatures may be derived by

$$T = T_{AMB} + P_{RF} \cdot R_{Th,RF} + I_{DC}^2 \cdot R_{DC} \cdot R_{Th,DC} \tag{4.3}$$

where the resulting temperature my not exceed 85 °C.

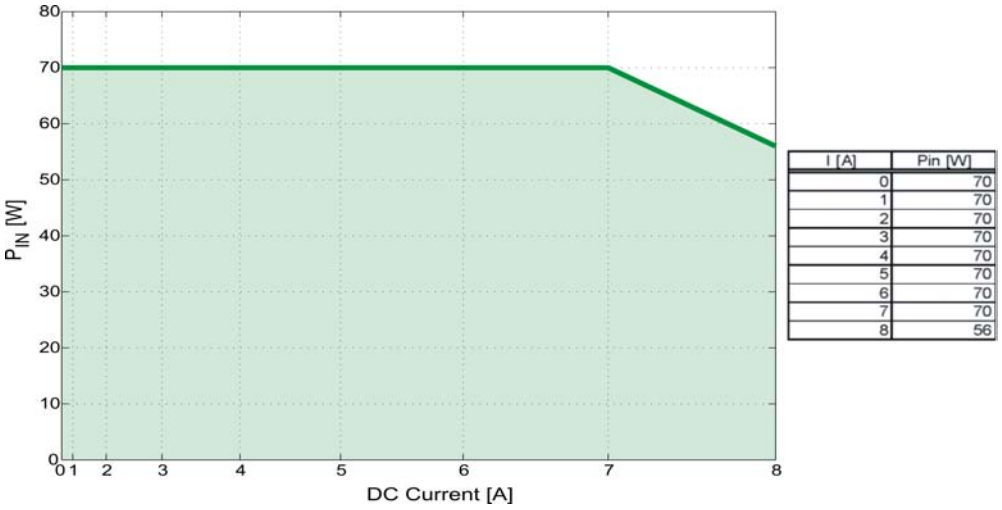

I [A]	Pin [W]
0	70
1	70
2	70
3	70
4	70
5	70
6	70
7	70
8	56

Figure 4.21: Safe Operation Area of the Bias-T

I_{max}	8 A	$T_{coupler}$ = 71 °C	T_{case} = 55 °C
P_{maxCW}	70 W	$T_{coupler}$ = 53 °C	T_{case} = 43 °C
$T_{maxCoupler}$	80 °C		
R_{DCpath}	75 mΩ		
$R_{Th,RF}$	1.2 °C/W		
$R_{Th,DC}$	2.8 °C/W		

Table 4.10: Limits of RF Power and DC Current

4.2.3 Measured DC Pulses

Additionally, also this bias-T was checked whether there is any distortion of pulses by the bias-T. Therefore, the measurement setup from Fig. 4.12 was used and a pulse with a length of 100 ns and one with 100 μs were measured.

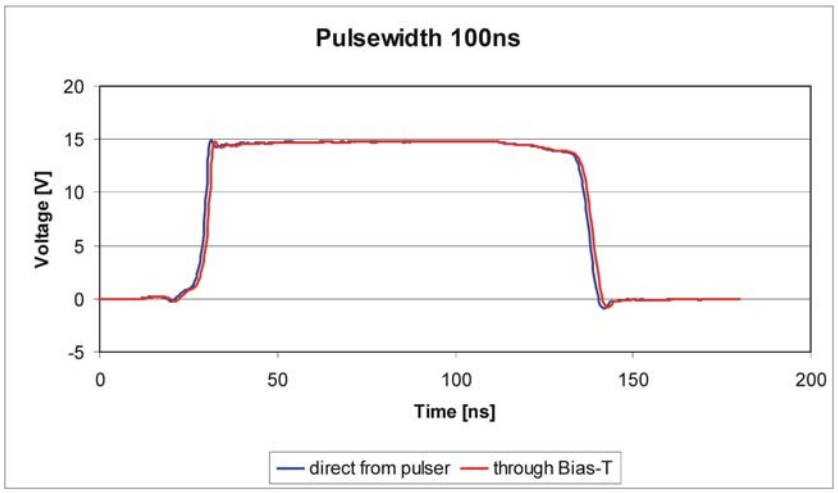

Figure 4.22: Short Pulse Measured

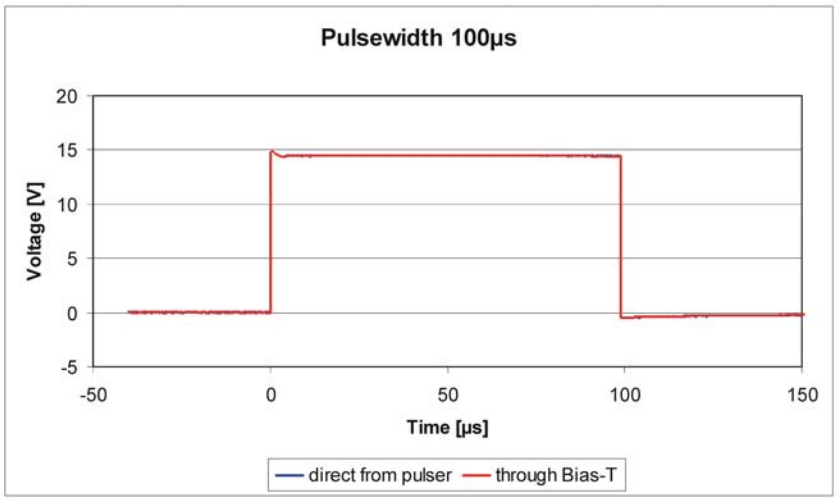

Figure 4.23: Long Pulse Measured

In both cases, there is no distortion of the pulse by the bias-T. In Fig. 4.22, only the short delay time of the pulse through the bias-T can be seen.

4.3 2^{nd} Bias-T without Harmonic Matching

This bias-T is built for a higher frequency range. Therefore, the Anaren Xinger® Hybrid Model 1M803 with a frequency range from 5 GHz to 6 GHz was used. But there is also no high pass filter included for harmonic frequencies (similar to 4.2).

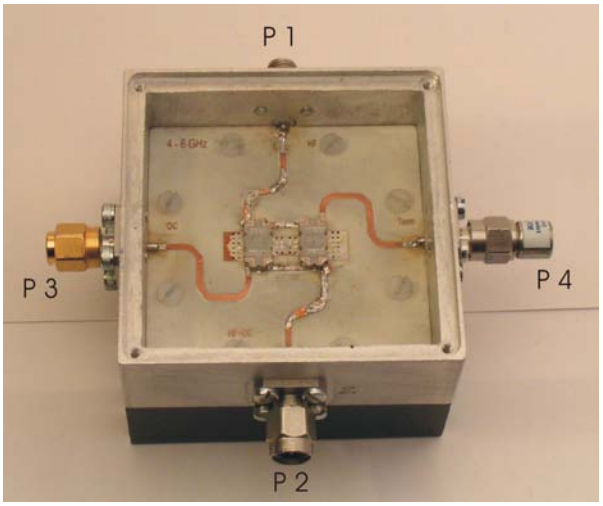

Figure 4.24: 2^{nd} Bias-T without Harmonic Matching

Port 1	RF
Port 2	RF+DC
Port 3	DC
Port 4	Termination

The used coupler 1M803 has smaller dimensions than the coupler 11306-3. This is a benefit for the resistance of the DC path since this is clearly reduced. But the disadvantage is, that the coupler is only specified for a continuous wave RF power up to 20 W.

4.3.1 S-Parameters

For this bias-T the same mechanical case as for the 1^{st} bias-T without harmonic matching is used. Therefore, the same resonance frequencies, as shown in table 4.6, are valid. Also for this bias-T, the dielectric absorber LS-10055 with a thickness of 3.1 mm and a frequency range from 4 to 26 GHz was used, in order to eliminate these resonance frequencies.
In Fig. 4.25, the S-parameters of the final bias-T with closed cap and mounted dielectric absorber are shown.

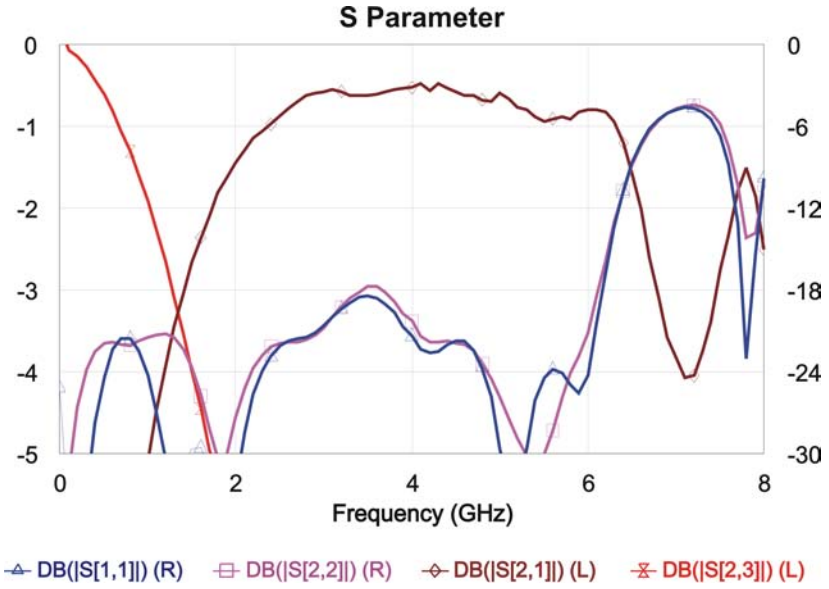

Figure 4.25: Finished Bias-T for Higher Frequencies

As shown in Fig. 4.25, the return loss in the expected frequency range from 2.3 GHz to 6.3 GHz is better than 17 dB and the insertion loss depends on the frequency range as listed in the table below.

Insertion Loss [dB]	Frequency Range [GHz]
0.5	4.0...4.3
0.6	2.8...4.5
0.7	2.7...5.1
0.8	2.5...5.2
0.9	2.45...6.2
1.0	2.3...6.3

Table 4.11: Insertion Losses from 2.3 to 6.3 GHz

4.3.2 Thermal Test with RF Power and DC Current

RF Power

It was not possible to measure the heating of the couplers and the heatsink with RF power because there was no high power amplifier available for the required frequency range. The specification from Anaren for the coupler model 1M803 is a maximum RF power of 20 W, but with the large heatsink we are confident that the bias-T can be used up to an RF power of 30 W.

DC Current

At this bias-T, also the thermal heating was measured up to a current of 8 Ampere. The resistance of the DC path is 47 mΩ.

I [A]	P [W]	T_{coup} [°C]	T_{case} [°C]	ΔT [°C]
1	0.05	25.3	25.3	0
2	0.18	25.8	25.6	0.2
3	0.42	28.6	28.0	0.6
4	0.75	31.0	30.0	1.0
5	1.18	35.1	33.3	1.8
6	1.69	39.3	36.8	2.5
7	2.30	43.3	39.8	3.7
8	3.00	49.4	44.7	4.7

Table 4.12: DC Current Measurement Results

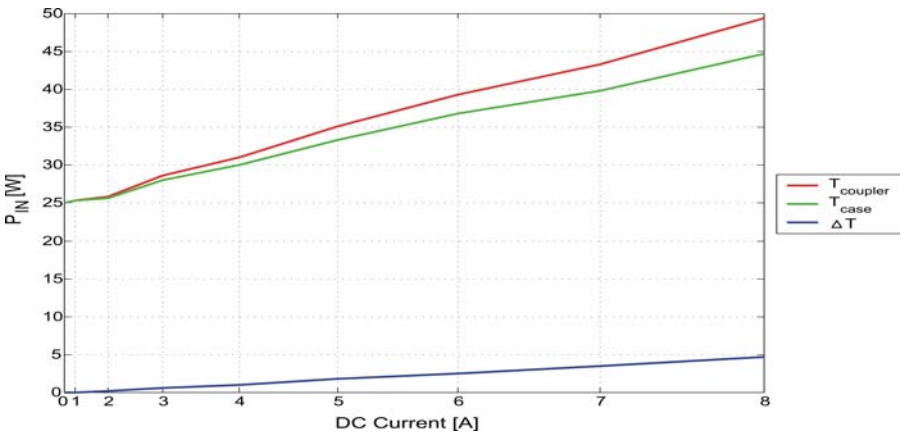

Figure 4.26: Bias-T Temperature vs. DC Current

With a DC current of 8 A the power loss is 3 W, the temperature of the couplers is 49.5 °C and the temperature of the heatsink is 44.7 °C. For a maximum temperature of 85 °C of the couplers the current of 8 A is no limit. But there is a risk that the couplers get damaged with more current, because of the small dimensions of their strip lines.

Summary of Thermal Measurements

It is not possible to describe an exactly safe operation area because of the missing measurements with RF power. But we are confident that there will be no thermal problems using the bias-T with an RF power of 30 W and a DC current of 8 A together, because of the low resistance of the DC path of 47 mΩ.

I_{max}	8 A	$T_{coupler}$ = 50 °C	T_{case} = 45 °C		$T_{maxCoupler}$	80 °C
P_{maxCW}	30 W	$T_{coupler}$ = °C	T_{case} = °C		R_{DCpath}	47 mΩ

4.3.3 Measured DC Pulses

Additionally also with this bias-T it was checked, if there is any distortion of pulses by the bias-T. Therefore, the measurement setup from Fig. 4.12 was used and a pulse with a length of 100 ns and one with 100μs were measured.

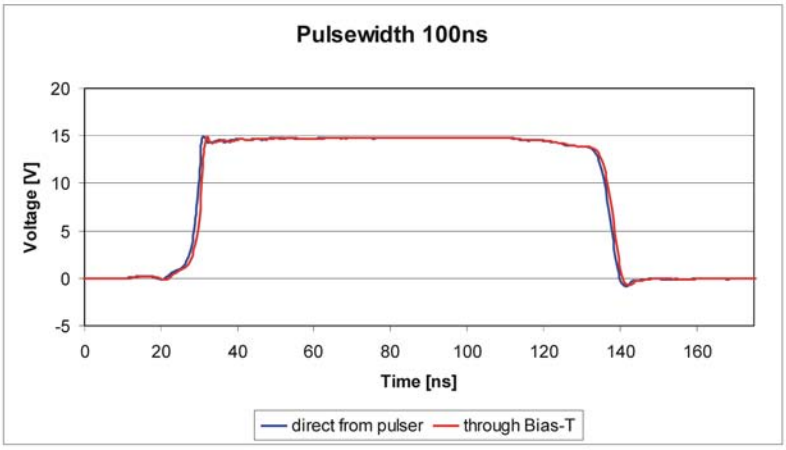

Figure 4.27: Short Pulse Measured

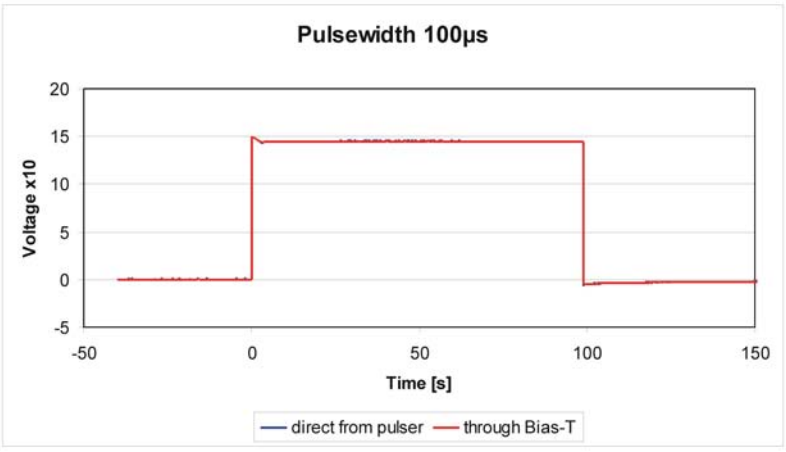

Figure 4.28: Longe Pulse Measured

As expected, no distortion of the pulses by the bias-T occured. According to the smaller dimensions of the coupler the delay time of the pulse through the bias-T is shorter than at the bias-Ts for a lower frequency range.

4.4 Bias-T to combine DC-Pulse and DC

For the bias-T which combines the DC pulse and DC only the classic design with high pass filter and low pass filter is possible. Because the frequency of the LF path of the bias-T ranges from 100 Hz to 200 MHz and it is not possible to design couplers for these low frequencies.
In the LF path, there is a capacitor with a value of 300 μF and in the DC path, there is an inductor of 100 mH which is necessary so that the distortion of the pulse with a length of 100 μs is negligible. A capacitor of 100 μF is placed at the DC input for DC buffering. The realized circuit schematic is shown in Fig. 4.29.

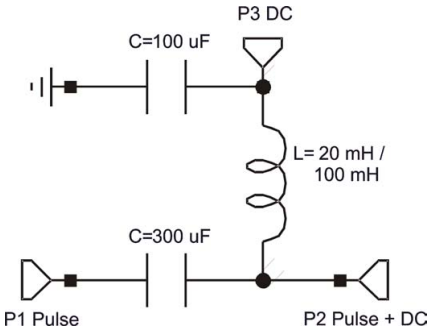

Figure 4.29: Circuit Schematic for Bias-T Pulse + DC

The disadvantage of the high inductivity of 100 mH is that the resistance of the DC path gets very high with a value of 210 mΩ. This resistance produces a DC offset at higher currents that has a negative influence on the measurement of the transistors when this bias-T is used (baseband modulation).
Therefore, a second bias-T for DC and pulse was built with an inductor of 20 mH and a resistance of 35 mΩ for a pulsewidth up to 10 μs.

4.4.1 Bias-T for Pulses up to 10 μs Pulsewidth

The bias-T as shown in Fig. 4.30 is designed for a maximum DC current of 10 A and a maximum voltage, pulse and DC, of 100 V.

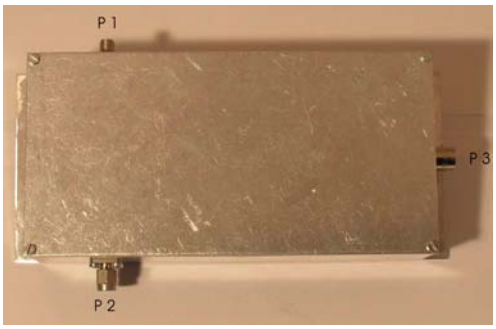

Figure 4.30: Bias-T for Pulses up to 10 μs

Port 1	RF
Port 2	RF+DC
Port 3	DC

S-Parameters

In Fig. 4.31 the S-parameters of the bias-T measured with closed case are shown. An absorber material was not necessary because of the low frequency range.
The insertion loss S_{21} is better than 2.1 dB in the required frequency range from 500 Hz to 200 MHz
The return losses S_{11} and S_{22} are better than 11 dB.

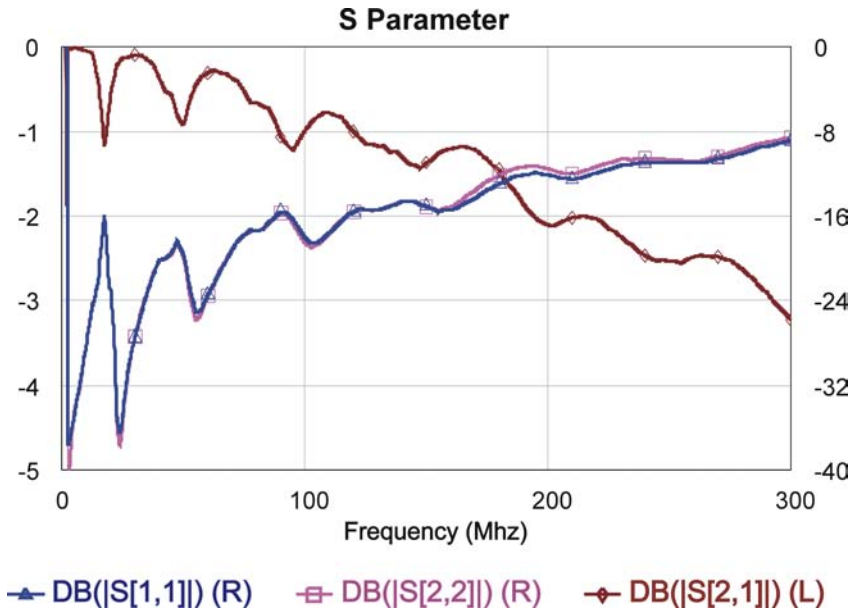

Figure 4.31: Small Bias-T for DC + Pulse

DC Pulses

The most important property of the bias-T is that there is no distortion of a pulse by it. Therefore, a lot of pulse responses with different pulsewidths were measured with the measurement setup from Fig. 4.12. In the figures below some of the results are shown.

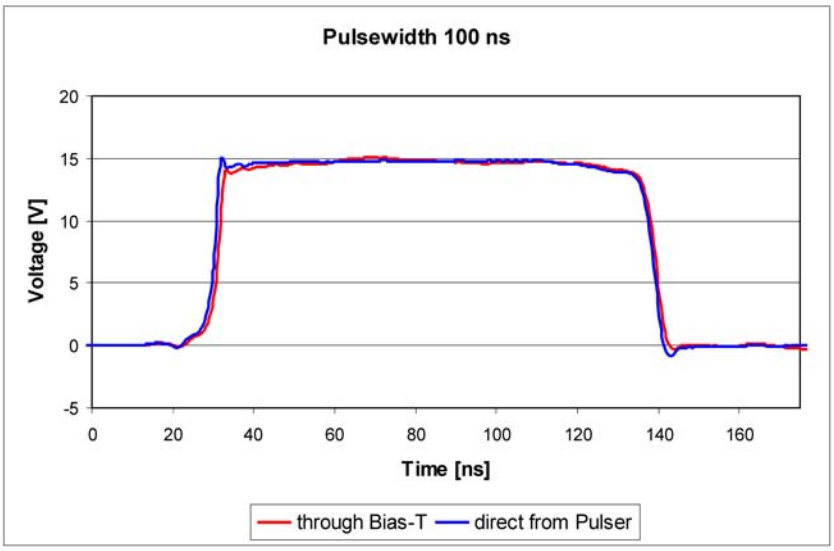

Figure 4.32: Short Pulse

In Fig. 4.32 the shortest pulse available from the pulser is displayed. The only difference which can be seen is the short delay time through the bias-T.

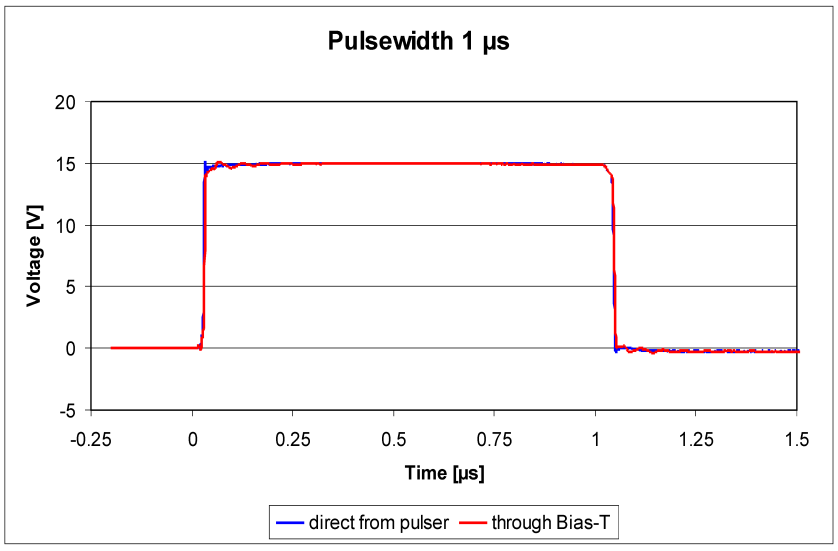

Figure 4.33: Pulse Inside the Range of the Bias-T

In Fig. 4.33 the pulse through the bias-T has exactly the same shape as the direct pulse from the pulser.

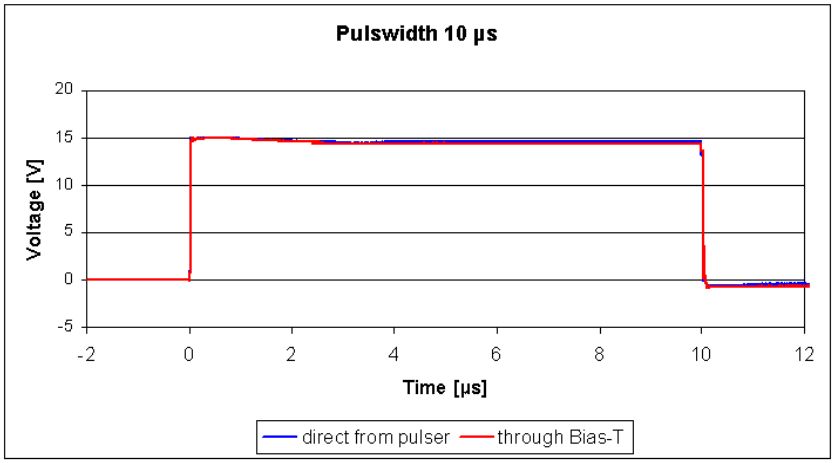

Figure 4.34: Maximum Pulsewidth

In Fig. 4.34 a small degradation at the end of the pulse is identifiable, but it is tolerable and, therefore, this is the longest pulse possible for this bias-T.

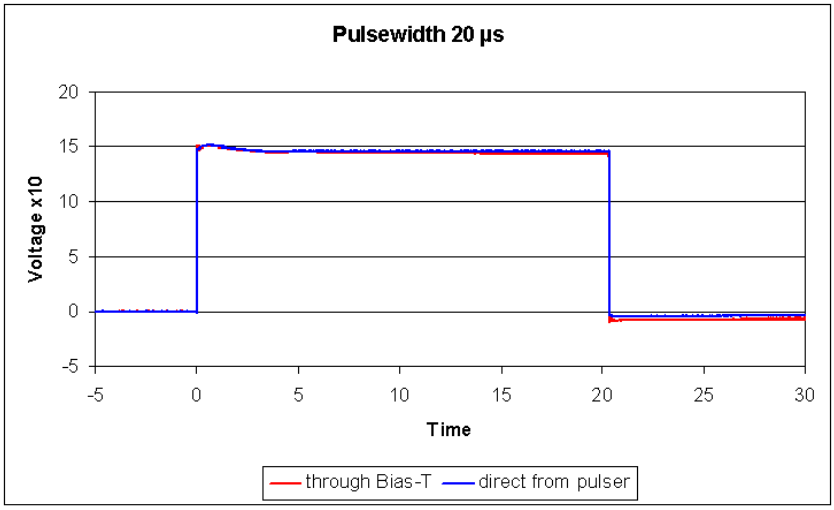

Figure 4.35: Distorted Pulse

In Fig. 4.35 a clear distortion of the pulse by the bias-T is to see, this pulse is too long for this bias-T.

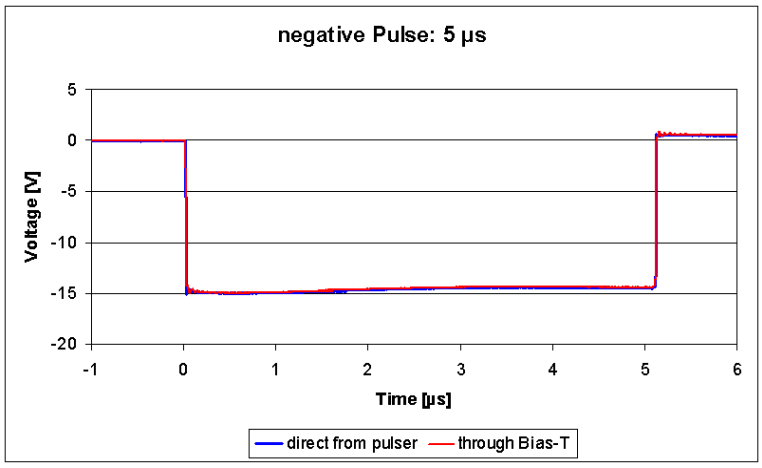

Figure 4.36: Negative Pulse Through the Bias-T

In Fig. 4.36 a negative pulse with a pulsewidth of 5 μs was measured. This was done to check if the bias-T has the same properties for positive and negative pulses and there was no difference to observe.

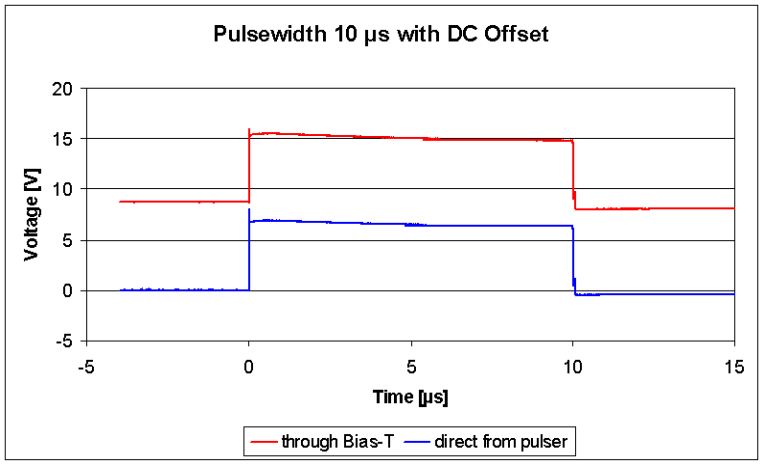

Figure 4.37: Pulse + DC

In Fig. 4.37 the combination of a pulse and DC is shown. The bias-T works well for pulses with a pulsewidth from 100 ns to 10 μs. It has a low resistance in the DC path and satisfactory S-parameters. This will be the most used bias-T for the combination of pulse and DC, because of its low resistance and the fact that in the most of the cases a pulsewidth of 10 μs will be long enough for transistor measurement.

4.4.2 Bias-T for Pulses up to 100 μs Pulsewidth

This bias-T, as shown in Fig. 4.38 is also built for a DC current up to 10 A and a maximum voltage, pulse and DC, of 100 V. This bias-T can be used for all available pulsewidths of the pulser ranging from 100 ns to 100 μs. But the resistance of the DC path is now 210 mΩ.

Figure 4.38: Bias-T for Pulses up to 100 μs

Port 1	RF
Port 2	RF+DC
Port 3	DC

S-Parameters

In Fig. 4.39 the S-parameters of the bias-T measured with closed case are shown. An absorber material was not necessary because of the low frequency range.
The insertion loss S_{21} is better than 0.9 dB in the required frequency range from 100 Hz to 200 MHz
The return losses S_{11} and S_{22} are better than 20 dB.

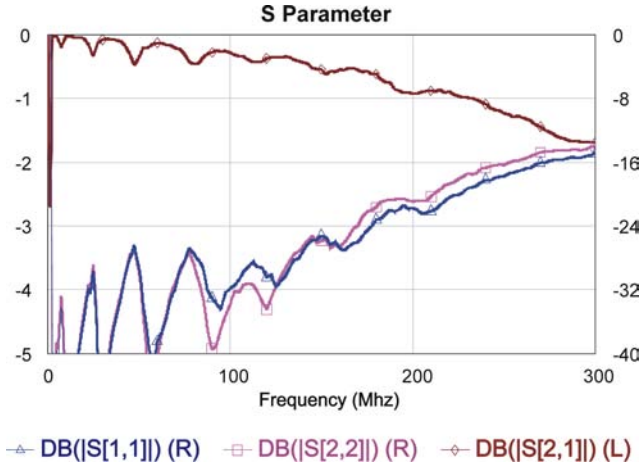

Figure 4.39: Large Bias-T for DC + Pulse

Because of the larger value of the inductivity of 100 mH, the S-parameters are better than for the bias-T presented in 4.4.1. The insertion loss is better than 0.9 dB and the return losses are better than 20 dB at the LF port and the LF+DC port are really good, but unfortunately with a reasonably high resistance.

DC Pulses

Also for this bias-T some characteristic pulses are shown below:

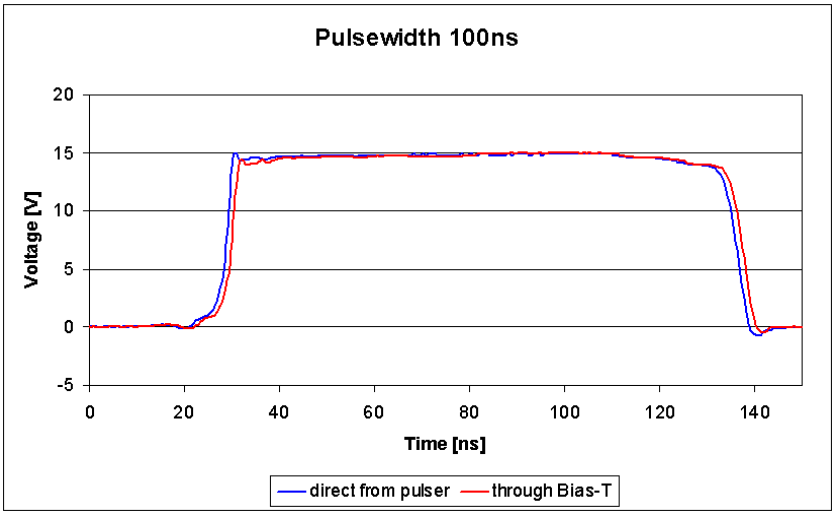

Figure 4.40: Short Pulse

In Fig. 4.40 the response to the shortest pulse available from the pulser is shown. The only difference which can be observed is the short delay time through the bias-T.

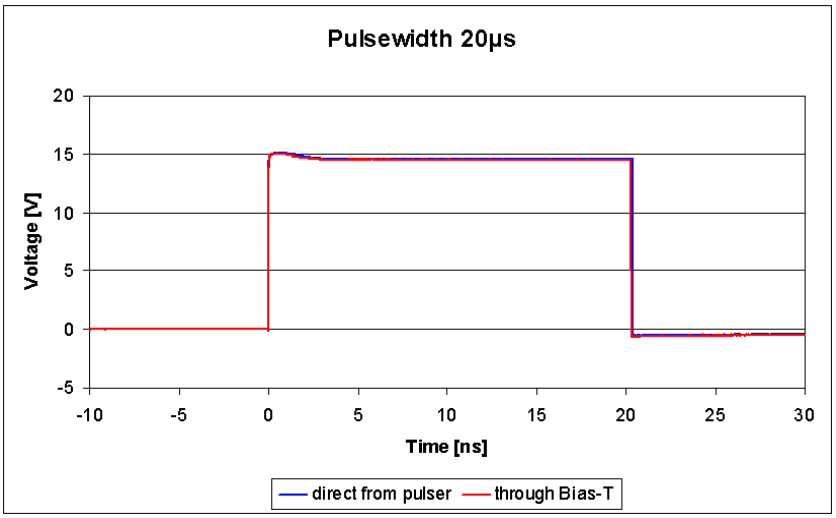

Figure 4.41: Pulsewidth 20 μs

In Fig. 4.41 the response to a pulse with a pulsewidth of 20 μs is shown. This pulse was distorted by the small bias-T, which is described in 4.4.1, but now there is no distortion.

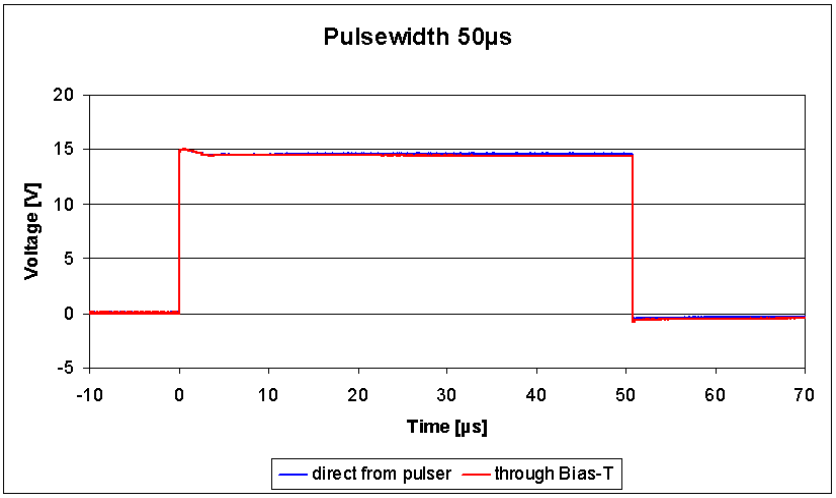

Figure 4.42: Pulsewidth 50 μs

In Fig. 4.42 the response to a pulse with a pulsewidth of 50 μs is shown with no distortion.

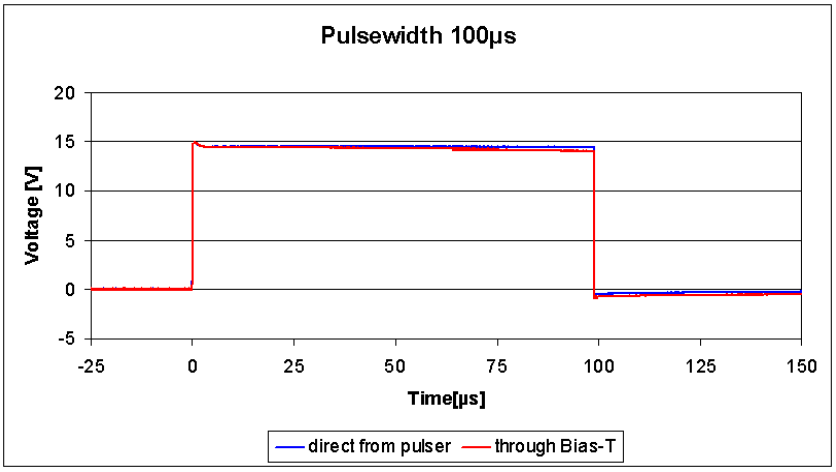

Figure 4.43: Largest Available Pulse

In Fig. 4.43 the response to the longest pulse available from the pulser is shown. There is a negligible distortion at the end of the pulse. This distortion is tolerable and additionally, such a long pulse will be only used rarely.

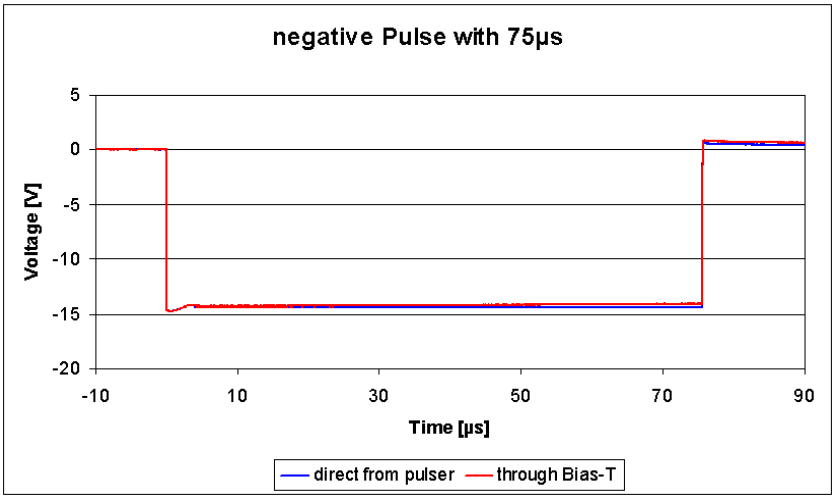

Figure 4.44: Negative Pulse with Pulsewidth 75 μs

In Fig. 4.44 the response to a negative pulse with a pulsewidth of 75 μs is presented. This was measured to check if the bias-T has the same properties for positive and negative pulses and there, no difference can be observed.

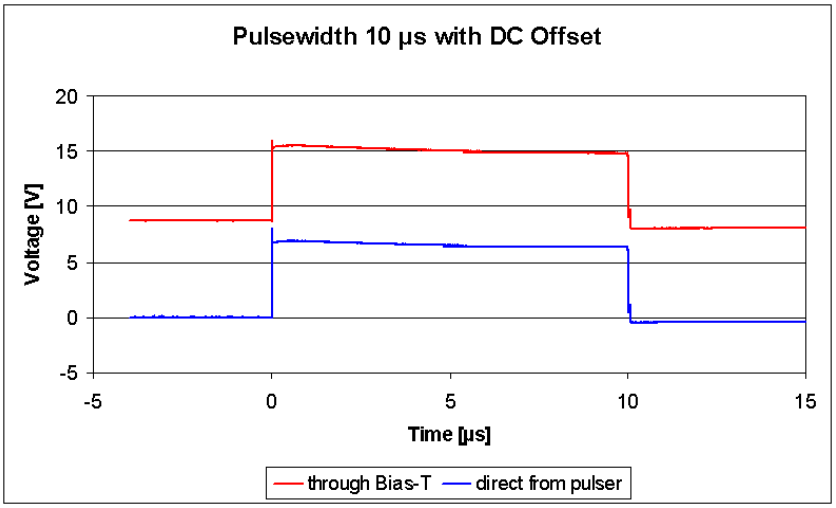

Figure 4.45: Pulse + DC

In Fig. 4.45 a combination of a pulse and DC is shown.

Both designed and built bias-Ts are usable to combine the DC pulse and DC. For applications where only shorter pulsewidth than 10 μs are necessary the smaller bias-T of these two will be preferable. The S-parameters of this bias-T are a little bit worse than the ones of the larger bias-T, but the resistance of the DC path is 6 times better.

Chapter 5

Summary and Outlook

5.1 Summary

The aim of this diploma thesis was to design a bias-T which is able to combine RF, DC-pulse and DC for a fundamental frequency range from 1.8 GHz to 2.5 GHz with a matching of the harmonics up to 3^{rd} order at the RF+DC port, which is equivalent to a frequency range from 3.6 GHz to 7.5 GHz.
To allow more flexibility in use, the bias-T in order to combine all three signals, was splitted into two bias-Ts where one combines the DC-pulse with DC (LF bias-T) and another combines RF with DC+Pulse (RF bias-T). Two basically different designs for the RF bias-T were evaluated.
The first design approach for the RF bias-T was a conventional design based on high pass and low pass filters with discrete components for a frequency range from 1.8 GHz to 7.5 GHz. One drawback of this design approach is that with high pass and low pass filters of first order the desired isolation between the RF path and the DC path of 20 dB is not possible to realize. Therefore, high pass and low pass filters of higher order were necessary. Higher order filters require additional lumped elements. Simulations with realistic lumped element models have shown that the resonance frequencies of the chosen inductors deteriorate the performance of the bias-T by far when compared to simulation results with ideal components. Those simulation results indicated a very delicate circuit design procedure where a robust design can be hardly achieve.
To overcome this drawback a second design based on 3 dB 90° hybrids with forward coupling was evaluated. It is possible to build a bias-T based on two hybrids with a physically uninterupted DC path through the couplers to which the RF is coupled, while there is no physical connection between the RF and DC port. Therefore, it is important to use directional couplers and not branch line couplers, since branchline couplers do not offer isolated branches which are the basis for this bias-T design.
In the beginning a design of a directional coupler for the whole frequency range from 1.8 GHz to 7.5 GHz was started. This design failed due to the problem that the design process delivered physical dimensions which were not manufacturable and would also not be able to bear the required DC current. To substitute those commercially available broadband couplers, couplers with a restricted range of frequency were used where a small modification in the design of the bias-T was necessary. To match the harmonics up to the 3^{rd} order a high pass filter at the RF+DC path was added. Finally, a set of different bias-Ts were designed and manufactured to offer high flexibility in their use for different applications. One bias-T with up to 3^{rd} order harmonic matching was built for a fundamental frequency range from 1.8 GHz to 2.5 GHz fulfilling the required specifications. Additionally, for more flexibility, two bias-Ts which do not comprise harmonic matching for a frequency range from 1.8 GHz to 4 GHz and from 3 GHz to 6 GHz, respectively, were built. The detailed technical data of these bias-Ts are shown in the next section.
In order to combine the DC pulse with a bandwidth of 200 MHz and DC offset, two additional bias-Ts in classical design with a capacitor as high pass filter and an inductor as low pass filter were built. Since the inductor's series resistance which is located in the DC path cause a voltage drop, baseband modulation of the supply voltage can occur for RF signals with non-constant envelope. Therefore, it is essential to reduce the inductor's series resistance to a minimum. Out of this reason, one LF bias-T was built for a maximum pulsewidth of 10 μs with considerably reduced series resistance and a second one was built being capable to transfer pulses with the maximum required pulsewidth of 100 μs without distortion. The detailed technical data of these bias-Ts are shown in the next section as well.

5.2 Bias-Ts Technical Data Sheets

5.2.1 Bias-T with Harmonic Matching

This bias-T has five ports. The schematic of the arrangement of the ports is shown in Fig. 5.1:

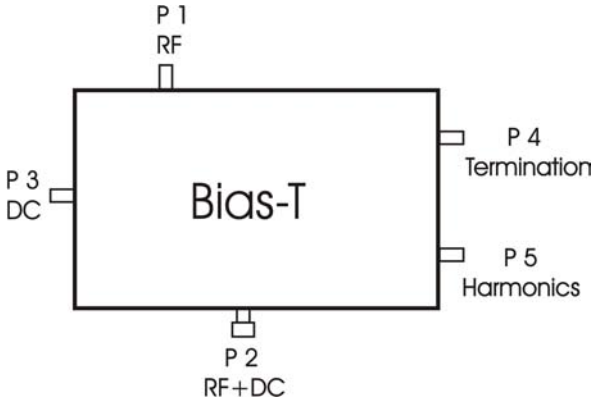

Figure 5.1: Ports of the 1^{st} Bias-T

The Technical Data are:

- Fundamental frequency range: 1.8 ... 2.5 GHz
  - Insertion loss: $\leq$ 0.53 dB
  - Return loss S_{11} and S_{22}: $\geq$ 17 dB
- Harmonic frequency range up to 3^{rd} order: 3.6 ... 7.5 GHz
- Return loss S_{22}: $\geq$ 10 dB
- max. RF_{CW} power: 70 W
- max. DC_{pulsed} current: 8 A
- max. $DC_{cont.}$ current: 8 A
- R_{DCpath}: 78 mΩ
- max. $T_{coupler}$: 85 $°C$
- max. T_{bias-T}: 50 $°C$
- no distortion of the DC pulses with a pulsewidth range from 100 ns to 100 μs

5.2.2 1^{st} Bias-T without Harmonic Matching

This bias-T has four ports. The schematic of the arrangement of the ports is shown in Fig. 5.2:

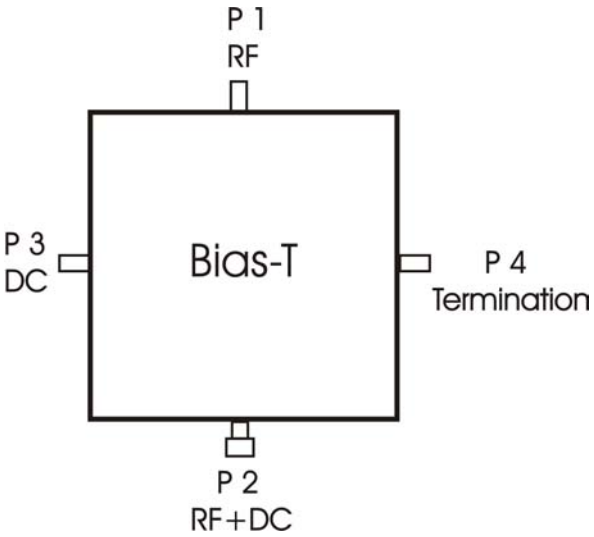

Figure 5.2: Ports of the 2^{nd} Bias-T

The Technical Data are:

Insertion Loss [dB]	Frequency Range [GHz]
0.5	1.68...2.35
0.6	1.50...3.30
0.7	1.43...3.80
0.8	1.35...4.10
0.9	1.28...4.26
1.0	1.25...4.33

- Return loss S_{11} and S_{22}: $\geq$ 17 dB
- max. RF_{CW} power: 70 W
- max. DC_{pulsed} current: 8 A
- max. $DC_{cont.}$ current: 8 A
- R_{DCpath}: 75 mΩ
- max. $T_{coupler}$: 80 $°C$
- max. T_{bias-T}: 50 $°C$
- no distortion of the DC pulses with a pulsewidth range from 100 ns to 100 μs

5.2.3 2^{nd} Bias-T without Harmonic Matching

This bias-T has four ports. The schematic of the arrangement of the ports is shown in Fig. 5.3:

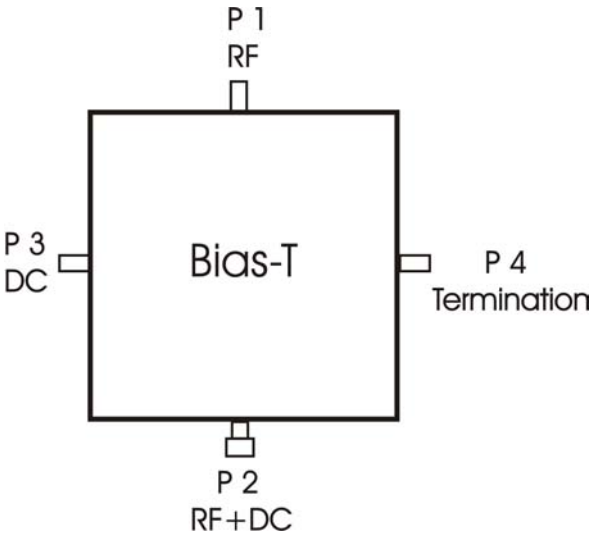

Figure 5.3: Ports of the 3^{rd} Bias-T

The Technical Data are:

Insertion Loss [dB]	Frequency Range [GHz]
0.5	4.0...4.3
0.6	2.8...4.5
0.7	2.7...5.1
0.8	2.5...5.2
0.9	2.45...6.2
1.0	2.3...6.3

- Return loss S_{11} and S_{22}: $\geq$ 17 dB
- max. RF_{CW} power: 30 W
- max. DC_{pulsed} current: 8 A
- max. $DC_{cont.}$ current: 8 A
- R_{DCpath}: 47 mΩ
- max. $T_{coupler}$: 80 $°C$
- max. T_{bias-T}: 50 $°C$
- no distortion of the DC pulses with a pulsewidth range from 100 ns to 100 μs

5.2.4 1^{st} Bias-T for DC-Pulse and DC

This bias-T has four ports. The schematic of the arrangement of the ports is shown in Fig. 5.4:

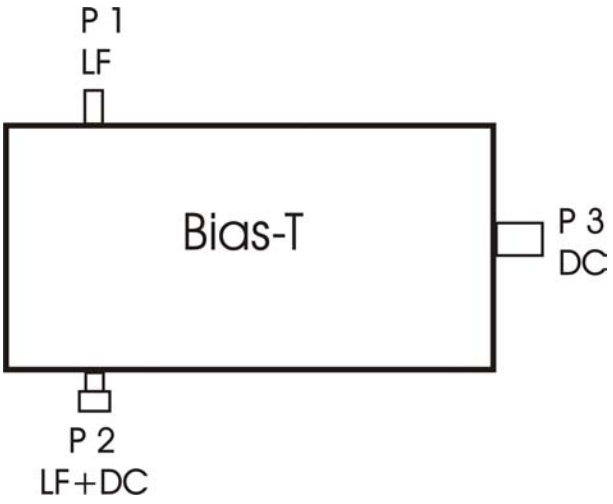

Figure 5.4: Ports of the 4^{th} Bias-T

The Technical Data are:

- Pulsewidth of the DC pulse: 100 ns ... 10 μs
- Frequency range: 600 Hz ... 200 MHz
- Insertion loss: $\leq$ 2.1 dB
- Return loss: $\geq$ 11.5 dB
- R_{DCpath}: 35 mΩ
- max. voltage: 100 V
- max. DC current: 8 A

5.2.5 2^{nd} Bias-T for DC-Pulse and DC

This bias-T has four ports. The schematic of the arrangement of the ports is shown in Fig. 5.5:

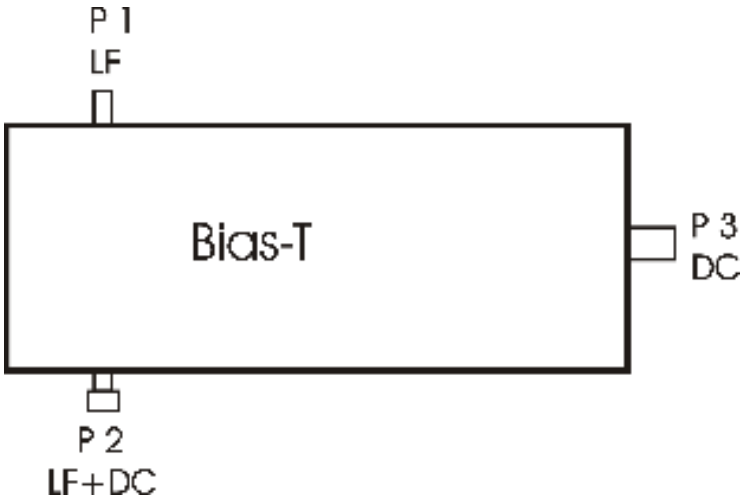

Figure 5.5: Ports of the 5^{th} Bias-T

The Technical Data are:

- Pulsewidth of the DC pulse: 100 ns ... 100 μs
- Frequency range: 100 Hz ... 200 MHz
- Insertion loss: $\leq$ 0.9 dB
- Return loss: $\geq$ 20.9 dB
- R_{DCpath}: 210 mΩ
- max. voltage: 100 V
- max. DC current: 8 A

5.3 Outlook

If it is necessary to build more of these bias-Ts, the following issues should be noted for a redesign:

- The transmissions lines between the connectors and the couplers should be as short as possible to reduce the insertion loss.
- It was also seen at the measurements, that straight transmission lines are better as curved ones, even if the radius of the curves is chosen large enough, so that they have in theory no influence to the insertion and return loss.
- Before using the same Rogers subtrate it is advisable to measure ε_r of this substrate because there were some problems with the correct line width of the transmission lines. This also increased the insertion loss. The use of a substrate with a lower ε_r will result in a larger line width of the transmission lines which will decrease the resistance of the DC path.
- At the end of this thesis a new generation of Xinger® hybrids from Anaren was available. Therefore, it would be helpful to check, if there are new models with a better suited frequency range or a lower insertion loss available.

Bibliography

[1] Bahl, I., *Lumped Elements for RF and Microwave Circuits*, Artech House, ISBN 1-58053-309-4

[2] Collin, R. E., *Foundations for Microwave Engineering*, McGraw-Hill, New York 1966

[3] Shelton, J. P., *Impedances of Offset Parallel-Coupled Strip Transmission Lines*, IEEE *Trans.*, Vol. MTT-14, Jan. 1966, pp. 7-15. Corrections: *ibid*, 1996, p. 249

[4] Mongia R., Bahl I., Bhartia P., *RF and Microwave Coupled-Lines Circuits*, Artech House, ISBN 0-89006-830-5, 1999

[5] Hornstein, R., *Broadband Reflectometer*, Diploma Thesis Vienna University of Technology, April 2002

[6] Bonek, E., *Vorlesung Wellenausbreitung 1*, Vienna University of Technology, Okt. 1997

[7] Bharita, P. and P. *Pramanic, Computer-Aided Design Models for Broadside-Coupled Striplines and Millimeter-Wave Suspeded Substrate Microstrip Lines*, *IEEE Trans.*, Vol. MTT-36, Nov. 1988, pp. 1,476-1,481. Corrections: *ibid*, 1996, p. 249.

Chapter 6

Appendix

6.1 Appendix A - MatLab® Function

Matlab- File for the determination of a directional coupler:

```
Z0=50;                                          reference transmission line impedance
Elem=40;                                        number of elements of one half
C=3.01;                                         coupling in dB
Z=[1.05391 1.14328 1.33137 1.80742 5.36886];    z-values for C=3 and
B10
B=10.356;                                       bandwidth
N=9;                                            number of reference segments
er=2.1;                                         relative dielectric constant of the substrate
b=6.45;                                         overall height of the substrate
s=0.1;                                          space between the lines
n=(N+1)/2;                                      number of Z-values
fu=1e9;                                         lower frequency limit
fo=fu*B;                                        upper frequency limit
f0=(fu+fo)/2;                                   center frequency
R=10^(-C/20);                                   linear coupling factor
L=n*pi/2/pi*3e8/f0/sqrt(er)*1e3;                overall length
LElem=round(100*L/Elem/2)/100;                  elements rounded to 2 decimals
LGes=2*Elem*LElem;                              overall lengths rounded to 2 decimals
w=zeros(1,5);
for i=0:3,                                      weighting factor
w(1+i)=(2*i+1)*pi/4/R*log(Z(5-i)/Z(4-i));
end
w(5)=9*pi/4/R*log(Z(1));
syms u
winkelteil=10*pi/Elem;                          integration steps
coupler=zeros(Elem+1,14);                       field definition
for i=0:Elem,                                   for all elements
winkel=-10*pi+i*winkelteil;                     integration area
Sum=0;                                          summing variable
for j=1:5,                                      for all weighting factors
if winkel>((j-5)*2*pi)                          start of integration
                                                weighting factors

Sum=Sum+w(6-j)*int((sin(u/2))^2/(u/2),(j-6)*2*pi,(j-5)*2*pi);
elseif and ((winkel>(j-6)*2*pi),(winkel<=(j-5)*2*pi))
Sum=Sum+w(6-j)*int((sin(u/2))^2/(u/2),(j-6)*2*pi,winkel);
else
Sum;
```

```
end
end                                                    end of integration
coupler(i+1,1)=winkel;                                 angular position -10pi...0
coupler(i+1,2)=winkel/(4*2*pi*f0*sqrt(er)/3e8)*1000;   absolute position -L/2...0 in mm
Sum=-Sum*R/pi*2;                                       intermediate value
coupler(i+1,3)=Z0*exp(Sum);                            even mode impedance at the det. position
coupler(i+1,4)=(Z0*Z0/coupler(i+1,3));                 odd mode impedance at the det. position
end                                                    phys. shape accomp. with odd- and even mode
                                                       imp. for all elements
```

Determination of the physical parameters of the broadside coupler:

```
sn=s/b;                                                normalizing s to b
ro=zeros(1,Elem);                                      filling the matrix with zeros
A=zeros(1,Elem);
B=zeros(1,Elem);
p=zeros(1,Elem);
r=zeros(1,Elem);
Cfo=zeros(1,Elem);
Co=zeros(1,Elem);
wn=zeros(1,Elem);
won=zeros(1,Elem);
dC=zeros(1,Elem);
K=zeros(1,Elem);
a=zeros(1,Elem);
q=zeros(1,Elem);
Cf=zeros(1,Elem);
wcn=zeros(1,Elem);
Cfa=zeros(1,Elem);
wnloos=zeros(1,Elem);
for i=1:Elem+1,
ro(i)=coupler(i,3)/Z0;                                  determining for tight coupling
A(i)=exp((60*pi^2)/(sqrt(er)*Z0)*((1-((ro(i)^2)*sn))/ro(i)));
B(i)=(A(i)-2+sqrt(A(i)^2-4*A(i)))/2;
p(i)=((B(i)-1)*((1+sn)/2)+sqrt((B(i)-1)^2*((1+sn)/2)^2+4*sn*B(i)))/2;
r(i)=sn*B(i)/p(i);
Cfo(i)=(1/pi)*(-2/(1-sn)*log(sn)+(1/sn)*log((p(i)*r(i))/((p(i)+sn)*(1+p(i))*(r(i)-sn)*(1-r(i)))));
Co(i)=120*pi*ro(i)/(sqrt(er)*Z0);
wn(i)=(sn*(1-sn)*(Co(i)-Cfo(i))/2);                    the normalized line width
won(i)=((1/(2*pi))*((1+sn)*log(p(i)/r(i))+(1-sn)*log((1+p(i))*(r(i)-sn)/((sn+p(i))*(1-r(i))))));
coupler(i,5)=(wn(i)*b);                                the line width
coupler(i,6)=(won(i)*b);                               line offset
coupler(i,7)=(coupler(i,6)-coupler(i,5));              the difference between width and offset
coupler(i,8)=(20*log10((coupler(i,3)-coupler(i,4))/(coupler(i,3)+coupler(i,4))));
                                                       determining for loose coupling
dC(i)=120*pi/sqrt(er)/Z0*(ro(i)^2-1)/ro(i);
K(i)=1/(exp(pi*dC(i)/2)-1);
a(i)=abs(sqrt(((sn-K(i))/(sn+1))^2+K(i))-(sn-K(i))/(sn+1));
q(i)=K(i)/a(i);
Cf(i)=2/pi*(1/(1+sn)*log((1+a(i))/(a(i)*(1-q(i))))-1/(1-sn)*log(q(i)));
wcn(i)=1/pi*(sn*log(q(i)/a(i))+(1-sn)*log((1-q(i))/(1+a(i))));
Cfa(i)=-2/pi*(1/(1+sn)*log((1-sn)/2)+1/(1-sn)*log((1+sn)/2));
wnloos(i)=((1-sn^2)/4*(Co(i)-Cf(i)-Cfa(i)));
coupler(i,9)=(wnloos(i)*b);                            the line widths
coupler(i,10)=(wcn(i)*b);                              the difference between width and offset
coupler(i,11)=(wn(i)/(1-sn));                          first limit for tight coupling
```

```
coupler(i,12)=((wn(i)-won(i))/sn);                    second limit for tight coupling
coupler(i,13)=wnloos(i)/(1-sn);                       first limit for loose coupling
coupler(i,14)=((2*(wnloos(i)-wcn(i)))/(1+sn));        second limit for loose coupling
end
coupler
LGes;
LElem;
```

6.2 Appendix B - Directional Coupler - Design Parameters

Table 6.1, taken from [4], was used to design the directional coupler. With this table it is possible to calculate a directional coupler. B is the bandwidth ratio, δ is the maximum ripple factor, Z_i is the normalized even mode impedances and w is the fractional bandwidth of a directional coupler.

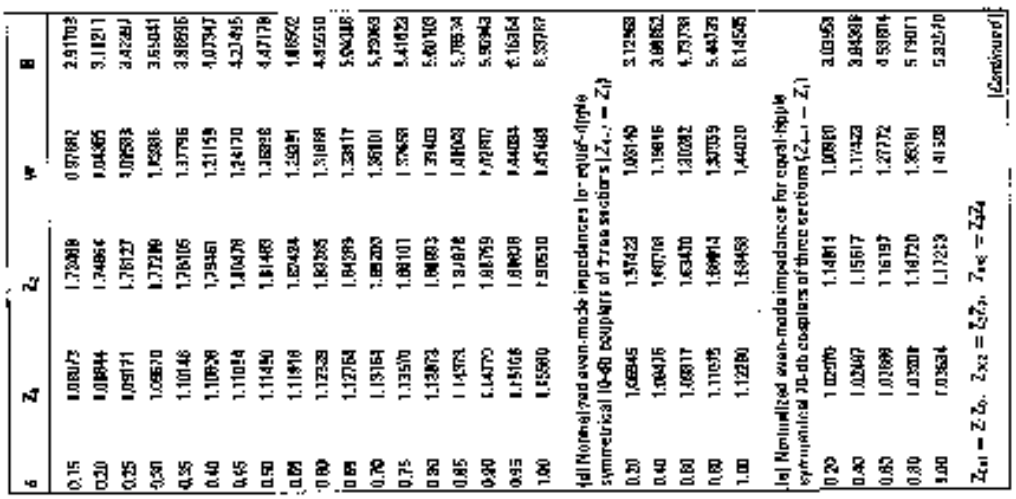

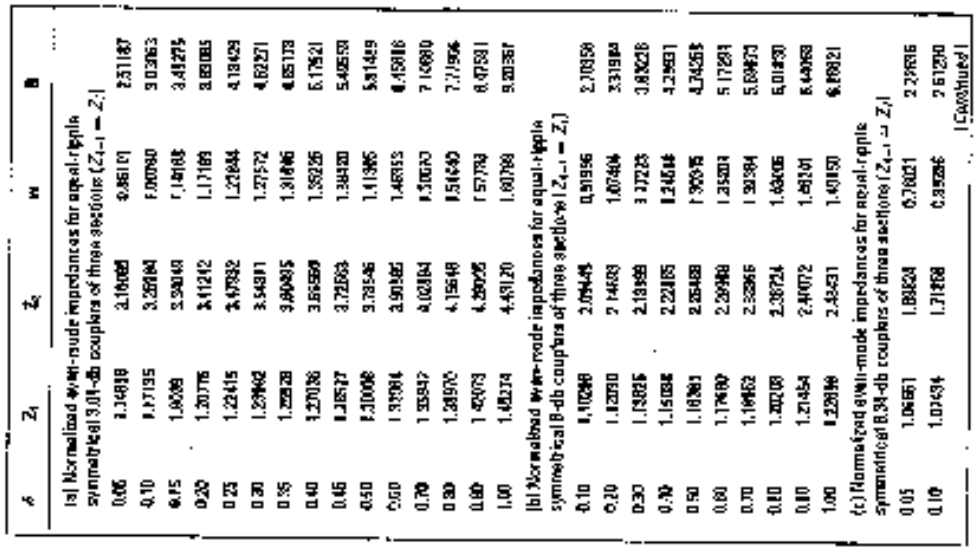

Table 6.1 (*Continued*)

δ	Z_1	Z_2	Z_3	W	B
(f) Normalized even-mode impedances for equal-ripple symmetrical 3.01-db couplers of five sections ($Z_{6-i} = Z_i$)					
0.05	1.06972	1.32824	3.81243	1.20488	4.03071
0.10	1.07354	1.37268	3.97615	1.32559	4.49114
0.15	1.09451	1.40890	4.10491	1.39899	5.05437
0.20	1.10921	1.44029	4.21023	1.45184	6.29714
0.25	1.12314	1.46863	4.30864	1.48033	6.88474
0.30	1.13858	1.48561	4.40069	1.52744	7.46482
0.35	1.14973	1.52091	4.48917	1.55539	8.01698
0.40	1.16288	1.54541	4.67481	1.58162	8.56845
0.45	1.17547	1.56926	4.65912	1.60371	9.09367
0.50	1.18822	1.59265	4.74253	1.62357	9.62609
0.60	1.21370	1.63364	4.90924	1.65791	10.69292
0.70	1.23941	1.68425	5.07867	1.68891	11.77588
0.80	1.26555	1.73013	5.25363	1.71198	12.86720
0.90	1.29235	1.77879	5.43856	1.73402	14.03060
1.00	1.31991	1.82486	5.62978	1.75370	15.24047
(g) Normalized even-mode impedances for equal-ripple symmetrical 8-db couplers of five sections ($Z_{6-i} = Z_i$)					
0.10	1.04501	1.21972	2.38157	1.25446	4.34522
0.20	1.06052	1.25302	2.46010	1.37765	5.45738
0.30	1.07392	1.27819	2.52068	1.45202	6.29363
0.40	1.08623	1.30203	2.57832	1.50648	7.09868
0.50	1.09818	1.32294	2.62159	1.54720	7.83365
0.60	1.10969	1.34262	2.66727	1.58135	8.55462
0.70	1.12089	1.36148	2.71142	1.61023	9.26242
0.80	1.13217	1.37978	2.75470	1.63520	9.96462
0.90	1.14328	1.39772	2.79760	1.65716	10.66721
1.00	1.15438	1.41542	2.84048	1.67673	11.37370
(h) Normalized even-mode impedances for equal-ripple symmetrical 8.34-db couplers of five sections ($Z_{6-i} = Z_i$)					
0.05	1.02539	1.14102	1.85802	1.11764	3.53328
0.10	1.03211	1.15680	1.89019	1.23184	4.20727
0.15	1.03770	1.16899	1.91418	1.30796	4.73524

(*Continued*)

Table 6.1 (*Continued*)

δ	Z_1	Z_2	Z_3	W	B
0.20	1.04271	1.17918	1.93644	1.35395	5.18150
0.25	1.04727	1.18822	1.95170	1.39442	5.60527
0.30	1.05179	1.19648	1.96764	1.42783	5.99090
0.35	1.05802	1.20417	1.98243	1.45627	6.35862
0.40	1.06012	1.21142	1.99635	1.48104	6.70767
0.45	1.06412	1.21838	2.00960	1.50296	7.04761
0.50	1.06803	1.22497	2.02232	1.52262	7.37898
0.55	1.07187	1.23136	2.03462	1.54043	7.70370
0.60	1.07565	1.23760	2.04858	1.55670	8.02323
0.65	1.07939	1.24387	2.05478	1.57168	8.33872
0.70	1.08309	1.24960	2.06971	1.58554	8.65112
0.75	1.08675	1.25542	2.08098	1.59844	8.96119
0.80	1.09039	1.26114	2.09210	1.61060	9.26909
0.85	1.09401	1.26876	2.10310	1.62182	9.57685
0.90	1.09761	1.27235	2.11401	1.63247	9.88347
0.95	1.10119	1.27786	2.12484	1.64253	10.18985
(i) Normalized even-mode impedances for equal-ripple symmetrical 10-db couplers of five sections ($Z_{6-i} = Z_i$)					
1.00	1.10478	1.28331	2.13562	1.65206	10.49635
0.20	1.03418	1.14318	1.70922	1.34442	5.10148
0.40	1.4784	1.16809	1.75305	1.47118	6.55407
0.60	1.05996	1.18815	1.78805	1.54875	7.82613
0.80	1.07140	1.20608	1.81943	1.60053	9.01322
1.00	1.08249	1.22280	1.84912	1.64210	10.17638
(j) Normalized even-mode impedances for equal-ripple symmetrical 20-db couplers of five sections ($Z_{6-i} = Z_i$)					
0.20	1.01016	1.04183	1.17872	1.32734	4.94856
0.40	1.01408	1.04859	1.18787	1.45350	6.31936
0.60	1.01747	1.05386	1.19463	1.52884	7.49338
0.80	1.02068	1.05851	1.20073	1.58281	8.50308
1.00	1.02371	1.06230	1.20633	1.62430	9.64410

$Z_{oo1} = Z_1Z_4$, $Z_{oo2} = Z_2Z_4$, $Z_{oo3} = Z_3Z_4$
$Z_{oo4} = Z_4Z_4$, $Z_{oo5} = Z_5Z_4$

(*Continued*)

Table 6.1 (*Continued*)

δ	Z_1	Z_2	Z_3	Z_4	w	B
(k) Normalized even-mode impedances for equal-ripple symmetrical 3.01-db couplers of seven sections ($Z_{s-i} = Z_i$)						
0.05	1.03635	1.14905	1.50280	4.39954	1.40024	5.6693
0.10	1.05240	1.18406	1.56753	4.61180	1.49705	6.9531
0.15	1.06643	1.21166	1.61640	4.77112	1.55447	7.9780
0.20	1.07950	1.23581	1.65795	4.90662	1.59539	8.8860
0.25	1.09201	1.25786	1.69523	5.02872	1.62715	9.7283
0.30	1.10419	1.27860	1.72975	5.14254	1.65308	10.5302
0.35	1.11615	1.29840	1.76238	5.25103	1.67497	11.3064
0.40	1.12798	1.31754	1.79367	5.35611	1.69388	12.0665
0.45	1.13975	1.33622	1.82400	5.45909	1.71051	12.8174
0.50	1.15149	1.35457	1.85365	5.56097	1.72534	13.5637
0.60	1.17505	1.39069	1.91172	5.76434	1.75090	15.0578
0.70	1.19890	1.42654	1.96915	5.97094	1.77238	16.5728
0.80	1.22323	1.46258	2.02682	6.18437	1.79087	18.1270
0.90	1.24820	1.49918	2.08545	6.40775	1.80710	19.7360
1.00	1.27399	1.53688	2.14586	6.64407	1.82155	21.4147
(l) Normalized even-mode impedances for equal-ripple symmetrical 6-db couplers of seven sections ($Z_{s-i} = Z_i$)						
0.10	1.02686	1.10756	1.32930	2.62516	1.44052	6.1494
0.20	1.04246	1.13419	1.37278	2.72038	1.53802	7.6583
0.30	1.05449	1.15540	1.40584	2.79246	1.59558	8.8908
0.40	1.06580	1.17408	1.43416	2.85438	1.63645	10.0026
0.50	1.07670	1.19128	1.45977	2.91078	1.66806	11.0505
0.60	1.08735	1.20755	1.48367	2.96391	1.69378	12.0626
0.70	1.09787	1.22318	1.50642	3.01511	1.71541	13.0553
0.80	1.10831	1.23839	1.52841	3.06523	1.73404	14.0396
0.90	1.11872	1.25331	1.54989	3.11486	1.75036	15.0232
1.00	1.12915	1.26805	1.57104	3.16446	1.76487	16.0119
(m) Normalized even-mode impedances for equal-ripple symmetrical 8.34-db couplers of seven sections ($Z_{s-i} = Z_i$)						
0.05	1.01460	1.06403	1.21141	1.99183	1.32568	4.9319
0.10	1.02033	1.07694	1.23301	2.03194	1.42127	5.9117

(*Continued*)

Table 6.1 (*Continued*)

δ	Z_1	Z_2	Z_3	Z_4	w	B
0.15	1.02519	1.06680	1.24822	2.06076	1.47818	6.6655
0.20	1.02963	1.09518	1.26167	2.08436	1.51889	7.3140
0.25	1.03379	1.10266	1.27297	2.10489	1.55059	7.9005
0.30	1.03778	1.10953	1.28316	2.12339	1.57653	8.4458
0.35	1.04163	1.11595	1.29256	2.14044	1.59848	8.9622
0.40	1.04538	1.12204	1.30135	2.15641	1.61749	9.4572
0.45	1.04905	1.12786	1.30969	2.17156	1.63423	9.9360
0.50	1.05265	1.13346	1.31764	2.18606	1.64919	10.4022
0.55	1.05621	1.13889	1.32528	2.20004	1.66270	10.8598
0.60	1.05972	1.14417	1.33267	2.21361	1.67500	11.3077
0.65	1.06320	1.14933	1.33984	2.22683	1.68629	11.7507
0.70	1.06666	1.15438	1.34684	2.23979	1.69672	12.1891
0.75	1.07009	1.15934	1.35368	2.25251	1.70640	12.6240
0.80	1.07350	1.16423	1.36040	2.26506	1.71543	13.0563
0.85	1.07689	1.16904	1.36700	2.27746	1.72389	13.4870
0.90	1.08028	1.17381	1.37351	2.28975	1.73184	13.9165
0.95	1.08365	1.17852	1.37993	2.30194	1.73934	14.3456
1.00	1.08702	1.18319	1.38629	2.31408	1.74643	14.7747
(n) Normalized even-mode impedances for equal-ripple symmetrical 10-db couplers of seven sections ($Z_{s-i} = Z_i$)						
0.20	1.02360	1.07622	1.20802	1.81699	1.51198	7.1965
0.40	1.03597	1.09725	1.23839	1.86715	1.61028	9.2638
0.60	1.04718	1.11444	1.26213	1.90649	1.66773	11.0383
0.80	1.05786	1.12991	1.28298	1.94149	1.70815	12.7059
1.00	1.06834	1.14444	1.30229	1.97446	1.73917	14.3359
(o) Normalized even-mode impedances for equal-ripple symmetrical 20-db couplers of seven sections ($Z_{s-i} = Z_i$)						
0.20	1.00697	1.02256	1.05976	1.20128	1.49853	6.9766
0.40	1.01052	1.02846	1.06767	1.21112	1.59672	8.9188
0.60	1.01369	1.03320	1.07372	1.21863	1.65421	10.5678
0.80	1.01669	1.03740	1.07894	1.22515	1.69472	12.1029
1.00	1.01958	1.04129	1.08368	1.23116	1.72584	13.5903

$Z_{0oi} = Z_i Z_0$

(*Continued*)

Table 6.1 (*Continued*)

δ	Z_1	Z_2	Z_3	Z_4	Z_5	w	B
0.15	1.01974	1.05735	1.13622	1.31862	2.18413	1.5858	8.658
0.20	1.02379	1.06452	1.14687	1.33341	2.21025	1.6190	9.499
0.25	1.02764	1.07099	1.15622	1.34822	2.23285	1.6446	10.256
0.30	1.03134	1.07697	1.16469	1.35771	2.25315	1.6656	10.960
0.35	1.03494	1.08261	1.17253	1.36825	2.27160	1.6832	11.627
0.40	1.03846	1.08798	1.17989	1.37809	2.28925	1.6985	12.265
0.45	1.04193	1.09314	1.18687	1.38738	2.30577	1.7119	12.883
0.50	1.04534	1.09813	1.19356	1.39622	2.32156	1.7238	13.484
0.55	1.04872	1.10298	1.19999	1.40471	2.33677	1.7346	14.072
0.60	1.05206	1.10771	1.20622	1.41290	2.35152	1.7444	14.650
0.65	1.05538	1.11234	1.21228	1.42085	2.36589	1.7534	15.221
0.70	1.05868	1.11689	1.21819	1.42858	2.37996	1.7617	15.785
0.75	1.06196	1.12137	1.22398	1.43615	2.39378	1.7694	16.345
0.80	1.06523	1.12579	1.22966	1.44356	2.40740	1.7766	16.901
0.85	1.06849	1.13016	1.23525	1.45084	2.42087	1.7833	17.455
0.90	1.07174	1.13448	1.24076	1.45802	2.43421	1.7896	18.008
0.95	1.07498	1.13877	1.24620	1.46511	2.44745	1.7955	18.560
1.00	1.07823	1.14302	1.25158	1.47211	2.46063	1.8011	19.111
(s) Normalized even-mode impedances for equal-ripple symmetrical 10-db couplers of nine sections ($Z_{10-i} = Z_i$)							
0.20	1.01889	1.05181	1.11743	1.26387	1.90628	1.6133	9.345
0.40	1.03041	1.07004	1.14313	1.29777	1.96074	1.6927	12.016
0.60	1.04103	1.08543	1.16344	1.32390	2.00313	1.7386	14.303
0.80	1.05127	1.09945	1.18139	1.34672	2.04073	1.7709	16.450
1.00	1.06133	1.11271	1.19805	1.36779	2.07614	1.7954	18.547
(t) Normalized even-mode impedances for equal-ripple symmetrical 20-db couplers of nine sections ($Z_{10-i} = Z_i$)							
0.20	1.00555	1.01529	1.03447	1.07471	1.21931	1.6024	9.061
0.40	1.00886	1.02054	1.04153	1.08328	1.22965	1.6818	11.571
0.60	1.01187	1.02485	1.04700	1.08974	1.23748	1.7278	13.697
0.80	1.01474	1.02871	1.05175	1.09527	1.24426	1.7601	15.674
1.00	1.01753	1.03232	1.05608	1.10028	1.25049	1.7848	17.588

$Z_{oa} = Z_i Z_0$

Table 6.1 (*Continued*)

δ	Z_1	Z_2	Z_3	Z_4	Z_5	w	B
(p) Normalized even-mode impedances for equal-ripple symmetrical 3.01-db couplers of nine sections ($Z_{10-i} = Z_i$)							
0.05	1.02680	1.09163	1.24706	1.66958	4.93133	1.5218	7.365
0.10	1.04112	1.12024	1.29488	1.74863	5.18240	1.6012	9.030
0.15	1.05391	1.14328	1.33137	1.80742	5.36886	1.6478	10.356
0.20	1.06598	1.16366	1.36260	1.85696	5.52654	1.6807	11.528
0.25	1.07763	1.18248	1.39075	1.90116	5.66814	1.7062	12.615
0.30	1.08904	1.20027	1.41691	1.94192	5.79985	1.7269	13.649
0.35	1.10030	1.21737	1.44168	1.98035	5.92523	1.7444	14.648
0.40	1.11149	1.23397	1.46548	2.01711	6.04655	1.7594	15.627
0.45	1.12264	1.25023	1.48856	2.05271	6.16540	1.7726	16.594
0.50	1.13379	1.26625	1.51114	2.08747	6.28296	1.7844	17.554
0.60	1.15624	1.29789	1.55536	2.15551	6.51769	1.8046	19.475
0.70	1.17904	1.32941	1.59902	2.22278	6.75634	1.8216	21.423
0.80	1.20234	1.36117	1.64277	2.29038	7.00316	1.8362	23.421
0.90	1.22630	1.39348	1.68712	2.35918	7.26188	1.8490	25.498
1.00	1.25107	1.42660	1.73250	2.42995	7.53602	1.8604	27.644
(q) Normalized even-mode impedances for equal-ripple symmetrical 6-db couplers of nine sections ($Z_{10-i} = Z_i$)							
0.10	1.02201	1.06888	1.17282	1.42807	2.83542	1.5550	7.989
0.20	1.03437	1.09137	1.20736	1.47877	2.94305	1.6345	9.943
0.30	1.04554	1.10967	1.23393	1.51678	3.02373	1.6809	11.535
0.40	1.05615	1.12599	1.25686	1.54902	3.09269	1.7136	12.969
0.50	1.06645	1.14117	1.27768	1.57805	3.15533	1.7389	14.319
0.60	1.07658	1.15561	1.29716	1.60504	3.21427	1.7594	15.622
0.70	1.08662	1.16957	1.31574	1.63070	3.27103	1.7765	16.900
0.80	1.09661	1.18320	1.33370	1.65546	3.32658	1.7913	18.166
0.90	1.10661	1.19661	1.35125	1.67962	3.38161	1.8042	19.431
1.00	1.11663	1.20989	1.36852	1.70342	3.43663	1.8157	20.702
(r) Normalized even-mode impedances for equal-ripple symmetrical 8.34-db couplers of nine sections ($Z_{10-i} = Z_i$)							
0.05	1.01032	1.03838	1.10598	1.27508	2.10668	1.4599	6.406
0.10	1.01536	1.04904	1.12341	1.30048	2.15200	1.5392	7.681

(*Continued*)

6.3 Appendix C - Directional Coupler - Table of Physical Parameters

U	x/mm	Z_{0E}/Ω	Z_{0O}/Ω	Tight		
				W	W_O	W_O-W
-31,42	-45,57	50,00	50,00	6,82	7,11	0,28
-30,63	-44,44	50,03	49,97	6,82	7,10	0,28
-29,85	-43,30	50,22	49,78	6,79	7,07	0,28
-29,06	-42,16	50,66	49,35	6,72	6,99	0,28
-28,27	-41,02	51,29	48,74	6,62	6,89	0,27
-27,49	-39,88	51,94	48,13	6,52	6,78	0,26
-26,70	-38,74	52,43	47,68	6,45	6,71	0,26
-25,92	-37,60	52,66	47,47	6,41	6,67	0,26
-25,13	-36,46	52,70	47,44	6,41	6,66	0,26
-24,35	-35,32	52,75	47,40	6,40	6,66	0,26
-23,56	-34,18	53,06	47,12	6,35	6,61	0,25
-22,78	-33,04	53,77	46,50	6,25	6,50	0,25
-21,99	-31,90	54,80	45,62	6,11	6,35	0,24
-21,21	-30,76	55,89	44,73	5,97	6,19	0,23
-20,42	-29,62	56,72	44,08	5,86	6,08	0,22
-19,63	-28,48	57,12	43,77	5,81	6,03	0,22
-18,85	-27,34	57,18	43,72	5,80	6,02	0,21
-18,06	-26,21	57,27	43,65	5,79	6,01	0,21
-17,28	-25,07	57,89	43,19	5,72	5,93	0,21
-16,49	-23,93	59,32	42,15	5,55	5,74	0,20
-15,71	-22,79	61,45	40,68	5,31	5,49	0,18
-14,92	-21,65	63,77	39,20	5,07	5,23	0,16
-14,14	-20,51	65,60	38,11	4,90	5,04	0,14
-13,35	-19,37	66,49	37,60	4,82	4,95	0,13
-12,57	-18,23	66,64	37,51	4,80	4,94	0,13
-11,78	-17,09	66,84	37,40	4,78	4,92	0,13
-11,00	-15,95	68,19	36,66	4,67	4,79	0,12
-10,21	-14,81	71,46	34,99	4,40	4,49	0,09
-9,42	-13,67	76,63	32,63	4,02	4,08	0,06
-8,64	-12,53	82,65	30,25	3,64	3,65	0,01
-7,85	-11,39	87,74	28,49	3,37	3,34	-0,03
-7,07	-10,25	90,41	27,65	3,23	3,19	-0,04
-6,28	-9,11	90,89	27,51	3,21	3,16	-0,05
-5,50	-7,98	91,57	27,30	3,18	3,13	-0,05
-4,71	-6,84	96,59	25,88	2,96	2,87	-0,09
-3,93	-5,70	110,81	22,56	2,45	2,27	-0,18
-3,14	-4,56	139,68	17,90	1,75	1,39	-0,36
-2,36	-3,42	187,88	13,31	1,11	0,45	-0,66
-1,57	-2,28	253,03	9,88	0,71	0,29	-0,43
-0,79	-1,14	315,69	7,92	0,55	0,75	0,20
0,00	0,00	342,61	7,30	0,52	0,92	0,41

k / dB	Lo ose		tight w'/(1-s')	tight w_c'/s'	loose w'/(1-s')	loose $2w_0$'/(1+s')
	W	W_C	≥ 0,35	≥ 0,7	≥ 0,35	≥ 0,85
NaN	NaN	NaN	1,07	-2,85	NaN	NaN
-64,44	5,54	-12,34	1,07	-2,84	0,87	5,46
-47,02	5,54	-8,22	1,07	-2,82	0,87	4,20
-37,64	5,54	-6,01	1,06	-2,78	0,87	3,53
-31,90	5,53	-4,66	1,04	-2,72	0,87	3,11
-28,39	5,52	-3,84	1,03	-2,65	0,87	2,86
-26,48	5,51	-3,39	1,02	-2,60	0,87	2,72
-25,71	5,51	-3,21	1,01	-2,58	0,87	2,66
-25,59	5,51	-3,19	1,01	-2,57	0,87	2,65
-25,44	5,51	-3,15	1,01	-2,57	0,87	2,64
-24,54	5,50	-2,95	1,00	-2,54	0,87	2,58
-22,79	5,47	-2,55	0,98	-2,47	0,86	2,45
-20,78	5,44	-2,11	0,96	-2,37	0,86	2,30
-19,10	5,39	-1,75	0,94	-2,27	0,85	2,18
-18,03	5,35	-1,53	0,92	-2,19	0,84	2,10
-17,57	5,33	-1,43	0,92	-2,15	0,84	2,06
-17,50	5,32	-1,42	0,91	-2,15	0,84	2,06
-17,39	5,32	-1,40	0,91	-2,14	0,84	2,05
-16,75	5,28	-1,27	0,90	-2,08	0,83	2,00
-15,43	5,20	-1,03	0,87	-1,95	0,82	1,90
-13,84	5,06	-0,76	0,84	-1,77	0,80	1,78
-12,45	4,90	-0,55	0,80	-1,57	0,77	1,66
-11,54	4,77	-0,43	0,77	-1,42	0,75	1,59
-11,13	4,70	-0,38	0,76	-1,34	0,74	1,55
-11,07	4,69	-0,38	0,76	-1,33	0,74	1,55
-10,98	4,68	-0,37	0,75	-1,31	0,74	1,54
-10,44	4,58	-0,31	0,73	-1,20	0,72	1,49
-9,30	4,35	-0,20	0,69	-0,95	0,68	1,39
-7,90	4,00	-0,10	0,63	-0,55	0,63	1,25
-6,67	3,64	-0,02	0,57	-0,11	0,57	1,12
-5,85	3,36	0,02	0,53	0,25	0,53	1,02
-5,49	3,23	0,04	0,51	0,44	0,51	0,98
-5,43	3,21	0,04	0,51	0,47	0,51	0,97
-5,34	3,18	0,05	0,50	0,51	0,50	0,96
-4,77	2,96	0,08	0,47	0,86	0,47	0,88
-3,59	2,45	0,17	0,39	1,79	0,39	0,69
-2,24	1,75	0,35	0,28	3,60	0,28	0,43
-1,23	1,11	0,62	0,18	6,64	0,18	0,15
-0,68	0,71	0,98	0,11	4,27	0,11	-0,08
-0,44	NaN	NaN	0,09	-2,03	NaN	NaN
-0,37	NaN	NaN	0,08	-4,05	NaN	NaN

6.4 Appendix D - Datasheets of Anaren Xinger® Q-Hybrids

Anaren

Model 11306-3
Rev. A

Xinger®

Hybrid Couplers
3 dB, 90°

Description

The 11306-3 is a low profile 3dB hybrid coupler in an easy to use surface mount package covering 2.0 to 4.0 GHz. The 11306-3 is ideal for balanced amplifiers and signal distribution and can be used in most high power designs. Parts have been subjected to rigorous qualification testing and units are 100% tested. They are manufactured using materials with x and y thermal expansion coefficients compatible with common substrates such as FR4, G-10 and polyamide.

Features:

- 2.0 – 4.0 GHz
- Low loss
- High Isolation
- 90° Quadrature
- Surface Mountable
- Tape And Reel
- Convenient Package
- 100% Tested

ELECTRICAL SPECIFICATIONS**

Frequency	Isolation	Insertion Loss	VSWR	
GHz	*dB Min*	*dB Max*	*Max:1*	
2.0 – 4.0	20	0.35	1.30	
Amplitude Balance	**Phase Balance**	**Power**	**ΘJC**	**Operating Temp.**
dB Max	*Degrees*	*Ave. CW Watts*	*°C/ Watt*	*°C*
± 0.55	± 5	60	24.6	-55 to +85

**Specification based on performance of unit properly installed on microstrip printed circuit boards with 50 Ω nominal impedance. Specifications subject to change without notice.

Outline Drawing

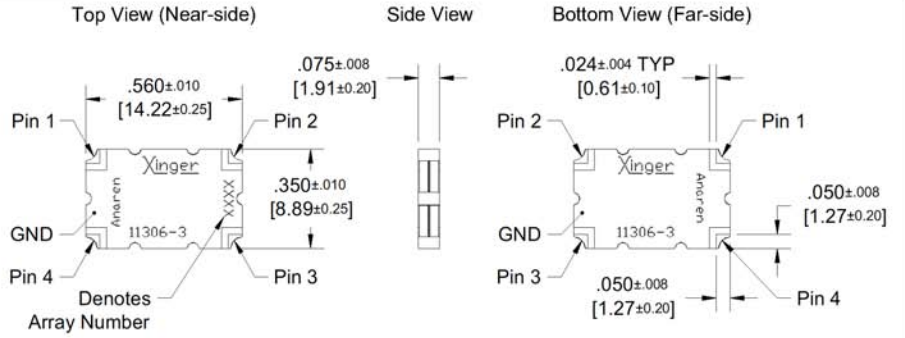

Dimensions are in Inches [Millimeters]
11306-3 Rev A Mechanical Outline

Part Is Symmetric About All Axis

Anaren
What'll we think of next

Available on Tape and Reel For Pick and Place Manufacturing.

USA/Canada: (315) 432-8909
Toll Free: (800) 544-2414
Europe: +44 2392-232392

Model 11306-3

Rev. A

Anaren

Xinger®

Typical Performance: 2.0 GHz. to 4.0 GHz.

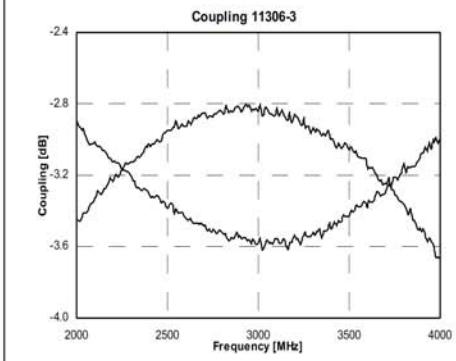

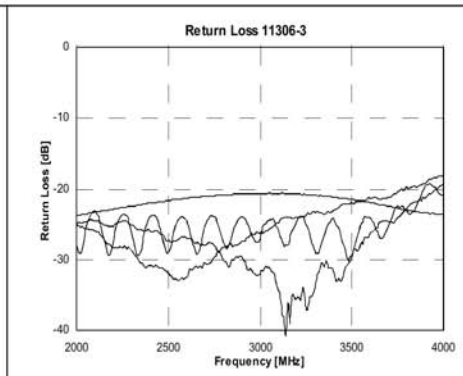

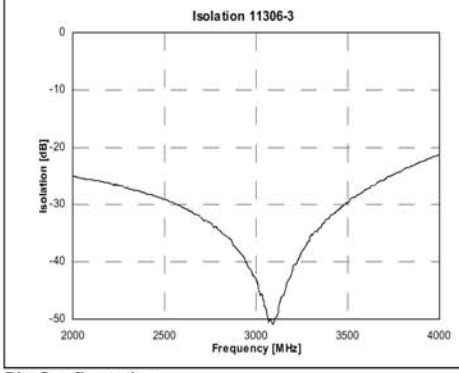

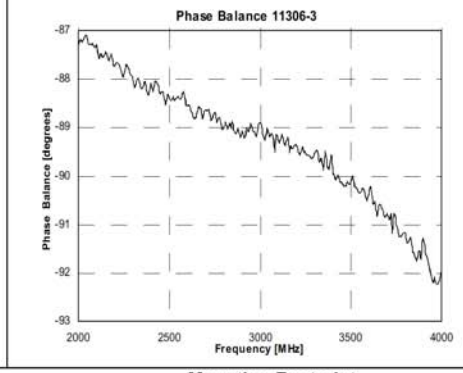

Pin Configuration

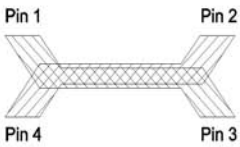

Hybrid Coupler Pin Configruation				
	Pin 1	Pin 2	Pin 3	Pin 4
Configuration #1	Input	Isolated	-3dB, -90°	-3dB, 0°
Configuration #2	Isolated	Input	-3dB, 0°	-3dB, -90°
Configuration #3	-3dB, -90°	-3dB, 0°	Input	Isolated
Configuration #4	-3dB, 0°	-3dB, -90°	Isolated	Input

Mounting Footprint

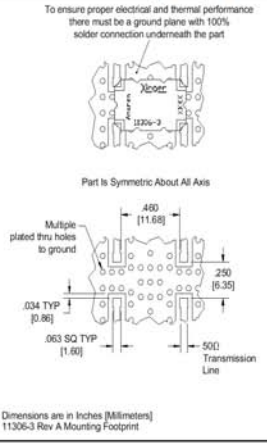

USA/Canada: (315) 432-8909
Toll Free: (800) 544-2414
Europe: +44 2392-232392

Available on Tape and Reel For Pick and Place Manufacturing.

Anaren

What'll we think of ne

Anaren

Model 1M803
Rev. B

Xinger®

Micro Xinger 3dB Hybrid Coupler

Description

The 1M803 Micro Xinger® is a low profile, miniature 3dB hybrid coupler in an easy to use surface mount package designed for U-NII, ISM and hyperLAN applications. The 1M803 is designed for balanced amplifiers and signal distribution and is an ideal solution for the ever increasing demands of the wireless industry for smaller printed circuit boards and high performance. Parts have been subjected to rigorous qualification testing and units are 100% tested. They are manufactured using materials with x and y thermal expansion coefficients compatible with common substrates such as FR4 and G-10.

Features:

- 5.0 – 6.0 GHz
- Very Low Loss
- High Isolation
- 90° Quadrature
- Surface Mountable
- Tape And Reel
- New Micro-Package
- 100% Tested

ELECTRICAL SPECIFICATIONS**

Frequency	Isolation	Insertion Loss	VSWR	
GHz	*dB Min*	*dB Max*	*Max:1*	
5.0 – 6.0	20	0.25	1.21	
Amplitude Balance	**Phase Balance**	**Power**	**ΘJC**	**Operating Temp.**
dB Max	*Degrees*	*Ave. CW Watts*	*°C/Watt*	*°C*
± 0.30	± 3	20	78.1	-55 to +85

**Specification based on performance of unit properly installed on microstrip printed circuit boards with 50 Ω nominal impedance. Specifications subject to change without notice.

Outline Drawing

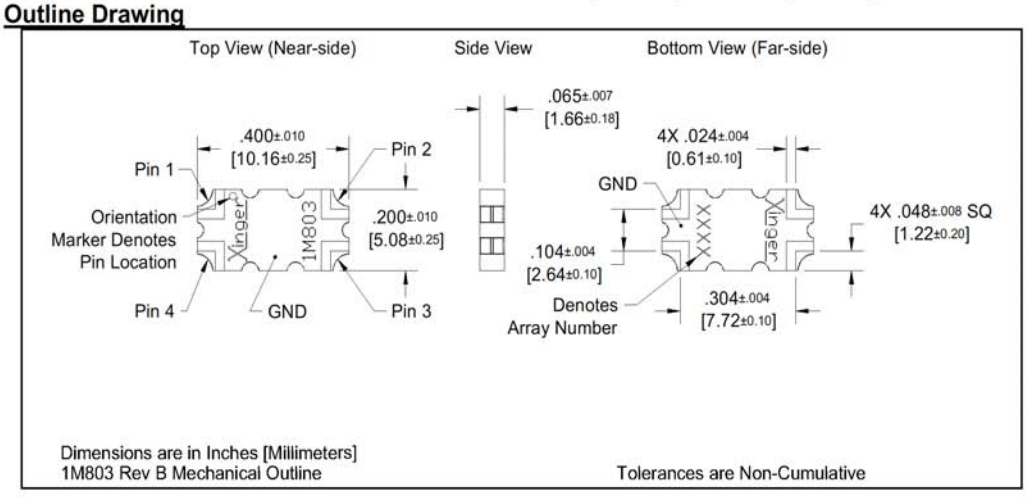

Anaren
What'll we think of next

Available on Tape and Reel For Pick and Place Manufacturing.

USA/Canada: (315) 432-8909
Toll Free: (800) 544-2414
Europe: +44 2392-232392

Model 1M803

Rev. B

Anaren

Xinger®

Typical Performance: 5.0 GHz. to 6.0 GHz.

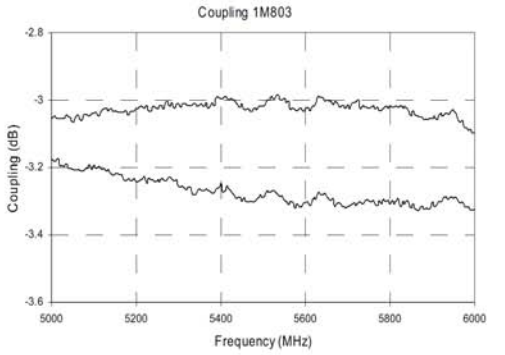

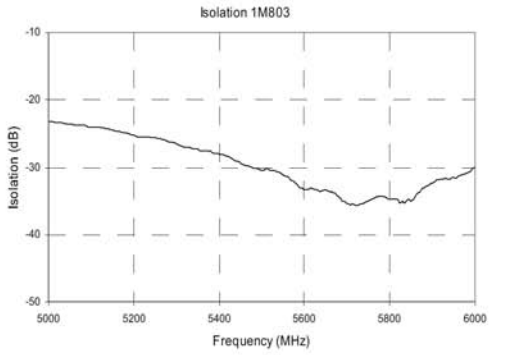

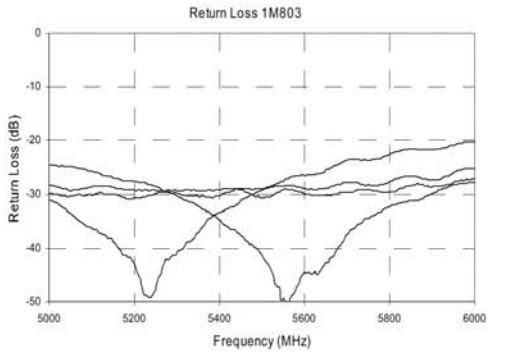

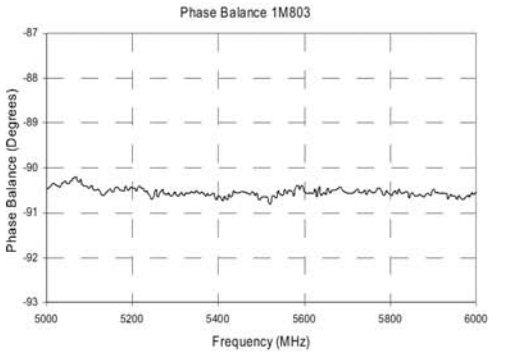

Pin Configuration

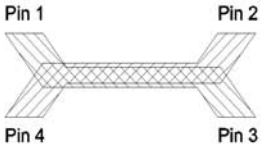

Hybrid Coupler Pin Configuration				
	Pin 1	Pin 2	Pin 3	Pin 4
Configuration #1	Input	Isolated	-3dB, -90°	-3dB, 0°
Configuration #2	Isolated	Input	-3dB, 0°	-3dB, -90°
Configuration #3	-3dB, -90°	-3dB, 0°	Input	Isolated
Configuration #4	-3dB, 0°	-3dB, -90°	Isolated	Input

Mounting Footprint

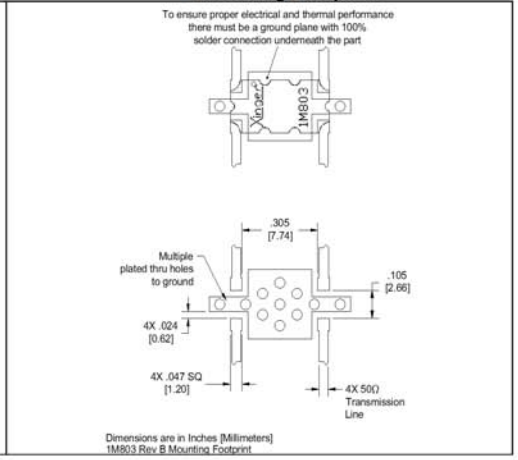

USA/Canada: (315) 432-8909
Toll Free: (800) 544-2414
Europe: +44 2392-232392

Available on Tape and Reel For Pick and Place Manufacturing.

Anaren
What'll we think of ne›

6.5 Appendix E - Subtrates

Taconic RF-35:

RF-35 TYPICAL VALUES					
Property	Test Method	Units	Value	Units	Value
Dielectric Constant @ 1.9 GHz	IPC-TM 650 2.5.5		3.50		3.50
Dissipation Factor @ 1.9 GHz	IPC-TM 650 2.5.5		0.0018		0.0018
Moisture Absorption (.060")	IPC-TM 650 2.6.2.1	%	.02	%	0.02
Peel Strength (1/2 oz. copper)	IPC-TM 650 2.4.8	lbs./linear inch	>8.0	N/mm	>1.5
Peel Strength (1 oz. copper)	IPC-TM 650 2.4.8	lbs./linear inch	>10.0	N/mm	>1.8
Dielectric Breakdown	IPC-TM 650 2.5.6	kV	41	kV	41
Volume Resistivity	IPC-TM 650 2.5.17.1	Mohm/cm	1.26×10^9	Mohm/cm	1.26×10^9
Surface Resistivity	IPC-TM 650 2.5.17.1	Mohm	1.46×10^8	Mohm	1.46×10^8
Arc Resistance	IPC TM 650 2.5.1	seconds	>180	seconds	>180
Flexural Strength Lengthwise	ASTM D 790	psi	>22,000	N/mm²	>152
Flexural Strength Crosswise	ASTM D 790	psi	>18,000	N/mm²	>124
Thermal Conductivity	Cenco-Fitch	BTU/in/hr/ft²/°F	1.416	W/m/K	0.20
Tensile Strength Lengthwise	ASTM D 638	psi	27,000	N/mm²	187
Tensile Strength Crosswise	ASTM D 638	psi	21,000	N/mm²	145
Dimensional Stability Lengthwise	IPC-TM 650 2.4.39	in/in	.00004	mm/mm	0.00004
Dimensional Stability Crosswise	IPC-TM 650 2.4.39	in/in	-.00010	mm/mm	-0.00010
x-y CTE	ASTM D 3386 (TMA)	ppm/°C	19-24	ppm/°C	19-24
z CTE	ASTM D 3386 (TMA)	ppm/°C	64	ppm/°C	64
Flammability	UL-94		V-0		V-0
Hardness	Rockwell M Scale		34		34

Type	Dk
TLY-5A	2.17
TLY-5	2.20
TLY-3	2.33
TLT-0 | TLX-0	2.45
TLT-9 | TLX-9	2.50
TLT-8 | TLX-8	2.55
TLT-7 | TLX-7	2.60
TLT-6 | TLX-6	2.65
TLE-95	2.95
TLC-27	2.75
TLC-30	3.00
TLC-32	3.20
RF-30	3.00
RF-35 | RF-35P	3.50
RF-60	6.15
CER-10	10

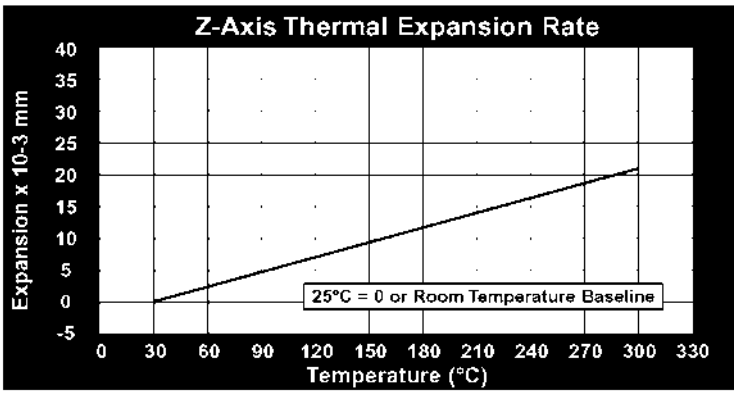

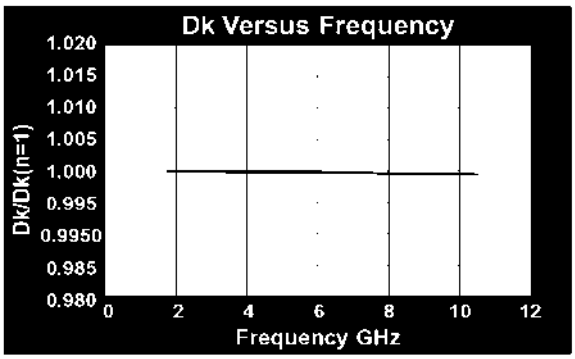

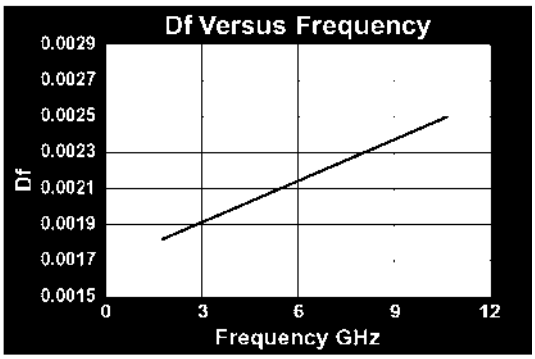

All reported values are typical and should not be used for specification purposes. In all instances the user shall determine suitability in any given application.

2/02

How to Order

Designation	Dielectric Constant
RF-35	3.5+/-.1

Available Thickness	Normal Dielectric Constant
0.0100" (0.25mm)	3.5
0.0200" (0.50mm)	3.5
0.0300" (0.76mm)	3.5
0.0600" (1.52mm)	3.5

Standard sheet size is 36" x 48" (914mm x 1220mm). Please contact our Customer Service Department for availability of other sizes and claddings.

RF-35 can be ordered with the following electrodeposited copper:

Designation	Weight	Copper Thickness	Copper Thickness
CH	1/2 oz./sq. ft.	~ .0007"	~18 µm
C1	1 oz./sq. ft.	~ .0014"	~ 35 µm
C2	2 oz./sq. ft.	~ .0028"	~ 70 µm

Panels may be ordered cut to size

Typical Panel Sizes	
12" x 18"	304mm x 457mm
16" x 18"	406mm x 457mm
18" x 24"	457mm x 610mm
16" x 36"	406mm x 914mm
24" x 36"	610mm x 914mm
18" x 48"	457mm x 1220mm

An example of our part number is: RF-35-0600-CH/CH-18" x 24" (RF-35-0600-CH/CH-457mm x 610mm)

TACONIC
ADVANCED DIELECTRIC DIVISION

P.O. Box 69 • 136 Coonbrook Road
Petersburgh, New York 12138 • USA
TEL: 518-658-3202 • FAX: 518-658-3988
TOLL FREE: 800-833-1805 • FAX: 800-272-2503

Mullingar Business Park
Mullingar, Co. Westmeath,
Republic of Ireland
TEL: +353-44-40477 • FAX: +353-44-44369

302 E-Dong Bundang Techno Park
151 Yatap-dong Bundang-gu
Sungnam-si, Kyungki-do, Republic of Korea
TEL: 82-31-/04-1868/9 • FAX: 82-31-/04-1857

Rogers R4003C:

PROPERTY	TYPICAL VALUE		DIRECTION	UNITS	CONDITION	TEST METHOD
	RO4003C™	RO4350B™[1]				
Dielectric Constant, ε	3.38±0.05	3.48±0.05*	Z	--	10 GHz/23°C 2.5 GHz/23°C	IPC-TM-650 2.5.5.5
Dissipation Factor tan, δ	0.0027 0.0021	0.0037 0.0031	Z	--	10 GHz/23°C 2.5 GHz/23°C	IPC-TM-650 2.5.5.5
Thermal Coefficient of ε	+40	+50	Z	ppm/°C	100°C to 250°C	IPC TM 650 2.5.5.5
Volume Resistivity	1.7 X 10[9]	1.2 X 10[10]		MΩ•cm	COND A	IPC-TM-650 2.5.17.1
Surface Resistivity	4.2 X 10[9]	5.7 X 10[9]		MΩ	COND A	IPC-TM-650 2.5.17.1
Electrical Strength	31.2 (780)	31.2 (780)	Z	KV/mm (V/mil)	0.51mm (0.020")	IPC-TM-650 2.5.6.2
Tensile Modulus	26,889 (3900)	11,473 (1664)	Y	MPa (kpsi)	RT	ASTM D638
Tensile Strength	141 (20.4)	175 (25.4)	Y	MPa (kpsi)	RT	ASTM D638
Flexural Strength	276 (40)	255 (37)	-	MPa (kpsi)		IPC-TM-650 2.4.4
Dimensional Stability	<0.3	<0.5	X,Y	mm/m (mils/inch)	after etch +E2/150°	IPC TM 650 2.4.39A
Coefficient of Thermal Expansion	11 14 46	14 16 50	X Y Z	ppm/°C	-55 to 288°C	IPC-TM-650 2.1.41
Tg	>280	>280	-	°C	A	IPC-TM-650 2.4.24
Thermal Conductivity	0.64	0.62	-	W/m/°K	100°C	ASTM F433
Moisture Absorption	0.04	0.04	-	%	48 hrs immersion 0.060" sample Temperature 50 C	ASTM D570
Density	1.79	1.86	-	gm/cm	23 C	ASTM D792
Copper Peel Strength	1.05 (6.0)	0.88 (5.0)		N/mm (pli)	after solder float 1 oz. EDC Foil	IPC-TM-650 2.4.8
Flammability	N/A	94V-0				UL

STANDARD THICKNESS:	STANDARD PANEL SIZE:	STANDARD COPPER CLADDING:
RO4003C™: 0.008" (0.203mm), 0.012" (0.305mm), 0.016 (0.406mm), 0.020" (0.508mm) 0.032" (0.813mm), 0.060" (1.524mm) **RO4350B™:** *0.004" (0.101mm), 0.0066" (0.168mm), 0.010" (0.254mm), 0.0133 (0.338mm), 0.0166" (0.422mm), 0.020" (0.508mm) 0.030" (0.762mm), 0.060" (1.524mm)	12" X 18" (305 X457 mm) 24" X 18" (610 X 457 mm) 24" X 36" (610 X 915 mm) 48" X 36" (1.224 m X 915 mm)	½ oz. (17µm), 1 oz. (34µm) and 2 oz. (70µm) electrodeposited copper foil

Approval needed for 0.004 mil material. Contact customer service.

(1) Dielectric constant and loss tangent are reported based on IPC-TM-2.5.5.5 @ GHz (stripline resonator). Departure from this test method or frequency may yeld different values. It has been reported that in some microstrip applications, a Delta (Δ) of 0.2 in dielectric constant has been observed for both RO4003 and RO4350B based on actual circuit measurement and circuit modeling comparisons. It is up to the user to determine which value best fits the application and modeling software used during the design process while Rogers ensures the repeatability of the product received.

(2) Dielectric constant typical value does not apply to 0.004 (0.101mm) laminates. Dielectric constant specification value for 0.004 RO4350B material is 3.36 ± 0.05.

Polyfon POLYGUIDE:

• Electrical

Dielectric Constant	
copper clad	2.320 ± 0.005
unclad	2.355 ± 0.010
Loss Factor	
unclad	1 x 10^{-5} @ 1.0 MHz
Attenuation	
copper clad	0.04 dB/m
Dissipation Factor	0.0002 ± .00005@1.0 MHz

• Thermal Properties

Coefficient of Expansion [ppm/deg C] Dielectric only (X,Y, & Z Axes)	108
Operating Temperature Range	-55 to 85° C
Solderability	Excellent
Decrease of Adhesion, Repeated Soldering	None

• Copper Clad & Unclad POLYGUIDE Dielectric

Dielectric Thickness inch.	(mm)	Thickness Variation inch.	(mm)
.020	.508	± .002	.051
.062	1.575	± .004	.102
.125	3.175	± .005	.127
.187	4.750	± .008	.203

• Copper Cladding Data

Type	Copper Thickness inch.	(mm)	Thickness Variation inch.	(mm)
½ .oz	.0007	.0178	± .00007	.00178
1 .oz	.0014	.0356	± .00014	.00356
2 .oz	.0028	.0711	± .00035	.00711

• POLYGUIDE Ordering Information

POLYGUIDE laminates and dielectrics are supplied in the following standard sheet sizes:

Dielectric Thickness	Sheet Size
.020	16.0" x 30.0"
.062	22.5" x 32.0"
.125	22.5" x 32.0"
.187	22.5" x 32.0"

• General Properties

Substrate

Dielectric Strength	500 volts/mil
Surface Resistivity	10^{12} ohms, min.
Volume Resistivity	10^{16} ohms
Water Absorption	<0.01%
Chemical Resistance	Resistant-to-very resistant: weak and strong acids, alkalis, & organic solvents.
Surface Outgas	Slight at 10^{-9} torr
Machinability	Will not alter properties
Thickness Variation	±.002"max, sheet-to-sheet

Laminate

Copper Foil Purity	99.5% (min)
Copper Foil Resistivity	0.15940 ohm-gm/m^2
Peel Strength	8.0 lbs/in (min)
Adhesives, Intermediates	None

Typical Ordering Code

PG - A - 62 -14- 14

Basic Type	Standard Line	Dielectric Thickness in mils	Copper Thickness in 0.1 mils.

• Processing Information

For information regarding the processing and handling of POLYGUIDE, please contact Polyflon. Also, as a service to our customers, Polyflon offers expert in-house circuit processing of most microwave laminates.

Polyfon CuFLON:

Electrical

Dielectric Strength:	
1-5 mils	2000 V/mil
10-20 mils	1000 V/mil
Dielectric Constant,23°C	
1MHz	2.1
1GHz	2.1
18GHz	2.1
Dissipation Factor,23°C	
1MHz	0.00010
1GHz	0.00045
18GHz	0.00045
Resistivity:Copper@23°C	1.75×10^{-6} ohm - cm
Volume Resistivity, Dielectric	10^{16} ohm - cm
Surface Resistivity, Dielectric	10^{16} ohm/sq.

Thermal

Operating Temperature Range	-55 to 175 °C
Short Term Maximum Temperature	225 °C
Solderability	Excellent
Decrease of Adhesion, Repeated Soldering	None
Coefficient of Expansion x 10^{-5} / °C (-55 to 100 °C) for 31 mil board with 1/2 oz. (0.7 mil) copper)	
Dielectric only, X, Y, Z axis	12.90
Plated Dielectric, Unetched, as Supplied, X and Y axis	2.61
Plated Dielectric, Unetched, as Supplied, Z axis	19.40
Typical Circuit, one side Groundplane	
X and Y axis	2.61
Z axis	12.90
Typical Circuit, two sides, Etched	
Along Circuit Conductors	2.61
Between Parallel Conductors	12.90
Z axis	12.90

Mechanical

Tensile Strength, Dielectric @23°C	3500 psi
Modulus of Elasticity, Dielectric @23°C	6000 psi

Dielectric Thickness	Dielectric Thickness Tolerance maximum
1-5 mils	10%
10-62 mils	+/- 1 mil
125 mils	+/- 3 mils

Standard Copper Cladding	Thickness	Tolerance
1/3 oz.	.5 mil	+/-.2mil
1/2 oz.	.7 mil	+/-.2mil
1 oz.	1.4 mil	+/-.35mil
2 oz.	2.8 mil	+/-.70mil

Peel Strength	8 lb/in
Water Absorption	<0.01%

CuFlon Ordering Information

PTFE dielectric thickness of 1/4 through 5 mils are provided in 9" x 9" sheets. Dielectric thicknesses of 10 mils and heavier are provided in 12" x 18" sheets.

Standard Thicknesses in mils:
1/4, 1/2, 1, 2, 3, 4, 5, 10, 15, 20, 31, 62*, 125**
* Not available with 1/3 oz copper
** Not available with 1/3 or 1/2 oz copper

Typical Ordering Code